2012

Numerical Simulation Of Electrolyte-supported Planar Button Solid Oxide Fuel Cell

Amjad Aman
University of Central Florida

NUMERICAL SIMULATION OF ELECTROLYTE-SUPPORTED PLANAR BUTTON SOLID OXIDE FUEL CELL

by

AMJAD AMAN
B.E. Visvesvaraya Technological University, India, 2006

A thesis submitted in partial fulfillment of the requirements
for the degree of Master of Science
in the Department of Mechanical, Materials and Aerospace Engineering
in the College of Engineering and Computer science
at the University of Central Florida
Orlando, Florida

Summer Term
2012

Major Professor: Nina Orlovskaya

ABSTRACT

Solid Oxide Fuel Cells are fuel cells that operate at high temperatures usually in the range of 600^{o}C to 1000^{o}C and employ solid ceramics as the electrolyte. In Solid Oxide Fuel Cells oxygen ions (O^{2-}) are the ionic charge carriers. Solid Oxide Fuel Cells are known for their higher electrical efficiency of about 50-60% [1] compared to other types of fuel cells and are considered very suitable in stationary power generation applications.

It is very important to study the effects of different parameters on the performance of Solid Oxide Fuel Cells and for this purpose the experimental or numerical simulation method can be adopted as the research method of choice. Numerical simulation involves constructing a mathematical model of the Solid Oxide Fuel Cell and use of specifically designed software programs that allows the user to manipulate the model to evaluate the system performance under various configurations and in real time. A model is only usable when it is validated with experimental results. Once it is validated, numerical simulation can give accurate, consistent and efficient results. Modeling allows testing and development of new materials, fuels, geometries, operating conditions without disrupting the existing system configuration. In addition, it is possible to measure internal variables which are experimentally difficult or impossible to measure and study the effects of different operating parameters on power generated, efficiency, current density, maximum temperatures reached, stresses caused by temperature gradients and effects of thermal expansion for electrolytes, electrodes and interconnects.

Since Solid Oxide Fuel Cell simulation involves a large number of parameters and complicated equations, mostly Partial Differential Equations, the situation calls for a sophisticated simulation technique and hence a Finite Element Method (FEM) multiphysics approach will be employed. This can provide three-dimensional localized information inside the fuel cell. For this thesis, COMSOL Multiphysics® version 4.2a will be used for simulation purposes because it has a Batteries & Fuel Cells module, the ability to incorporate custom Partial Differential Equations and the ability to integrate with and utilize the capabilities of other tools like MATLAB®, Pro/Engineer®, SolidWorks®.

Fuel Cells can be modeled at the system or stack or cell or the electrode level. This thesis will study Solid Oxide Fuel Cell modeling at the cell level. Once the model can be validated against experimental data for the cell level, then modeling at higher levels can be accomplished in the future. Here the research focus is on Solid Oxide Fuel Cells that use hydrogen as the fuel. The study focuses on solid oxide fuel cells that use 3-layered, 4-layered and 6-layered electrolytes using pure YSZ or pure SCSZ or a combination of layers of YSZ and SCSZ. A major part of this research will be to compare SOFC performance of the different configurations of these electrolytes. The cathode and anode material used are $(La_{0.6}Sr_{0.4})_{0.95\text{-}0.99}Co_{0.2}Fe_{0.8}O_3$ and Ni-YSZ respectively.

This thesis is dedicated to my parents, Mirza Mohamed Amanulla and Suhara Aman, who have loved me more than I could ever ask for; my siblings, Shabna and Arshad, with whom I always feel one. Finally I dedicate this thesis to my girlfriend, Janaki Palomar, who has always loved me and believed in me.

ACKNOWLEDGMENTS

This thesis is a result of the guidance, patience and support I have received from my advisors Dr. Nina Orlovskaya and Dr. Yunjun Xu. Dr. Nina taught me everything I know about fuel cells, gave me the opportunity to work with her and has always been available. Dr. Yunjun has been available and always provided useful feedback. To them, I express my deepest gratitude.

I am also very grateful to Rusty Gentile, who worked with me on this research and gave his valuable insights and his dedication.

I also would like to really thank Yan Chen, PhD candidate, who produced the electrolytes for this research. Big thanks to Dr. Xinyu Huang and Jay Nuetzler for testing these electrolytes at the University of South Carolina.

I would like to thank Dr. Tuhin Das for being on the thesis committee.

Last but not the least; I would like to thank the rest of my family and my friends who have supported me in this journey, especially Shruti Sanganeria, Jonathan Wehking, Rashmi Murthy, Vinu Paul and Niveditha Ratnam.

TABLE OF CONTENTS

CHAPTER 1: INTRODUCTION 1

1.1. Previous work 3

1.2. Background 5

CHAPTER 2: LITERATURE REVIEW 11

2.1 Solid Oxide Fuel Cell 11

2.1.1 Real Voltage output for a fuel cell 14

2.1.2 Efficiency and Power density 16

2.1.3 Advantages of SOFC 23

2.1.4 Applications of SOFC 25

2.2 Numerical Simulation 26

2.2.1 Numerical simulation of SOFC 28

2.2.2 Geometric design of the SOFC 29

2.2.3 Assumptions in SOFC modeling 30

2.2.4 Governing Equations 31

2.2.5 Boundary & Volume conditions 32

2.2.6 Post-processing 34

2.3. Basic Algorithm 36

CHAPTER 3: METHODOLOGY - SOFC SIMULATION USING COMSOL MULTIPHYSICS® VERSION 4.2A 39

3.1 About COMSOL Multiphysics® 39

3.2 Modeling Methodology 40

3.2.1 Secondary Current Distribution [11] 41
3.2.2 Transport of Concentrated Species [11] 45
3.2.3 Fluid Flow [11] 48
CHAPTER 4: RESULTS AND DISCUSSION 54
4.1 SOFC Geometry and material properties 54
4.2 Meshing 59
4.3 Modeling approach 61
4.4 Simulation Results 65
4.4.1 Results of 3-, 4-, 6-layered electrolyte SOFC 68
4.5. Model Validation 71
4.6. Parametric Study 73
CHAPTER 5: CONCLUSION 84
APPENDIX: COPYRIGHT PERMISSION LETTER 86
LIST OF REFERENCES 101

LIST OF FIGURES

Figure 1. The ideal electrolyte configurations of the SOFC. Each layer has a thickness of 30μm. 7

Figure 2. Actual SOFC electrolyte dimensions, after production. Units: μm. 8

Figure 3. The measured electrolyte conductivities for 3, 4, & 6 layered electrolytes for pure YSZ and SCSZ, shown as Arrhenius plot. 9

Figure 4. The measured electrolyte conductivities for 3, 4 & 6 layered electrolytes for composite layers of YSZ and SCSZ, shown as Arrhenius plot. The plot also includes 6-layered electrolytes of pure YSZ and SCSZ. 9

Figure 5. Planar (left) and tubular(right) designs of SOFC. 13

Figure 6. Cathode-supported (left), Anode-supported (middle) and Electrolyte-supported (right) design of SOFC. 14

Figure 7. Current density – Voltage or j-V curve for a fuel cell. 15

Figure 8. Power density curve for a fuel cell. 18

Figure 9. j-V curve demonstrating the efficiency of the fuel cell at constant flow rate and constant stoichiometry. 22

Figure 10. Screen shot of COMSOL desktop. 40

Figure 11. SOFC geometry. 55

Figure 12. SOFC geometry – side view, labeled. 56

Figure 13. Custom-flow: Oxygen mass fraction distribution in SOFC cathode and cathode flow channel. 57

Figure 14. Cross-flow: Oxygen mass fraction distribution in SOFC cathode and cathode flow channel 58

Figure 15. Algorithm of the modeling process 62

Figure 16. Measured SOFC electrolyte conductivities. 64

Figure 17. Comparison of the 'Layered' and 'Block' approach used to model the SOFC button cell. 65

Figure 18 Maximum power density versus number of electrolyte layers. 67

Figure 19 Maximum current density versus number of electrolyte layers. 67

Figure 20 Current-voltage plots of 3-Layered Electrolyte SOFC. Format: 3-Layered Block/Layered Electrolyte Material 68

Figure 21 Power-voltage plots of 3-Layered Electrolyte SOFC. Format: 3-Layered Block/Layered Electrolyte Material 69

Figure 22 Current-voltage plots of 4-Layered Electrolyte SOFC. Format: 4-Layered Block/Layered Electrolyte Material 69

Figure 23 Power density plots of 4-Layered Electrolyte SOFC. Format: 4-Layered Block/Layered Electrolyte Material 70

Figure 24 Current-voltage plots of 6-Layered Electrolyte SOFC. Format: 6-Layered Block/Layered Electrolyte Material 70

Figure 25 Power-current density plots of 6-Layered Electrolyte SOFC. Format: 6-Layered Block/Layered Electrolyte Material 71

Figure 26. Model validation – the simulation results are plotted against results from Sembler et al. [15] at 1123 K, 1023 K and 923 K. 73

Figure 27 Effect of anode partial pressure on current and power density. 76

Figure 28 Effect of anode partial pressure on current and power density. 76

Figure 29 Effect of cathode partial pressure on current and power density. 77

Figure 30 Effect of viscosity of gases at the cathode on current and power density. 77

Figure 31 Effect of anode exchange current density on current and power density. 78

Figure 32 Effect of cathode exchange current density on current and power density. 78

Figure 33 Effect of temperature on current and power density. 79

Figure 34 Effect of anode specific surface area on current and power density 79

Figure 35 Effect of cathode specific surface area on current and power density 80

Figure 36 Effect of permeability of anode electrode on current and power density..... 80

Figure 37 Effect of permeability of cathode electrode on current and power density..... 81

Figure 38 Effect of inlet boundary conditions of gases at electrodes, on current and power density. 81

Figure 39 Effect of equilibrium voltage at cathode on current and power density..... 82

Figure 40 Current and power density of SOFC at various values of anode (A) & cathode (C) exchange current density..... 82

LIST OF TABLES

Table 1. Table shows the SOFC electrolyte dimensions for different configurations, after production. 8

Table 2. The SOFC electrolyte conductivities measured at 800^{o}C at the Center for Fuel Cells, University of South Carolina. 10

Table 3. Summary of advantages of SOFC 24

Table 4. Dimensions of the button SOFC to be produced in the lab. 54

Table 5. Material properties of the electrodes and electrolyte 59

Table 6. Summary of meshing specifications. 60

Table 7. Measured electrolyte conductivities and average of YSZ & SCSZ conductivities. 63

Table 8. Summary of results – Power density. 66

Table 9. Summary of results – Current density. 66

Table 10 Summary of the parametric study on a SOFC 75

Table 1. Table shows the SOFC electrolyte dimensions for different configurations, after production. 8

Table 2. The SOFC electrolyte conductivities measured at 800^{o}C at the Center for Fuel Cells, University of South Carolina. 10

Table 3. Summary of advantages of SOFC 24

Table 4. Dimensions of the button SOFC to be produced in the lab. 54

Table 5. Material properties of the electrodes and electrolyte 59

Table 6. Summary of meshing specifications. 60

Table 7. Measured electrolyte conductivities and average of YSZ & SCSZ conductivities. 63

Table 8. Summary of results – Power density. 66

Table 9. Summary of results – Current density. 66

Table 10 Summary of the parametric study on a SOFC 75

CHAPTER 1: INTRODUCTION

Fuel Cells are devices that convert chemical energy of a fuel into electrical energy through electrochemical processes. The main difference between a battery and a fuel cell is that while a battery has a limited life, a fuel cell can continue to produce electricity as long as it is supplied with fuel. When compared with conventional combustion engines fuel cells are not limited by the Carnot cycle. Combustion engines convert chemical energy of the fuel into mechanical energy and heat is released in the process, then this mechanical and heat energy is converted into electrical energy. Instead fuel cells convert chemical energy of fuel directly into electrical energy and therefore have higher electrical efficiency. The first fuel cell was invented by the English scientist William Robert Grove in 1839 [3]. The conceptual Solid Oxide Fuel Cell was probably first demonstrated in 1937 by the Swiss scientists Emil Bauer and Hans Preis using zirconia ceramics as the electrolyte, Fe_3O_4 as the cathode, and C as the anode [4]. Currently, the most common Solid Oxide Fuel Cell uses yttria-stabilized zirconia as the electrolyte, which is an oxygen ion conductor.

High-temperature Solid Oxide Fuel Cells are receiving a lot of attention due to their superior energy conversion efficiency, fuel flexibility and minimal environmental impact. They are ideal for stationary, distributed power generation applications due to their durability, compactness, efficiency and ability to offer clean energy. The electrical efficiency of the Solid Oxide Fuel Cell is about 50-60%; in combined heat and power applications, efficiencies could reach 90% [1].
Although Solid Oxide Fuel Cells have a large number of advantages, there are a number of hurdles that are preventing their commercialization. The high operating temperature of these fuel

cells not only can be advantageous but also becomes the main cause of its negative impacts. The two main disadvantages are high energy costs and system reliability. Other obstacles are stack hardware, sealing and cell interconnect issues. The high temperatures also create difficulties in materials requirements, mechanical issues, and unmatched thermal expansion between system components.

For the past few decades there has been a lot of intense research conducted worldwide with the drive to overcome disadvantages and cause the commercialization of Solid Oxide Fuel Cells. Therefore the study of performance characteristics of these fuel cells is critical. There are numerous factors that contribute to the system performance like material composition, geometries, fuel stoichiometric factor, etc., which calls for a systematic study of the qualitative and quantitative effect of these parameters. Numerical simulation techniques will be used in this work and due to the complexity of the problem involved the situation calls for a sophisticated numerical simulation technique called Computational Fluid Dynamics. This technique has already been tested and proven to be reliable over years by its continued applications in many fields of science.

The main goal of this work is to build a working and reliable model of the Solid Oxide Fuel Cell at the cell level and study the effect of certain significant parameters on the efficiency and power density. The focus here is on planar button-shaped electrolyte-supported Solid Oxide Fuel Cells that use hydrogen as the fuel. In case of electrolyte-supported fuel cells, the conductivities, configuration and thickness of the electrolyte plays a very important role on the cell

performance. Yan Chen, a PhD candidate for Materials Science and Engineering at the University of Central Florida, under the supervision of faculty member Dr. Nina Orlovskaya, developed electrolytes of different thicknesses and configurations using Yttria-stabilized Zirconia (YSZ) and Scandia-doped Ceria Zirconia (SCSZ). Yan developed 3-layered, 4-layered and 6-layered electrolytes using pure YSZ or pure SCSZ or a combination of layers of YSZ and SCSZ. The thickness of each layer was in the range of 30 to 35 μm. The conductivities of these electrolytes were then tested by Dr. Xinyu Huang and Jay Nuetzler at the Center for Fuel Cells, University of South Carolina. A major part of this research will be to compare SOFC performance of the different configurations of these electrolytes. The cathode and anode material used are $(La_{0.6}Sr_{0.4})_{0.95\text{-}0.99}Co_{0.2}Fe_{0.8}O_3$ and Ni-YSZ respectively. A validation of the model against experimental results will be carried out. Our primary simulation tool is COMSOL Multiphysics® version 4.2a. In chapter 2 will include a review of the concepts of Solid Oxide Fuel Cells, followed by an introduction to numerical simulation, and then the modeling methodology adopted. Chapter 3 will include results and discussion, followed by conclusion and details of planned future work.

1.1. Previous work

There has been a lot of work done on numerical modeling of SOFC in the past decade. SOFC modeling can be done at the cell, stack or system level. The modeling of SOFC can be focused on the aspect of electrochemical reaction or fluid flow or heat transfer, or a comprehensive approach that takes into consideration all three aspects. There are also has been a lot of work

done on the control aspect of the fuel cell. The computational software or languages used for modeling include the C language as seen in the paper of Ferguson et al. [12], or FORTRAN as used in paper by Assadi et al. [13], or STAR-CD used by Ho et al. [14], or FLUENT by Sembler et al. [15] and Larrain et al. [18], or COMSOL Multiphysics by Akhtar et al. [16]. The software used in this research is COMSOL Mutiphysics. In terms of geometry the modeling research can be classified into planar, cylindrical (also called as micro-tubular) and flat-tube [22]. Research of modeling of planar SOFC can be seen in the work of Arpornwichanop et al. [17], Sembler et al. [15], Larrain et al. [18], Ho et al. [14]. Some of the micro-tubular SOFC research has been carried out by Ciano [19], Cheng and Cui [20] and Serincan et al. [21]. In the paper by Bae et al. [22], a study is done on performance of the various designs of flat-tube SOFCs and improvements are suggested. SOFCs can also be categorized as electrode-supported or electrolyte-supported. Under electrode-supported designs, there is not much work done on cathode-supported SOFCs. The paper by Arpornwichanop et al. [17] presents an overview of comparison between anode-supported, electrolyte-supported and cathode-supported fuel cells. The numerical method used is not mentioned and there is no model validation provided either. A study of cell performance shows that electrolyte-supported cells have higher ohmic resistance while anode-supported cells have higher activation losses. The effect of electrode and electrolyte thicknesses on cell performance shows that the performance increases when the anode and electrolyte thicknesses are lowered, but the performance is not significantly affected by cathode thickness. The paper also shows that the performance increases with temperature and operating pressure. Anode-supported SOFCs have gained a lot of interest in the past few years. Some of the advantages of anode-supported SOFC is given by Virkar et al. [23], stating that these SOFCs

are relatively easy to fabricate, are mechanically sturdy and have relatively high power densities. Other research on anode-supported SOFCs include the work of Haanappel et al. [25], Ho et al. [14], Assadi et al., Li et al. [24], most these are planar-designs. Interestingly, there is some work done on bi-electrode supported cell as seen in the work by Xue et al. [28], but there are some challenges presented by this design that need to be addressed. Electrolyte-supported SOFCs are known mainly for having lower activation losses and in some cases ease of mounting. Pasaogullari and Wang [26] mention that for higher operating temperatures around 1000^{o}C, the electrolyte-supported SOFC are preferred as the electrolyte ionic conductivity increases with temperature. This would make electrolyte-supported SOFCs ideal for Combined Heat & Power applications where operating at higher temperatures can be very beneficial. The work done by Hill et al. [27], suggests that in the test carried out although anode-supported SOFCs had a higher Open Circuit Voltage (OCV) and power density they were less stable and suffered significant structural damage from carbon formation over a 24h galvanostatic test. For all these purposes and also given that the testing facility available is favorable for electrolyte-supported, a planar button-shaped electrolyte-supported SOFC is chosen for this research.

1.2. Background

In the past decade, the commercialization of fuel cells has increased significantly. The fuel cell industry is striving to produce fuel cells with higher power density, efficiency, durability and cost-effectiveness. Researchers have been experimenting with the materials, operating conditions, manufacturing methods, chemical processes to achieve higher performance. The

SOFC research group at University of Central Florida in the Mechanical, Materials & Aerospace Engineering department has focused on use of better materials to improve the performance of SOFC. Yan Chen, a Doctoral candidate, under the guidance of Assistant Professor, Dr. Nina Orlovskaya, has done significant work on the electrolyte materials used in electrolyte-supported SOFC. Two materials showed superior properties favorable to SOFC applications – 8 mol% Y_2O_3 stabilized ZrO_2 [YSZ] and Scandia-doped Ceria Zirconia $Sc_{0.17}Ce_{0.08}ZrO_2$ [SCSZ]. SCSZ has higher ionic conductivity compared to YSZ and hence is more favorable to be used, but YSZ is chemically very stable and does not undergo phase transition like SCSZ at the operating conditions of SOFC. An electrolyte that contains both YSZ and SCSZ will have high ionic conductivity as well as stability. Therefore, a type of SOFC electrolyte was developed that would have layers of SCSZ sandwiched between a layer of YSZ. The YSZ layers will protect the SCSZ layers in the chemically harsh conditions and SCSZ layers will provide high conductivity. Each layer was designed to be 30 μm in thickness. Yan developed 3-layered, 4-layered and 6-layered electrolytes using layers of pure YSZ or pure SCSZ or a combination of layers of YSZ and

SCSZ. The figure 1 below shows the ideal case of the SOFC electrolytes to be produced.

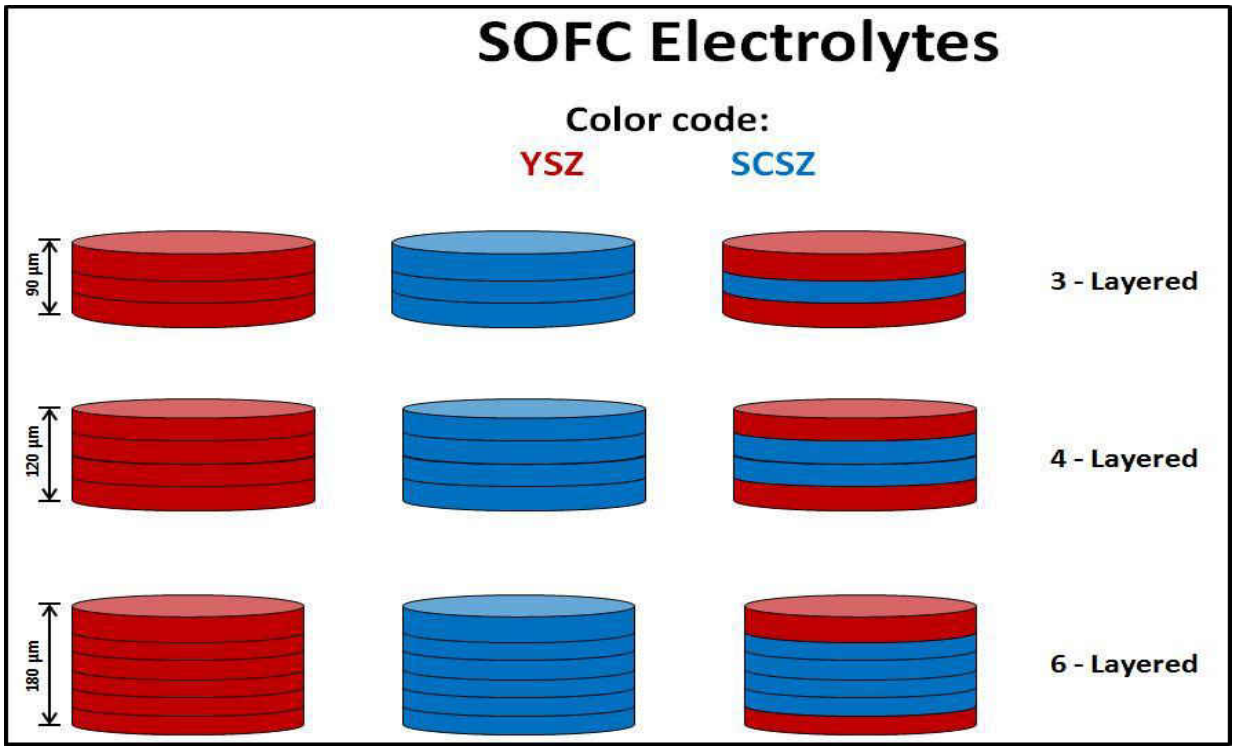

Figure 1. The ideal electrolyte configurations of the SOFC. Each layer has a thickness of 30µm.

The actual SOFC electrolytes that are developed are shown in the figure 2 below. As it can be seen the electrolyte thickness varies by the end of the production process. Table 1 summarizes the dimensions of the various configurations of electrolytes after production.

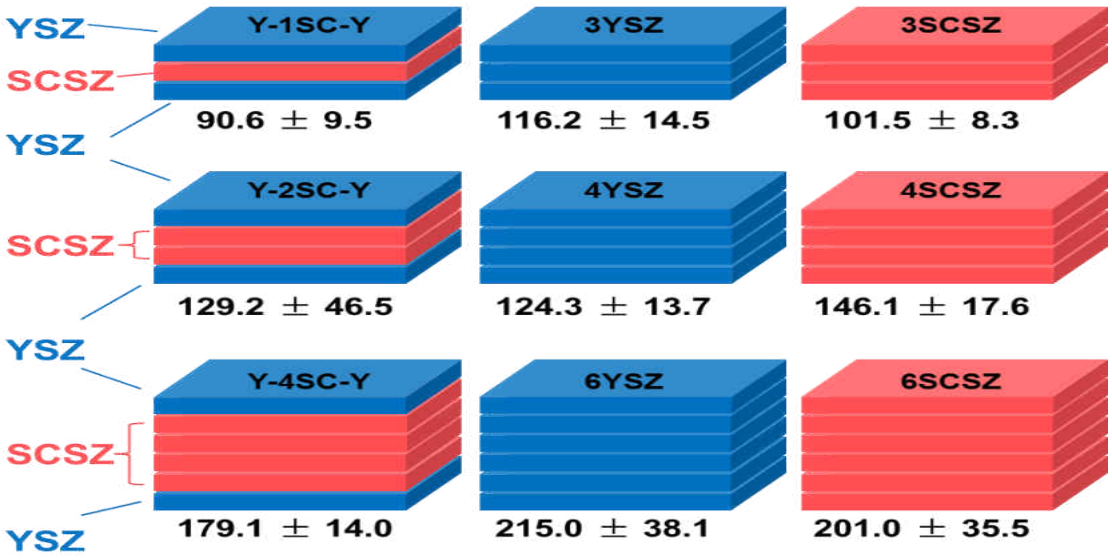

Figure 2. Actual SOFC electrolyte dimensions, after production. Units: µm.

Table 1. Table shows the SOFC electrolyte dimensions for different configurations, after production.

Design	Thickness [µm]			Average thickness per layer [µm]
	3-layers	4-layers	6-layers	
YSZ	116.2 ± 14.5	123.9 ± 13.7	215.0 ± 38.1	35.01
SCSZ	101.5 ± 8.3	146.1 ± 17.6	201.0 ± 35.5	34.51
YSZ-SCSZ-YSZ	90.6 ± 9.5	129.2 ± 46.5	179.11 ± 14.0	30.69

The electrolyte conductivities were tested by Dr. Xinyu Huang and Jay Nuetzler at the Center for Fuel Cells, University of South Carolina. The electrolytes were tested for different temperatures. The two graphs, graph 1 and graph 2 show the measured electrolyte conductivities.

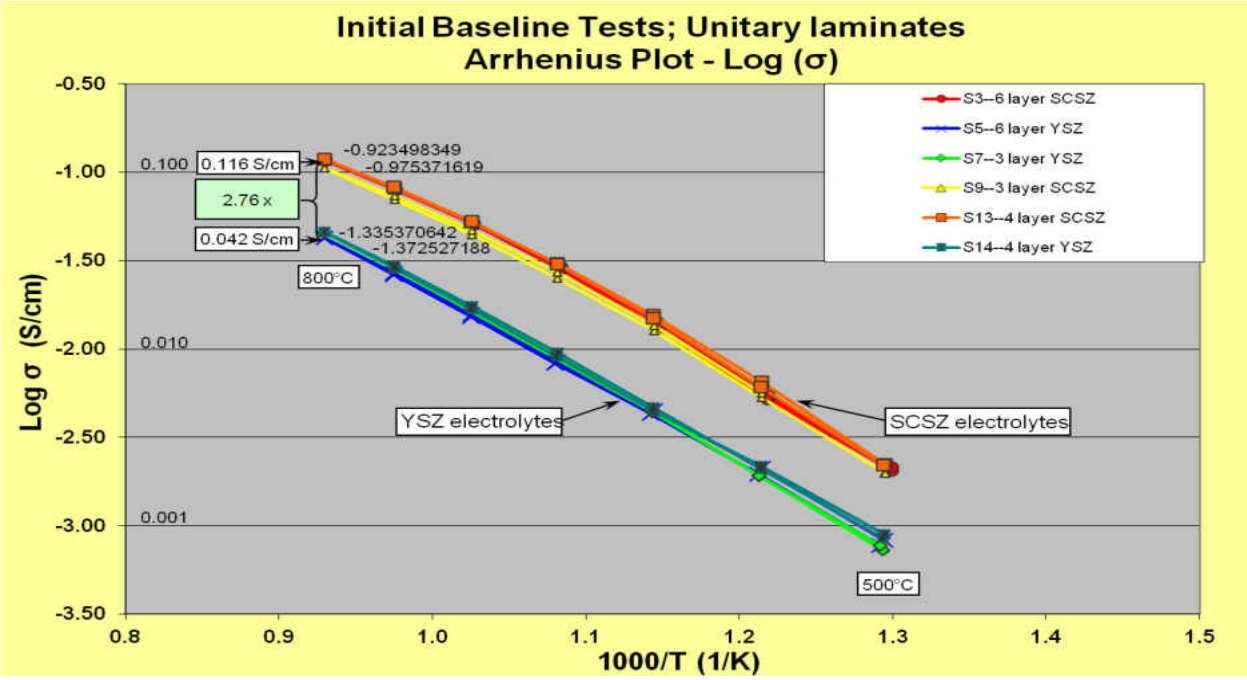

Figure 3. The measured electrolyte conductivities for 3, 4, & 6 layered electrolytes for pure YSZ and SCSZ, shown as Arrhenius plot.

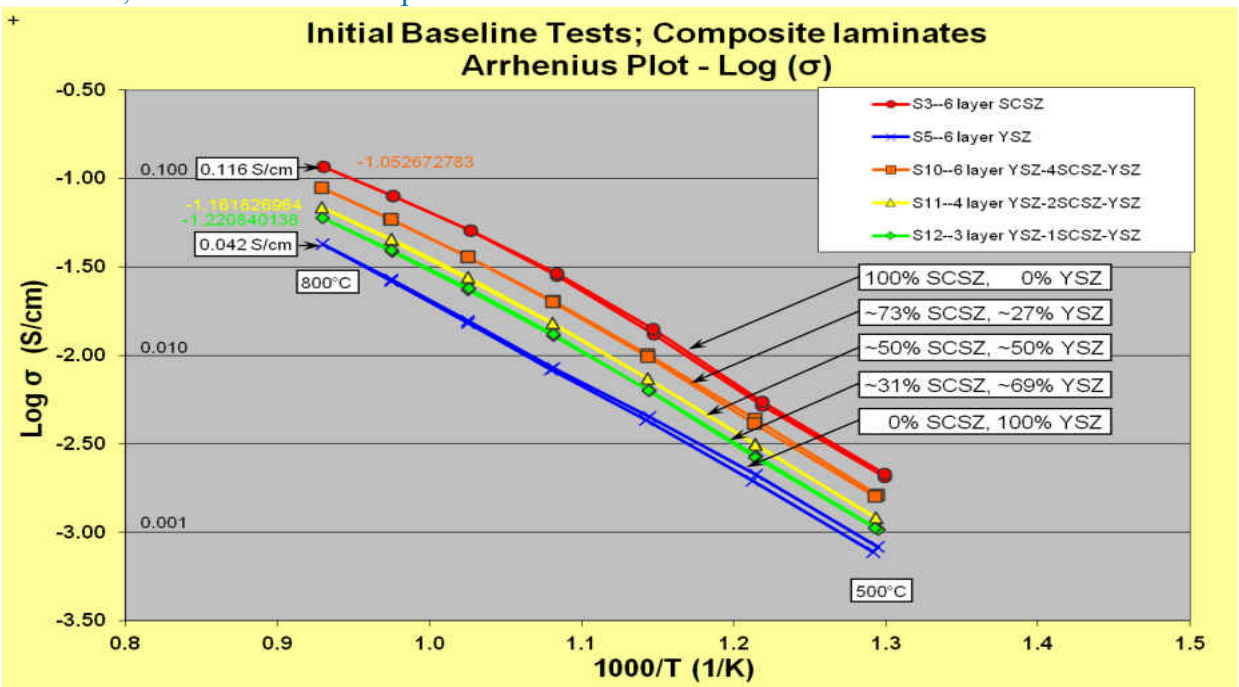

Figure 4. The measured electrolyte conductivities for 3, 4 & 6 layered electrolytes for composite layers of YSZ and SCSZ, shown as Arrhenius plot. The plot also includes 6-layered electrolytes of pure YSZ and SCSZ.

The initial simulations were carried out for the 800°C temperature specification. The results from these tests for 800°C are displayed in the table 2 below.

SOFC Electrolyte Conductivities at 800°C [S/m]			
	YSZ	**SCSZ**	**YSZ-SCSZ-YSZ**
3-layered (Block)	4.54	10.59	6.01
4-layered (Block)	4.62	11.93	6.89
6-layered (Block)	4.24	11.62	8.86

Table 2. The SOFC electrolyte conductivities measured at 800°C at the Center for Fuel Cells, University of South Carolina.

CHAPTER 2: LITERATURE REVIEW

2.1 Solid Oxide Fuel Cell

A fuel cell consists of four main functional components: anode, electrolyte, cathode, and interconnect. As mentioned before a Solid Oxide Fuel Cell (SOFC) use a solid ceramic electrolyte. The chemical reactions of a simple Solid Oxide Fuel Cell is stated.

Anode: $$H_2 + O^{2-} \rightarrow H_2O + 2e^-$$

Cathode: $$\frac{1}{2}O_2 + 2e^- \rightarrow O^{2-}$$

Anode is the electrode where oxidation process takes place and cathode is the electrode where reduction process takes place. Figure 1 shows the working of a simple tubular SOFC. In a SOFC hydrogen gas (fuel) is supplied at the anode and oxygen gas or air (oxidant) is supplied at the cathode. Oxygen undergoes reduction (process of electrons are consumed), the oxygen ions (O^{2-}) are transported through the electrolyte. At the anode the hydrogen atoms undergo oxidation (process of liberation of electrons), they combine with the oxygen ions to form water and releases two electrons in the process. The liberated electrons travel through an external circuit via current collectors, hence producing electricity, and reach the cathode where they combine with oxygen atoms to create more oxygen ions. Therefore, the function of the electrolyte is to facilitate the conduction of oxygen ions, prevent electronic conductance, prevent passing over of gases from one side to the other. The most popular SOFC electrolyte is yttria-stabilized zirconia (YSZ). The anode and cathode materials in a SOFC are different. The fuel electrode should possess the ability to withstand the highly reducing high-temperature environment at the anode, and the air electrode must possess the ability to withstand the highly oxidizing high-temperature

environment of the cathode. The most common material for the anode electrode in a SOFC is nickel-YSZ cermet (a cermet is a mixture of ceramic and metal) [1]. Conductivity and catalytic activity is the purpose of nickel, while YSZ adds ionic conductivity, thermal expansion compatibility, and mechanical stability and helps maintain high porosity and surface area of the anode structure. Mixed ion-conducting and electronically conducting (MIEC) ceramic materials are usually used for the cathode electrode. Some examples are strontium-doped lanthanum manganite (LSM), lanthanum-strontium ferrite (LSF), lanthanum-strontium cobaltite (LSC), and lanthanum strontium cobaltite ferrite (LSCF). High catalytic activity and good oxidation resistance are the reasons these materials are chosen for the cathode electrode. By varying the compositions of the materials at the cathode, anode and electrolyte different levels of properties like ionic conductivity, catalytic activity, and thermal expansion compatibility can be achieved.

The overall driving force for a SOFC is the chemical or concentration gradient of oxygen between the cathode where the partial pressure of oxygen is high to the anode where the partial pressure of the oxygen is low. The thermodynamic voltage output of a single SOFC based on the electrochemical half reactions is around 1.23 V at standard temperature and pressure conditions. As it can be noticed this voltage is low and inadequate for practical use. To produce voltage and power that is high enough to suffice energy requirements the individual cells can be connected in series and/or parallel with the aid of interconnectors and/or cell-to-cell connectors. The cell-to-cell connectors need to be ionic insulator and pure electronic conductors. This method is called stacking of cells and it is the way SOFC are designed for practical power generation. The complete fuel cell system consists of a number of stacks of individual fuel cells.

There are different designs of SOFC. Modern SOFC generally is made of a thin electrolyte film and a supporting substrate. The substrate is a porous or channeled dense body for gas transport, ad is made of anode and cathode electrodes, interconnect (metal or ceramic), or inactive insulator. The substrate can be classified geometrically as tubular (cylindrical or flattened and ribbed) as seen in figure 5. The tubular geometry design with one closed end feature allows for a seal-less design. Planar designs deal more sealing problems compared to tubular designs. In the tubular SOFC design, it is common to fabricate the thin fuel cell components directly onto the outside of a thickened porous support tube. The surface area available on the outside of each tube is often subdivided into a row of cells that are connected in series, a design referred to as segmented-in-series [5]. Additionally, the SOFC could be designed as anode-supported, cathode-supported, or electrolyte supported as seen in figure 6.

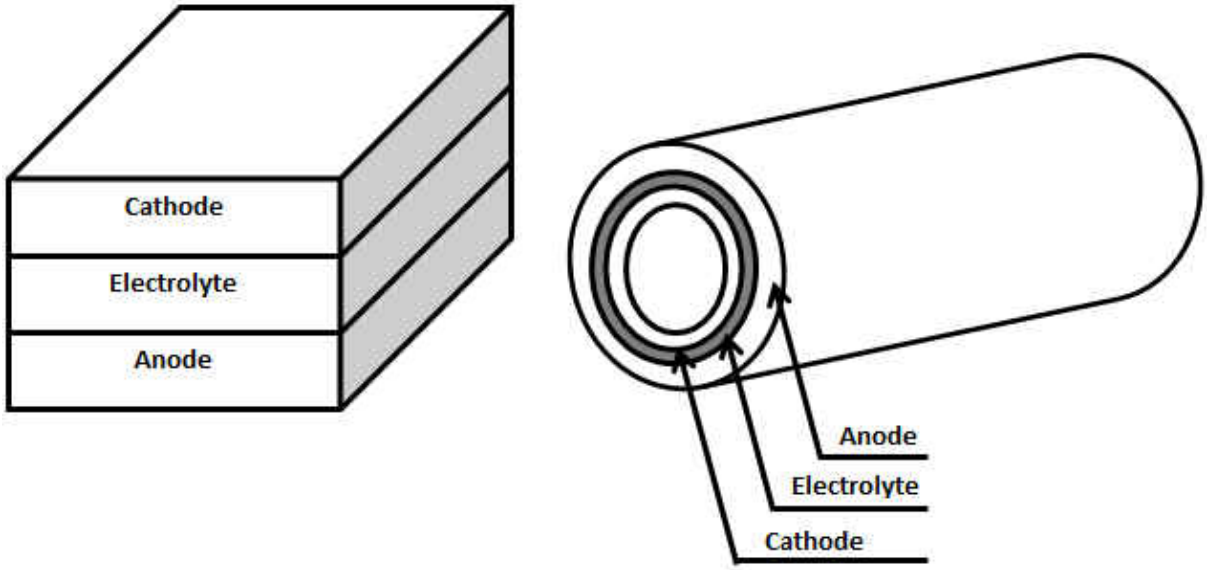

Figure 5. Planar (left) and tubular(right) designs of SOFC.

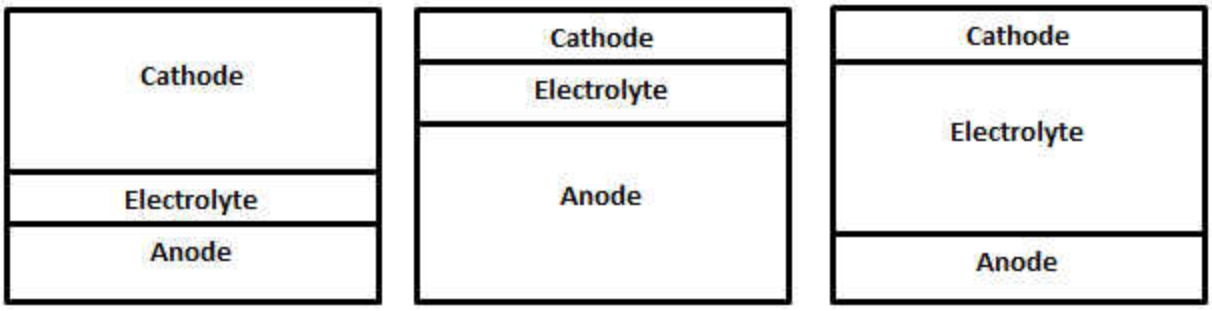

Figure 6. Cathode-supported (left), Anode-supported (middle) and Electrolyte-supported (right) design of SOFC.

2.1.1 Real Voltage output for a fuel cell

The thermodynamic reversible voltage is the open circuit voltage of the fuel cell without any losses. The real voltage output of a fuel cell is always less than the thermodynamically reversible voltage. For any fuel cell, the voltage output depends on the current that is being drawn from the fuel cell. Ideally the voltage of the fuel cell is supposed to stay constant, no matter what the amount of current is that is being drawn. Many losses come into play when a fuel cell is operated in reality, and hence the voltage keeps reducing as the current load keeps increasing. All of the above can be explained in a single graph called the j-V curve. Figure 9 shows an example of a j-V curve.

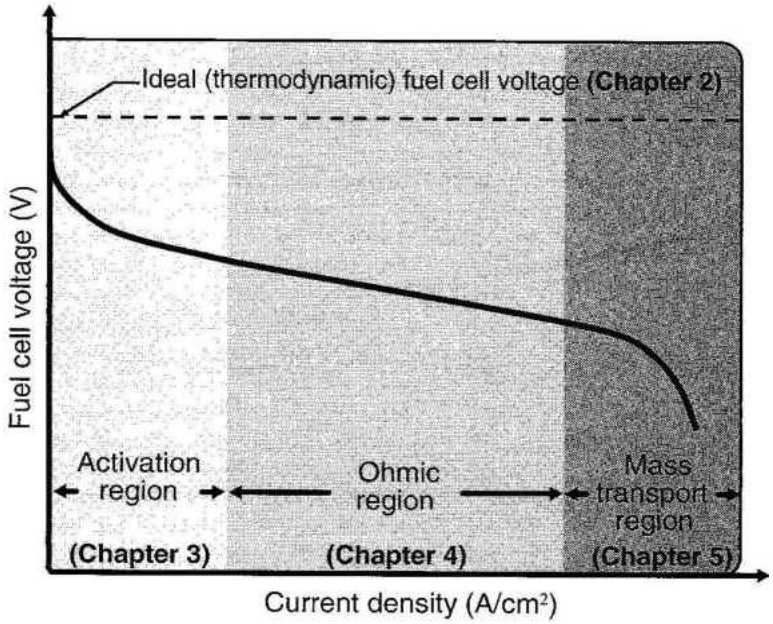

Source: Ryan O'Hayre, Suk-Won Cha, Whitney Colella, and Fritz B. Prinz, Fuel Cell Fundamentals, Wiley; 2nd edition, 2009. [1]

Figure 7. Current density – Voltage or j-V curve for a fuel cell.

The x-axis of the j-V curve has the current density, j [A/cm^2], and the y-axis has the fuel cell voltage, V [V]. Current density is the current per unit area, given by j = i / area. The graph could also be drawn as i-V curve, but normalizing the current will give an idea of the fuel cell size for a particular application. As it can be seen, the dashed line represents the thermodynamically reversible voltage which remains constant, independent of the current, i.e. without any losses. The dark line represents the relationship between real voltage of the fuel cell and the current. The relationship is not exactly linear. To understand this, it is important to understand the different losses that are encountered in a real fuel cell. The bottom of the graph is marked by three regions, these regions represent the source of the loss for that particular range of current. The equation for real voltage of a fuel cell:

$$V = E_{\text{thermodynamic}} - \eta_{\text{activation}} - \eta_{\text{ohmic}} - \eta_{\text{concentration}}$$

where, V is the real voltage output of the fuel cell, $E_{thermodynamic}$ is the thermodynamically reversible voltage output, $\eta_{activation}$ is the activation losses caused by reaction kinetics, η_{ohmic} is the ohmic losses due to resistance in the fuel cell components to the flow f electrons and ions, $\eta_{concentration}$ is the concentration losses due to the issues in transport of species throughout the fuel cell.

2.1.2 Efficiency and Power density

Power density for a fuel cell is defined as the amount of power supplied by the fuel cell per unit volume or per unit mass of the fuel cell.

$$P = iV$$

where i is the current drawn in amperes, and V is the voltage of the fuel cell is volts.

Power density can be categorized into two types – volumetric and gravimetric. Volumetric power density is the power that is supplied by the fuel cell per unit volume. Similarly, gravimetric power density is the power that is supplied by the fuel cell per unit mass. The unit for volumetric power density is usually [kW/m^3 or W/cm^3] and for gravimetric fuel power density is usually [kW/kg or W/g]. Power density is probably the most important of the fuel cell, since the whole purpose of the fuel cell is to produce power. Volumetric and gravimetric power densities can give us an idea of the total size or weight of the fuel cell that will meet the power requirements for a particular application. Therefore, power density is a major performance parameter that can be used to compare different fuel cells or fuel cells with combustion engines or batteries or other energy sources. It could also guide our assessment of the type of fuel cell to be used for different

applications. For example, the energy source for a mobile phone would definitely require a fuel cell that is light, occupies less volume and operates at or close to room temperature. This makes the polymer electrolyte fuel cell the best match. On the other hand, for power generation for a block of factories or houses, the size and weight of the fuel cell is not significant and hence SOFC is the ideal candidate for it high power density.

Power density varies with the current drawn. The power density usually increases as the amount of current drawn is increased, up to a certain point, after which the power density decreases with increase of current being drawn. This can easily be seen on a i-V or j-V curve as in figure 8.

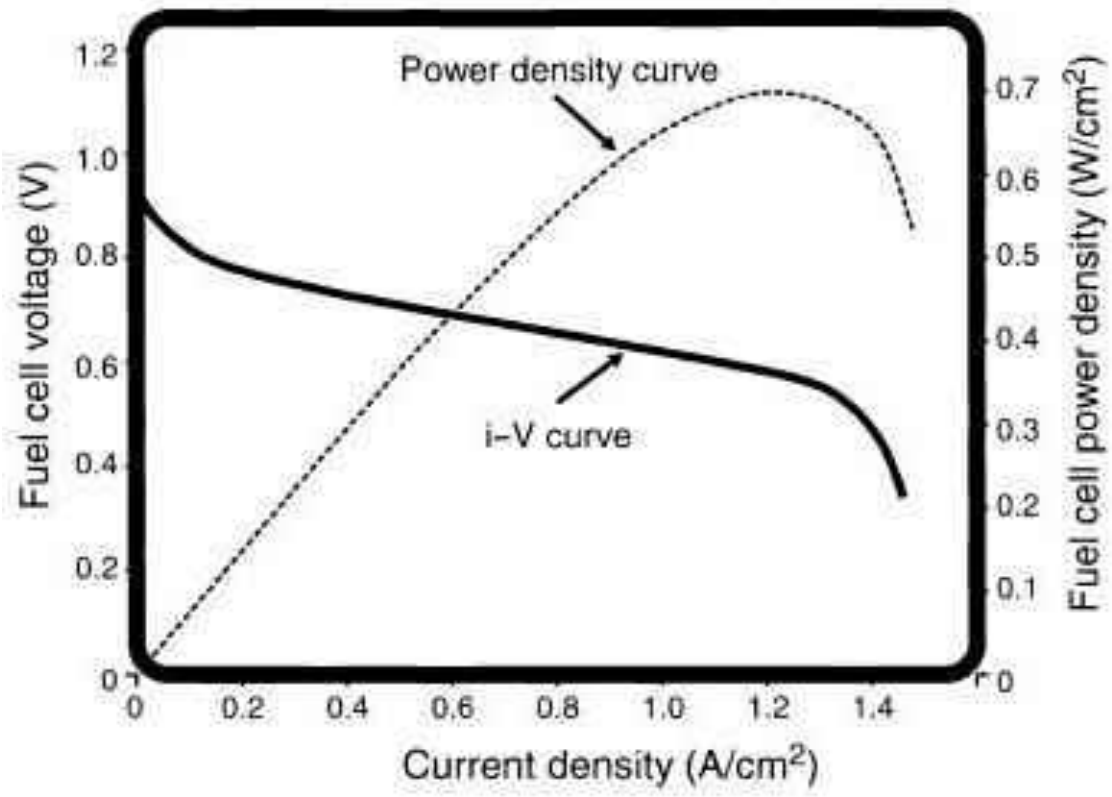

Source: Ryan O'Hayre, Suk-Won Cha, Whitney Colella, and Fritz B. Prinz, Fuel Cell Fundamentals, Wiley; 2nd edition, 2009.
Figure 8. Power density curve for a fuel cell.

Efficiency is a very important performance parameter for any energy conversion device. There are two kinds of efficiencies – ideal efficiency and real efficiency. Thermodynamically speaking, for a chemical reaction the electrical work available from a fuel cell is limited by the Gibbs free energy ΔG, and so the ideal efficiency is also limited by ΔG. This efficiency is the ideal efficiency and since it is limited, it is always less than 100%. The efficiency of any energy conversion device is given as the total useful work available during the process divided by the total energy evolved by that process. For a chemical reaction, the total energy available is given by the enthalpy change of the reaction.

$$\varepsilon = (\text{useful work} / \Delta \hat{h})$$

As mentioned before, the maximum amount of useful energy that can be extracted from a fuel cell is given by the Gibb's free energy. Hence, the thermodynamically reversible efficiency of a fuel cell is,

$$\varepsilon_{\text{thermodynamic}} = \Delta \hat{g}^0 / \Delta \hat{h}^0_{\text{HHV}} = 0.83 \text{ at STP}$$

where STP stands for standard temperature and pressure conditions, The thermodynamic efficiency, $\eta_{\text{thermodynamic}}$, is 83% because for a fuel cell that utilizes hydrogen as the fuel and oxygen as the oxidant the Gibb's free energy at STP is, $\Delta \hat{g}^0 = -237.3$ kJ/mol and the change in enthalpy of the reaction is, $\Delta \hat{h}^0_{\text{HHV}} = -286$ kJ/mol, where HHV stands for higher heating value of the product which is water in this case. Reversible efficiency can be calculated by dividing -237.3 kJ/mol by 286 kJ/mol, equal to 83%.

Now let us look the real efficiency of a fuel cell. The fuel cell is not a perfect device, meaning the real efficiency of the fuel cell should always be less that the ideal efficiency. In reality, the fuel cell during its operation has different types of losses. Of the myriads of losses in a typical fuel cell, two losses contribute the most – fuel utilization losses and voltage losses. Real efficiency of the fuel cell is terms of the thermodynamic efficiency, voltage efficiency and fuel utilization efficiency, given by:

$$\varepsilon_{\text{real}} = (\varepsilon_{\text{thermodynamic}}) * (\varepsilon_{\text{voltage}}) * (\varepsilon_{\text{fuel}})$$

One of the major obstacles in achieving maximum work and efficiency in the fuel cell is the reaction kinetics losses. The voltage efficiency of the fuel cell $\varepsilon_{\text{voltage}}$ accounts for these losses due to irreversible kinetic effects.. The voltage efficiency can defined in terms of the voltage (V)

that can be obtained from the fuel cell under operation at a particular current load and the open circuit voltage (E). Ohm's law states that voltage is directly proportional to the current.

$$V \alpha I$$

For a fuel cell the voltage (V) at any time of the fuel cell under operation is directly related to the current (i) that is being drawn from the fuel cell at that time. With a increase in the current being drawn from the fuel cell the voltage across its end drop, and hence the efficiency also drops.

$$\varepsilon_{voltage} = V / E$$

Now, let us look at the next term in the real voltage equation - fuel utilization efficiency.

$$\varepsilon_{fuel} = (i / nF) / (v_{fuel})$$

where, i (amperes) is the current being drawn, n is the number of moles of electrons that are transferred during the reaction. For a hydrogen-oxygen fuel cell reaction n = 2. F in the equation is Faraday's constant (F = 96,400 C/mol) and v_{fuel} is the fuel supply rate (mol/s).

In an ideal fuel cell the amount of fuel supplied will be fully utilized to generate electricity. But in reality, not all of the fuel supplied is used up in the intended reactions. Some of the fuel may undergo some side reactions. If hydrogen is the fuel being supplied, it may react with the impurities present in the anode or catalyst layers. Also, if the rate of fuel supplied is high compared to the fuel required for that particular current load, then some of the fuel will just flow through with undergoing any reactions. The amount of fuel supplied must always be higher than what is required, to avoid fuel cell starvation and all the problems following that. In the situation where the amount of fuel supplied is constant can be called constant stoichiometry condition. Under this condition, the constant fuel supply rate is set a little for than the fuel required at

maximum current load. Alternatively, the fuel cell can be supplied with fuel such that the supply rate of the fuel at any instance is a little higher than the amount of fuel required for the current load at that instance. This is called the fuel stoichiometry condition. It is obvious that the latter method leads to less wastage of the fuel. SOFC already have higher operating costs and if we are using hydrogen as the fuel for stationary power generation, then the operating costs will go even higher. So designing a feedback control to accomplish fuel stoichiometry condition is very important. The fuel stoichiometric factor is said to be 1.6 if the amount of fuel supplied is 1.6 times the amount of fuel required for the current load at that instant. Fuel stoichiometric factor is given by,

$$\lambda = v_{fuel} / (i / nF)$$

hence,

$$\varepsilon_{fuel} = 1 / \lambda$$

Going back to the real efficiency of the fuel cell, it can re-written as,

$$\varepsilon_{real} = (\Delta \hat{g} / \Delta \hat{h}) * (V/E) * ((i / nF) / v_{fuel})$$

or,

$$\varepsilon_{real} = (\Delta \hat{g} / \Delta \hat{h}) * (V/E) * (1 / \lambda)$$

Fuel stoichiometric factor is a very important factor. This can be clearly seen in figure 7. It shows a j-V curve for a fuel cell. On the x-axis is the current density, j [A/cm^2], and on the y-axis is the fuel cell voltage V in volts. The y-axis on the right is the efficiency axis. The dark dashed line shows the j-V curve for a constant fuel flow rate. The dark line represents the j-V curve for constant stoichiometric fuel flow condition. The graph below shows how the efficiency for the constant fuel flow rate and the constant fuel stoichiometry condition end up at the same point on

the efficiency axis, which means that the efficiency is the same for the two conditions at maximum current density. But it is quite obvious that the constant fuel stoichiometry condition results in much higher fuel cell efficiency when compared with the constant fuel flow rate condition.

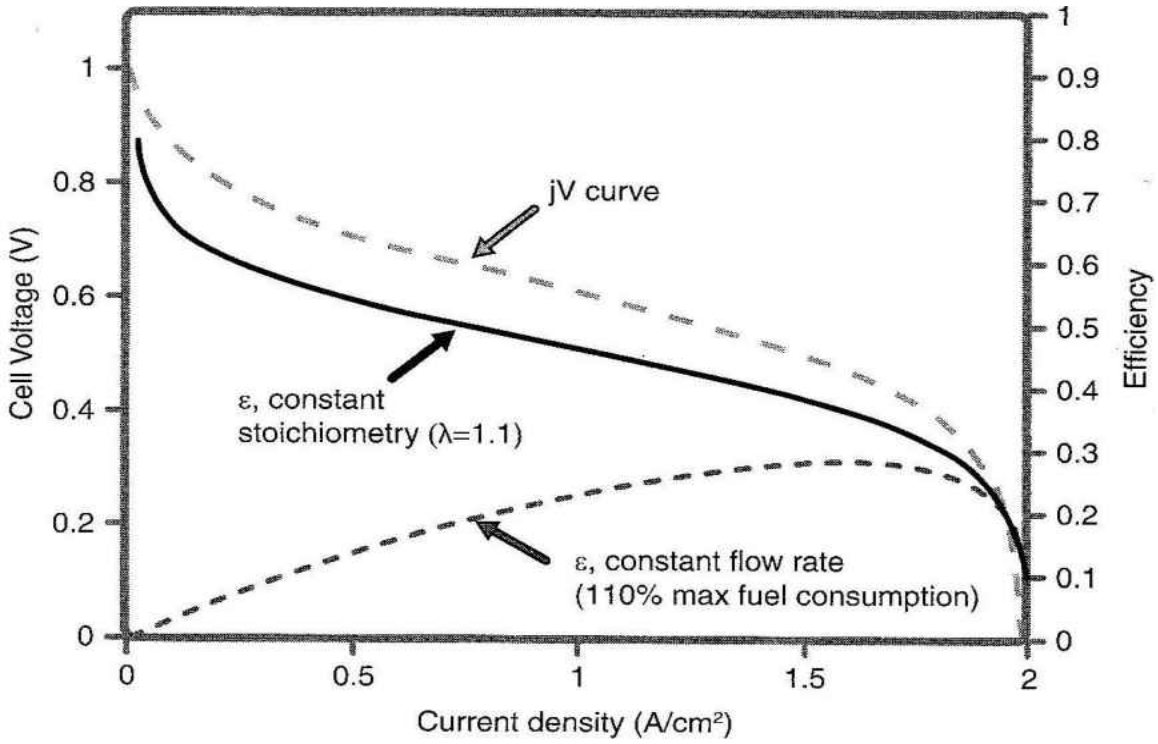

Source: Ryan O'Hayre, Suk-Won Cha, Whitney Colella, and Fritz B. Prinz, Fuel Cell Fundamentals, Wiley; 2nd edition, 2009. [1]
Figure 9. j-V curve demonstrating the efficiency of the fuel cell at constant flow rate and constant stoichiometry.

Therefore one of the main goals of our research is to study the relationship between fuel stoichiometric factor, λ, and the real efficiency, η_{real}, and the power density of the fuel cell and to find the optimum value for the constant fuel stoichiometric factor to achieve maximum power density and efficiency.

2.1.3 Advantages of SOFC

Solid Oxide Fuel Cells have numerous advantages. They are one of the most studied and researched fuel cells currently. There is a real drive to their commercialization. Here are some the advantages of SOFCs:

- Flexibility in the type of fuel used.
- High electrical efficiency compared to other types of fuel cells in the range of 50-60% [1].
- Wide power generated range, 10 – 100,000 kW [1]
- Could be sued in stationary and portable power generation.
- Lower CO2 emissions per unit electricity produced (if the fuel used is a hydrocarbon) when compared with combustion engines [3].
- Less prone to CO poisoning and therefore suitable for coal-based fuel.
- Higher electrical efficiency when compared with conventional heat engines, since they are not limited by Carnot cycle.
- Nickel could be used as catalyst instead of platinum, which is very cost effective.
- Negligible greenhouse gases emission if hydrogen is the fuel used.
- High quality waste heat, which makes co-production of heat and power (CHP) possible.
- No moving parts, therefore less vibrations and noise.

Table 3. Summary of advantages of SOFC

Solid Oxide Fuel Cells – Attributes	
High electric-conversion efficiency	• Demonstrated – 47%
	• Achievable – 55%
	• Hybrid – 65%
	• Combined Heat & Power – 80%
Superior environmental performance	• No NO_x
	• Lower CO_2 emissions
	• Sequestration capable
	• Quiet; no vibrations
Cogeneration – Combined Heat & Power	• High-quality exhaust heat for heating, cooling, hybrid power generation, and industrial use
	• Co-production of hydrogen with electricity
	• Compatible with steam turbine, gas turbine, renewable technologies, and other heat engines for increased efficiency
Fuel Flexibility	• Low- or high- purity H_2

Solid Oxide Fuel Cells - Attributes	
	• Liquefied natural gas
	• Pipeline natural gas
	• Diesel, coal gas, fuel oil, gasoline
	• Biogases
Size and siting flexibility	• Modularity permits wide range of system sizes
	• Rapid siting for distributed power
Transportation and stationary applications	• Watts to megawatts

Source: Mark C. Williams, Joseph P. Strakey and Wayne A. Surdoval, U.S. Department of Energy's Solid Oxide Fuel Cells: Technical Advances, Int. J. Appl. Ceram. Technol., 2 (4) 295–300 (2005). [7]

2.1.4 Applications of SOFC

The primary use of Solid Oxide Fuel Cells is for stationary power generation applications. But, there has been a lot of research conducted regarding the portable applications of SOFC including electric cars. In their paper, Wolfgang Winkler and Hagen Lorenz say that the integration of a solid oxide fuel cell (SOFC)–GT (gas turbine) power system in an all electric car concept seems to be possible [8]. The stationary applications of SOFC can also be quiet wide in range. John B. Goodenough and Kevin Huang, in their book [3], have categorized the stationary applications of SOFC into four markets:

- Residential: Targeted for powering a home with a power rating range of 1 – 10 kWe. Fuel used could be coal gas or pipeline natural gas.

- Industrial: Targeted for a small industrial unit. Power rating range of 100 – 1000 kWe. Fuel used could be pipeline natural gas.
- Dispersed: Targeted for a large industrial unit. Power rating range of 2 – 10 MWe. Fuel used could be coal-derived or natural gas.
- Central: Power rating range of 100MWe. Fuel used could be coal-derived or pipeline natural gas.

Commercialization of SOFC is the ultimate dream and motivation of researches. The company – Bloom Energy® - founded in 2001 by Dr. KR Sridhar, has definitely demonstrated the commercial uses of SOFC. Their patented SOFC technology has been used to create a type of distributed power generator called Energy Server™ that uses renewable and fossil fuels to generate power in the range of 100 kW [9]. Their customers include big corporations like Google, The Coca-Cola Company, Walmart, California Institute of Technology, and many more.

With all these applications, commercialization, funding and upcoming research, the future of SOFC looks promising.

2.2 Numerical Simulation

Numerical simulation is a theoretical method of research that uses mathematical discretization and computational resources. By using theoretical knowledge of the equations and relations and some experimental data and software packages or programming languages to determine the

performance characteristics of the SOFC. Typically for SOFC it is required to solve partial differential equations (PDEs). Also, the number of variable and parameters is very large. Since these equations are quiet complex, the situation calls for a sophisticated modeling tool. Computational fluid dynamics (CFD) is a perfect candidate. CFD has been used over decades in various fields of research and has proven its reliability and worth. CFD combines mathematics, computing and physics to create a superb tool that can be used foe numerical simulation. Once a model developed in CFD can be validated, it becomes an invaluable tool. There are certain parameters that are either difficult or impossible to measure through experimentation. CFD gives the advantage of providing localized information. For example, the concentration distribution of oxygen ions in the electrolyte can be solved for. CFD packages are usually a complete package that has the ability to model a SOFC from start to finish. Commercial CFD packages include Fluent®, STAR-CD®, CFD-ACE® and COMSOL Multiphysics®. For this research COMSOL Multiphysics® will be used.

COMSOL Multiphysics® has a 'Batteries and Fuel cells' module that allows incorporating/entering of custom PDEs to modify the model based on the problem. It can integrate closely with MATLAB® and Simulink® from MathWorks®. It has the LiveLink™ feature for MATLAB®, Pro/Engineer®, SolidWorks® which allows the import and the modification of the parent file modeled using any of the above software. The testimony of Galip Guvelioglu, PhD student, Lehigh University: "COMSOL Multiphysics® gave me the opportunity to focus on the fuel-cell problem instead of devoting time to learning a specific tool."

2.2.1 Numerical simulation of SOFC

A Solid Oxide Fuel Cell can be modeled at the cell/stack/system level. Here, we will focus on fuel cell modeling at the cell level. Also we could model the SOFC in 1D, 2D or 3D. We could start with 1D or 2D modeling, but 3D modeling gives us the complete picture. There are many approaches to model the SOFC. We will discuss the following steps in modeling:

- Geometric design of the fuel cell: Creating a computerized geometric model of the fuel cell that represents the physical dimensions of the real fuel.
- Assumptions: Make logical and reasonable assumptions to simplify the SOFC model, and save computational time and resources.
- Governing Equations: A defined set of governing equations that define the relationships between the various relevant parameters and characteristics of the SOFC.
- Boundary and Volume conditions: Define the different conditions at the boundary and within the SOFC.
- Post-processing: Interpretation, analysis and validation of the results obtained against experimental data.
- Model reduction: An optional additional time and resources saving step includes deducing the fundamental nature of different equations and parameters, in order to reduce the model complexity, with an accepted level of reduction in the accuracy of the results. For example, converting a certain relation or equation of an exponential nature to a exponential equation.

2.2.2 Geometric design of the SOFC

The first step is to build a geometric model of the SOFC. Most of the CFD software available gives the user to build a geometry in the same software. COMSOL Multiphysics® has this option available. If the geometry is complex and highly detailed, it is recommended to use software packages specifically designed for these purposes, such as Pro/Engineer®, SolidWorks®. Building the computerized fuel cell geometry is a critical step in SOFC modeling where we need to build a model that represents the real fuel cell as closely as possible in terms of physical dimensions. At the same time, neglecting certain details or approximations of certain aspects could help save time and resources, without affecting the validity of the results. Inside of building the SOFC geometry, different parts of the SOFC are divided into distinct domains. Each domain has its own set of assumptions, governing equations, and boundary and volume conditions. For example, the flow channel that transports the fuel to the anode is a domain created separately from the anode electrode domain. We want to minimize the size of the model, so it is possible for certain domains when we can approximate that certain properties are constant throughout, we can skip developing the whole domain and develop just the surface with the boundary conditions. Once, we have created and assembled all the domains to represent a real SOFC, the next step is to discretize each domain into several elements. This is achieved by 'grid generation' where the domain is filled with small elements of defined shapes. Numerical calculations are performed in each of these elements to get a discretized solution. By reducing the size of the elements we can get finer, more accurate results and by increasing the size of the elements the accuracy of the results go down and so does the computation time. There are software packages available specifically designed for grid generation, that could be used if

required. Grid refinement is an ‘art’ that comes with experience. For instance, flow channels could use coarse grids while the electrolyte definitely needs a fine grid. The 3D elements used to make these grids can be tetrahedral, pyramids, prisms, etc. When the grid is generated automatically by the computer, it is called unstructured grid. Here the user does not have much control over the placement and size of the grid elements. It is a time saving process, but it could be computationally very expensive. Another way of grid generation allows the user to select the shape and placement of the grid elements manually. This could be tedious process, but on the long run, it could be very economic computationally. Again, this comes with experience. For example, in the grid generation of the flow channels one could use coarse grid throughout, but near the interface of the flow channel and the anode electrode if we are interested in the combined convection and diffusion process of different species, it would be a good idea to use finer grid. To summarize geometric design of a SOFC model includes creating the model geometry to match the physical dimensions of the real SOFC, the components are separated into distinct domains and then the domains are discretized by grid generation.

2.2.3 Assumptions in SOFC modeling

Modeling a SOFC can be a very cumbersome and time consuming process due to the complexity of the SOFC design, the sophisticated set of governing equations and high number of parameters involved. Therefore, we should strive to simplify the model as much as possible. Making reasonable and logical assumptions comes with knowledge and experience. If we make valid assumptions we could save a lot of time and resources. Making assumptions that are not valid

and logical, on the other hand, could result in minor or severe inaccuracies. An example, is as mentioned in Prinz et al., water could be assumed to exist in a single phase – in the form of water vapor in the SOFC. This is a very valid assumption since the operating temperatures for SOFC is between 600^{o}C and 1000^{o}C. Another example is as mentioned is Singhal et al., the flow of species in the SOFC could be assumed to be laminar. This again is a valid assumption. Reynolds number defines the relationship between inertial and viscous forces, and is categorized as laminar if the two forces are comparable depending on the flow dimensions. In a SOFC we do not reach high species flow speeds and the viscous and inertial forces seem to have comparable order of magnitude. There will be numerous assumptions made as we go further ahead.

2.2.4 Governing Equations

Governing equations bring together all the relevant parameters and variables involved the SOFC processes, and define their relationship to each other. SOFC has different types of processes happening at the same time. We could broadly classify these governing equations into three models.

- Flow model, or fluid dynamics model: accounts for all the fluid flow physics.
- Thermal or heat transfer model: accounts for the energy transfer involved through exchange of heat between components.
- Electrochemical model: accounts for all the electrochemical processes happening between different species in a SOFC.

Typically our final goal is to generate the i-V or j-V curve for the SOFC. This gives us the opportunity to calculate efficiency, power density, activation overvoltage, etc. To start, we could either specify or assume the current or the voltage and finally calculate the other. Usually to achieve the required results we solve for all the three models of governing equations. The scope of this thesis is limited to solving the governing equations for fluid flow and electrochemistry. A detailed discussion on the governing equations used in the model will be discussed in the Modeling Methodology section 3.2.

2.2.5 Boundary & Volume conditions

Boundary and volume conditions are used to define the conditions at the interface between domains, condition within each domain and conditions of the external surrounding environment. Boundary and volume conditions are specified based on the values of different parameters that are known to us. They are combined with the governing equations and assumptions to determine the values of the unknowns.

Volume conditions:

Here are some of the volume conditions that need to be specified for a fuel cell as given by Prinz et al.

Porosity (ε): Porosity in the flow channels is 1, 0 for solid structures, typical values for electrode and catalyst layers is 0.3 to 0.6, and so on for other parts.

Permeability (k) [m^2]: typical permeability values is assigned to electrode and catalyst layers, almost 0 for solid structures and very large for flow channels.

Exchange current density (j_0) [A/m^3 or A/cm^3]: this value is calculated separately for anode and cathode electrodes due to difference in reaction kinetics.

Transfer coefficient (α): ideally to be 0.5 but will be different for anode and cathode due to difference reaction kinetics.

Electronic conductivity (σ_{elec}) [S/m or S/cm]: is set to 0 for flow channels and electrolyte, and assigned values for other domains based on experimental observations.

Ionic conductivity (σ_{ion}) [S/m or S/cm]: typically set to 0 for all domains except electrolyte and catalyst layers. Instead on using a constant value, we could use Arhenius equation that calculates σ_{ion} based on local temperature.

Tortuosity (τ): typical values in porous fuel cell media like electrodes vary from 1 to 4.

Thermal Conductivity (k) [W/m^2K]: assigned for all domains. In case of fluid mixtures in the flow channels, this property can be calculated from kinetic theory of gases.

Density (ρ) (kg/m^3): calculated from ideal gas equation for the gas-phase regions.

Viscosity (μ) [$N \cdot s/m^2$] *& Diffusivity (D)* [m^2/s]: like thermal conductivity, these two properties are usually calculated from the kinetic theory of gases.

Effective Diffusivity (D_{eff}): in most CFD codes this property can be calculated using different equations based on the nominal diffusivity, turtuosity and porosity.

Boundary conditions

The common boundary conditions are:

Inlet condition: specified at the flow inlet face of the fuel cell geometry with the knowledge of the composition, velocity and temperature of the fluid entering. Fluid velocity is determined based on the desired fuel and the stoichiometry numbers.

Outlet condition: specified at the flow outlet face of the fuel cell geometry. Typically based on pressure, and the outlet is usually exposed to atmospheric pressure (could be set as 1 atm)

Wall condition: Apart from the inlet and outlet, most exterior surfaces in the fuel cell model are walls – no fluid can go in or out. Two important types: thermal & electric wall conditions.

Common Thermal wall conditions: Adiabatic (well-insulated) & Isothermal (uninsulated).

Electric wall conditions: applied to exterior surface of the anode & cathode current collector plates. The difference in voltage applied to the anode versus the cathode walls represents the overpotential (η) driving the fuel cell. η can be controlled through the electric wall conditions. The fuel cell output voltage is calculated as $V = E_{thermo} - \eta$. As η increases, j_0 increases. Hence, we can get the complete j-V curve.

Symmetry condition: If a fuel cell has identical structural and physical model geometry across a "symmetry plane" then we simulate only one half and the solution for the other half can be obtained by mirroring. This saves computational time and resources. Use of the symmetry boundary condition seems quiet improbable, since it is hard to find symmetry conditions in SOFC.

2.2.6 Post-processing

We have already designed the SOFC geometry, made suitable assumptions, defined asset of governing equations and specified the boundary and volume conditions. The final step in modeling is solving for the unknowns. Most CFD codes employ an iterative process to find the

value of the unknowns. After an initial guess of the unknown values, the iterative process is started. At the end of each iteration we get a value for the unknown variable. The iterative process continues till the solution 'converges'. Convergence of a solution is said to be reached when the value of the solution for consecutive iterations are within a specified range or tolerance or accuracy. This rage could be about 1% error range or lower. If the solution 'diverges', which means it becomes unstable and the solution from consecutive iterations keeps growing apart, then we need to stop the process and go back and look for errors made with the geometry, governing equations, assumptions, boundary & volume conditions. Once we make the required corrections and the solution reaches convergence, the next step is data validation. The data or solution obtained from the numerical simulation of the SOFC is compared against the experimental data that is available. If the results vary from the experimental data within a reasonable range, the numerical simulation is declared to be successful.

We can then continue onto to result analysis, where we can interpret and draw various conclusions from the final solution. An example is that if we started off by specifying the voltage and finding the corresponding current value, then we can use this set of voltage and current values to draw a i-V or j-V curve. This step is also referred to as data visualization where we draw graphs and plots to study the results in depth.

2.3. Basic Algorithm

The basic algorithm will give us an understanding of how the governing equation, that we have are used to obtain the desired solutions. Let us consider the set of governing equations given in the book by Singhal et al. [2], and the process of solving them. This is one basic algorithm, but in section 4.3 the algorithm that was used in this thesis will be shown.

STEP 1: Assume or specify a current or current density value. We will determine the corresponding voltage value through the following steps.

STEP 2: Using the mass and momentum conservation equations we can solve for fluid velocity (v), species diffusion velocity (U_i) and species density (ρ_i). We have 3 equations and 3 unknowns. All other terms are known from experimental data.

$$\frac{\partial(\rho v_k)}{\partial t} + \nabla \bullet (\rho v_k v) = \rho g_k - \frac{\partial P}{\partial X_k} + \nabla \bullet (\mu_e \nabla v_k) + \Omega_k + \tau_k$$

$$\frac{\partial \rho_i}{\partial t} + \nabla \bullet [\rho_i (v + U_i)] = \omega_i$$

$$\rho_i U_i = -\rho D_{im} \nabla c_i$$

Note: the pressure drop term in the first equation can be calculated by first assuming that the flow in the SOFC is laminar. Then we can calculate pressure drop through a channel as, $\Delta P = (1/2) * (\rho v^2 f1) / (Re D_h)$

where, D_h is the hydraulic diameter of the channel, Re is Reynolds number based on D_h, l is the length of the flow path, f is the friction factor that depends on the shape of the cross-section of the channel.

STEP 3: Using the above results, we can determine the temperature (T) profile from the energy equation. The last four terms of the energy equation can be estimated from experimental data or approximated.

$$\frac{\partial(\rho c_p T)}{\partial t} + \nabla \bullet (\rho c_p T v) = \nabla \bullet (\lambda \nabla T) + Q + \frac{\partial P}{\partial t} + Q_{vis} + W^v + E^k$$

STEP 4: This step will allow us to calculate the voltage for the given current. Start with the potential balance equation. We need t determine the LHS value. All the terms on the RHS are currently unknown and need to be calculated.

$$V(i) = E_{eq} - iR_i - \eta_{Ca} - \eta_{Cc} - \eta_{Aa} - \eta_{Ac}$$

To determine the thermodynamic reversible voltage, we use the equation:

$$E_{eq} = -\frac{\Delta G^0}{2F} + \frac{RT}{4F} \ln \frac{P_{O_2} P_{H_2}^2}{P_{H_2O}^2} = E^0 + \frac{RT}{4F} \ln \frac{P_{O_2} P_{H_2}^2}{P_{H_2O}^2}$$

Activation overvoltage can be calculated from:

$$j = i / a = i_0 \{\exp[-\alpha z F \eta_a / RT] - \exp(1-\alpha) z F \eta_a / RT]\}$$

Then, the concentration overvoltage is determined from:

$$\eta_C = (RT / nF) \ln(1 - i / i_C)$$

here ic is the limiting current of the species and for hydrogen-oxygen fuel cell we can use:

$$i_{O_2} = (2 p_{O_2} D_{eff(C)} / Cl_C)[P / (P - p_{O_2}^0)]$$

$$i_{H_2} = 2 p_{H_2} D_{eff(a)} / (Cl_a)$$

Hence we finally obtain the voltage V as a function of the current:

$$V(i) = E_{eq} - iR_i - \eta_{Ca} - \eta_{Cc} - \eta_{Aa} - \eta_{Ac}$$

STEP 5: Data validation: The previous step is repeated for the whole range of current load to achieve the corresponding voltage. We can plot a j-V curve from the results obtained. Then we compare it with the experimental data we have. If the two match within reasonable range, then we can declare that the numerical simulation was a success.

STEP 6: Model reduction: We can try and reduce different equations and relations to their fundamental nature like exponential, linear, etc. Then we modify our model and after the solution process we can validate the results and if the results are within acceptable range of error, then we can say that the model reduction step was successful. This will save a lot of time and resources.

CHAPTER 3: METHODOLOGY - SOFC SIMULATION USING COMSOL MULTIPHYSICS® VERSION 4.2A

3.1 About COMSOL Multiphysics®

COMSOL Multiphysics is a modeling software developed by the COMSOL Group founded by Svante Littmarck and Farhad Saeidi in 1986 [10]. The unique feature that distinguishes COMSOL Multiphysics from much other modeling software available in the market is that it can be used for 'Multiphysics modeling'. Generally available modeling software incorporates a single or a few aspects of physics. Multiphysics modeling is a method of modeling that incorporates a diverse range of physics like heat transfer, electrochemistry, geophysics, electromagnetic, fluid dynamics, optics, plasma physics, etc. COMSOL Multiphysics uses the Finite Element Method (FEM) method of modeling in solving Partial Differential Equations (PDE) that are used to mathematically express physical and scientific phenomena. COMSOL Multiphysics is a comprehensive modeling tool because it allows the user to create the model geometry, mesh the geometry, add the relevant physics equations, derive a solution and finally visualize the results. The software offers additional modules that are specific to each area of physics. For the research work presented here the 'Batteries and Fuel Cells' module has been used. The Batteries and Fuel Cells module provides the user the ability to build models of electrodes and electrolytes in detail. In addition, it includes all the relevant aspects of fuel cell physics namely chemical species transport, electrochemistry, fluid flow and heat transfer. To

fulfill on the research purpose of this thesis a ‘Materials library’ was also used. A screen shot of the COMSOL desktop can seen below in figure 10.

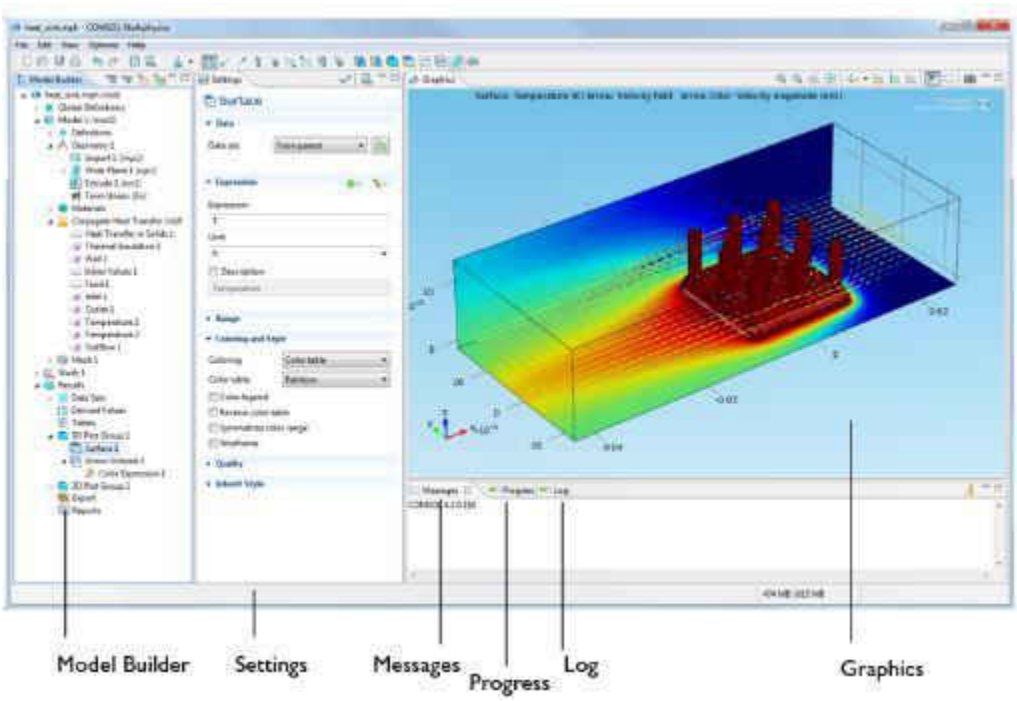

Source: COMSOL® Multiphysics® version 4.2 Help
Figure 10. Screen shot of COMSOL desktop.

3.2 Modeling Methodology

The methodology that will be used for the modeling purpose is very critical. The choice of concepts, equations, coefficients and other relevant parameters determines the accuracy of the final result. The Batteries and Fuel Cells module in COMSOL Multiphysics offers a number of choices with regards to each aspect of physics involved. This section will present all the choices of physics interface and the reason behind choosing a particular interface.

There are four major phenomena that need to be taken into consideration in modeling of a Solid Oxide Fuel Cell:

I. Electrochemistry or current distribution

II. Chemical Species Transport

III. Fluid Flow

IV. Heat Transfer

We will take into consideration the first three, although heat transfer is an important physical phenomenon it is out of the scope of this thesis.

I. Electrochemistry: This interface in COMSOL Multiphysics is used to calculate the current distribution and the potential distribution within a SOFC. It takes into account the electrochemical reaction kinetics of the SOFC, while ignoring the ohmic and concentration losses. This interface has three categories – Primary, Secondary and Tertiary Current Distribution. Of these the Secondary Current Distribution is the feature that is best suited to calculate the activation overpotential losses in the fuel cell.

3.2.1 Secondary Current Distribution [11]

The transfer of current in fuel cells takes place through the transport of electrons in the electrodes and the transport of ions in the electrolyte. The secondary current distribution interface is used for this purpose. It accounts for the charge balance in the anode electrode, cathode electrode and the electrolyte. The fundamental assumption is that the electrolyte does not undergo any change in its composition and its properties remain uniform. The dependent variable for the electrolyte is

the electrolyte potential and for the electrode it is the electric potential. The Butler-Volmer and sometimes Tafel equations are used to express the electrochemical reactions. The generation or consumption of different chemical species is expressed as sources and sinks respectively at the boundaries or domains of the fuel cell. The current generation in the fuel cell domains can be expressed using the equation:

$$\nabla \cdot i_k = Q_k$$

where i stands for the current density vector, k represents the notation that is s for the electrodes and l for the electrolyte, and Q_k stands for the source term. The current density vector in the electrolyte can be described as:

$$i_l = -\sigma_l \nabla \Phi_l$$

where Φ_l is the electrolyte potential and σ_l is the electrolyte conductivity. Similarly for electrodes:

$$i_s = -\sigma_s \nabla \Phi_s$$

where Φ_s is the electrode potential and σ_s is the electrode conductivity.

The activation overpotential, η, represents the loss in voltage that the fuel cell needs to sacrifice to overcome the activation barrier. The activation overpotential is related to the electrode potential, electrolyte potential and the equilibrium potential. This can be shown in the following equation for an electrode reaction with index m,

$$\eta_m = \Phi_s - \Phi_l - E_{eq,m}$$

where $E_{eq,m}$ represent the equilibrium potential for the m reaction.

The Butler-Volmer equation is the equation that can be used to relate current and voltage in a fuel cell. It basically shows the relationship between the current density and the activation overpotential. The equation is below [1]:

$$j = j^{0}{}_{0}\left[\frac{c_R^*}{c_R^{0*}}\exp\left\{\frac{n\alpha F}{RT}\eta\right\} - \frac{c_P^*}{c_P^{0*}}\exp\left\{\frac{-n(1-\alpha)F}{RT}\eta\right\}\right]$$

j: current density

$j^0{}_0$: current density measured at the reference reactant and product concentration values

$c^*{}_R$: actual concentration of the reactant involved in the electrochemical reaction

$c^*{}_P$: actual concentration of the product involved in the electrochemical reaction

$c^{0*}{}_R$: reference concentration of the reactant involved in the electrochemical reaction

$c^{0*}{}_P$: reference concentration of the product involved in the electrochemical reaction

n: number of charges transferred

α : transfer coefficient (ranges generally between 0.2 and 0.5)

For a fuel cell, the potential balance of the fuel cell [2] can be written as:

$$V(i) = E_{eq} - iR_i - \eta_{Ca} - \eta_{Cc} - \eta_{Aa} - \eta_{Ac}$$

i : current density.

iR_i : ohmic potential drop.

ηC_a : overpotential of the cathode due to activation loss.

ηC_c : overpotential of the cathode due to concentration loss.

ηA_a : overpotential of the anode due to activation loss.

ηA_c : overpotential of the anode due to concentration loss.

E_{eq} : thermodynamic cell potential/equilibrium voltage, given by

$$E_{eq} = -\frac{\Delta G^0}{2F} + \frac{RT}{4F}\ln\frac{P_{O_2}P_{H_2}^2}{P_{H_2O}^2} = E^0 + \frac{RT}{4F}\ln\frac{P_{O_2}P_{H_2}^2}{P_{H_2O}^2}$$

R : gas constant.

T : Temperature.

F : Faraday constant.

ΔG^0 : standard free-energy change of the reaction at standard pressure (1 atm).

E^0 : standard cell potential or standard emf (depends only on temperature).

P_{O2}, P_{H2}, P_{H20} : partial pressures of oxygen, hydrogen and water respectively.

In COMSOL, for charge balance in porous electrodes the charge transfer current density is included as a source or sink, while in non-porous electrodes it can be included as a boundary condition. Under the Secondary Current distribution feature, for electrodes the equilibrium potential and potential during operation are defined and the driving potential (V_{cell}) for the current through the fuel cell is given by the difference in the polarization of the electrodes and the equilibrium potential given as:

$$V_{cell} = \Phi_s - \Phi_l - E_{eq,m}$$

II. Chemical species transport: The role of this interface is to provide the ability to solve the equations, boundary conditions and parameters that account for the chemical transport of different species involved in the fuel cell reactants and products.

3.2.2 Transport of Concentrated Species [11]

The transport of chemical species involved in the chemical reactions of the fuel cell occurs mainly by diffusion and convection. Convection is the process of transport of the chemical species as a bulk through the fluid, and is governed by the laws of fluid flow and heat transfer. Convection in fuel cells occurs mainly in the flow channels of the electrodes and is driven by a pressure gradient. Diffusion is the process of transport of chemical species usually driven by concentration gradient of the species itself. Generally in a SOFC the diffusion process dominates the transportation of chemical species through the electrodes. In COMSOL Multiphysics the 'Transport of Concentrated Species' supports the modeling of chemical species transport by offering the equations, boundary conditions and reaction terms for convection, diffusion and migration in 1D, 2D and 3D. This can be achieved by solving for the mass fractions. The diffusion model offered is either Mixture-average diffusion model or Fick's model. Fick's law model is computationally more expensive and is used when the chemical transport mechanism is not dominated by molecular diffusion and a lower order but robust model is required. The Mixture-average model of diffusion employs the Maxwell-Stefan diffusivities and is computationally less expensive. The mixture-averaged model is used in this thesis.

To explain the multicomponent mass transport of individual species in a reacting flow which consists of a mixture of i = 1, ..., Q species and j = 1, ..., N reactions, the following equation can be used:

$$\frac{\partial}{\partial t}(\rho\omega_i) + \nabla \cdot (\rho\omega_i u) = -\nabla \cdot j_i + R_i$$

ρ: mixture density (kg/m^3)

u: mass average velocity (m/s)

ω_i: mass fraction

j_i: mass flux relative to the mass average velocity (kg/(m^2s)) [this term can include contributions from molecular diffusion, thermal diffusion, mass flux due to migration in an electric field]

R_i: consumption or production rate (kg/(m^3s))

The conservation of mass equation can be deduced by the summation of the above transport equation over all the species present in the reaction,

$$\frac{\partial \rho}{\partial t} + \nabla \cdot (\rho u) = 0$$

by using the assumption,

$$\sum_{i=1}^{Q} \omega_i = 1 \qquad \sum_{i=1}^{Q} j_i = 1 \qquad \sum_{i=1}^{Q} R_i = 1$$

Using the above conservation of mass equation, the transport of an individual chemical species, I, is given by:

$$\rho \frac{\partial}{\partial t}(\omega_i) + \rho(u \cdot \nabla)\omega_i = -\nabla \cdot j_i + R_i$$

The above equation can be used to solve for Q-1 of the individual species independently. The mass fraction of the Qth species can be computed using the fact that the summation of all mass fractions is equal to 1:

$$\omega_Q = 1 - \sum_{i=1}^{Q-1} \omega_i$$

The Maxwell-Stefan diffusion model for the transport of species' mass can be expressed as:

$$\rho\frac{\partial}{\partial t}(\omega_i) + \rho(u\cdot\nabla)\omega_i = \nabla\cdot\left(\rho\omega_i\sum_{k=1}^{Q}\widetilde{D}_{ik}d_k + D_i^T\frac{\nabla T}{T}\right) + R_i$$

T: temperature (K)

D_i^T: thermal diffusion coefficients (kg/(ms))

d_k: diffusional driving force acting on species k (1/m)

$\widetilde{D}_{ik}$: multicomponent Fick diffusivities (m^2/s) [$\widetilde{D}_{ik} = \widetilde{D}_{ki}$] - symmetric

The multicomponent Maxwell-Stefan diffusivities, D_{ik}, are related to the Fick diffusivities,$\widetilde{D}_{ik}$, through the relation [29]:

$$\frac{x_i x_k}{D_{ik}} = -\omega_i\omega_k\frac{\sum_{j\neq i}(adjB_i)_{jk}}{\sum_{j\neq i}\widetilde{D}_{ij}(adjB_i)_{jk}}$$

$$(B_i)_{jk} = \widetilde{D}_{kj} - \widetilde{D}_{ij}$$

$$i \neq j$$

where $(adjB_i)_{jk}$ is the jk^{th} component of the adjoint of the matrix B_i. For low-density gas mixtures, the multicomponent Maxwell-Stefan diffusivities, D_{ij}, can be replaced with binary diffusivities for the species pairs that are involved in the reaction.

The diffusional driving force for ideal gas mixtures is given by,

$$d_k = \nabla x_k + \frac{1}{p}\left[(x_k - \omega_k)\nabla p - \rho\omega_i g_k + \omega_k\sum_{l=1}^{Q}\rho\omega_l g_l\right]$$

p: partial pressure (Pa)

g_k: external force acting on the species k, per unit mass. For ionic species, the electric field causes the external force. Note: when the external force acting on all the species is the same, like gravity, then the last two terms of the above equation can be dropped.

x_k: mole fraction calculated using,

$$x_k = \frac{\omega_k}{M_k} M$$

M: mean molar mass (kg/mol) given by,

$$\frac{1}{M} = \sum_{i=1}^{Q} \frac{\omega_i}{M_i}$$

For the cases when isothermal and isobaric conditions are assumed, the mixed-average diffusion coefficient can be derived from the Maxwell-Stefan equations [30]:

$$D_i^m = \frac{1 - \omega_i}{\sum_{k \neq i}^{N} \frac{x_{ki}}{D_{ik}}}$$

3.2.3 Fluid Flow [11]

The fluid flow in SOFC is modeled in COMSOL Multiphysics using the 'Free and Porous Media Flow' interface. The Free and Porous Media Flow interface combines laminar flow physics and physics of flow through porous media; by providing the equations, boundary conditions and volume forces for modeling fluid flow through open and porous regions. It uses the Navier-Stokes equations for describing flow through the open domains like the flow channels and the Brinkman equations for the flow through porous media like the electrodes. This interface solves for the velocity field, u, and pressure field, p, in both the porous and free flow regions. Therefore the assumption made is that the pressure and velocity field is continuous in the porous domain

and the free flow domain and over the interface between the two domains. This means that the free flow fluid velocity and the Darcy velocity in the porous domain are continuous. This is an approximation and one of several ways of modeling the interface between the two domains [31]. This continuity in u and p also means that there is a discontinuity in stress at the interface between free flow domains and porous domains, the difference in stress assumed to be absorbed by the rigid porous matrix which is a result of the Navier-Stokes and Brinkman equation calculations.

The fluid flow through open domains is modeled as Laminar flow using the Navier-Stokes equations assuming compressible flow at Ma < 0.3. The compressibility factor is considered since the density of the fluid could undergo changes at the operating temperatures of the SOFC (600^{o}C to 1000^{o}C). The Navier-Stokes equations [32] [33] are solved for single-phase (by default) flows using the compressible version of the continuity and momentum equations. The continuity equation is given by,

$$\frac{\partial \rho}{\partial t} + \nabla \cdot (\rho u) = 0$$

ρ: density of the fluid (kg/m^3)

u: velocity vector (m/s)

The momentum equation is given by,

$$\rho \frac{\partial u}{\partial t} + \rho u \cdot \nabla u = -\nabla p + \nabla \cdot \left[\mu(\nabla u + (\nabla u)^T) - \frac{2}{3}\mu(\nabla \cdot u) I \right] + F$$

p: pressure (Pa)

F: volume force vector (N/m^3)

μ : dynamic viscosity of the fluid (Pa·s)

I: identity tensor

Mach number, Ma, is a dimensionless quantity defined as:

$$Ma = \frac{|u|}{a}$$

a: speed of sound (m/s)

Normally problems involving air or other gases are considered incompressible with Ma = 0, which means that the speed of sound could be considered infinity or relatively very high. The Navier-Stokes equations consider the speed of sound to be finite and to spread throughout the domain instantaneously. This means that Ma for a flow is usually higher than zero no matter how small the value might be. For cases where the Mach number is lower than one, the fully compressible Navier-Stokes equations demonstrate sharp gradients once the Mach number goes beyond the moderate value. As a rule of thumb, this value is 0.3. Therefore, although for a SOFC small changes in density can be considered due to the high operating temperatures; the Mach number needs to be assumed as Ma<0.3.

The fluid flow dynamics are different in porous media and therefore by averaging the properties and variables over a control volume surrounding a point, the fluid properties and variables at that point inside the porous media is estimated. The control volume chosen for this purpose must be small compared to the typical macroscopic dimensions as used in the Navier-Stokes equations, but large enough to encompass many pores and solid matrix elements. Porosity in this case can

vary from zero for a solid non-porous media to a value of unity for open channels. The fluid properties (viscosity, pressure, density) are defined as intrinsic volume averages for a unit volume of pores. This way of defining the properties facilitates the properties to be assumed as continuous and experimentally measurable. Similarly, fluid flow velocities are defined as superficial volume averages, where the unit volume includes both matrix and pores. These velocities can be defined as the volume flow rates divide by cross sectional area of the medium and are sometimes referred to as Darcy velocities.

The Brinkman equations [34] are composed of the continuity and momentum equations for porous media, given by:

$$\frac{\partial}{\partial t}(\varepsilon_p \rho) + \nabla \cdot (\rho u) = Q_{br}$$

$$\frac{\rho}{\varepsilon_p}\left(\frac{\partial u}{\partial t} + (u \cdot \nabla)\frac{u}{\varepsilon_p}\right) = -\nabla p + \nabla \cdot \left[\frac{1}{\varepsilon_p}\left\{\mu(\nabla u + (\nabla u)^T) - \frac{2}{3}\mu(\nabla \cdot u)I\right\}\right] - \left(\frac{\mu}{k} + Q_{br}\right)u + F$$

μ : dynamic viscosity of the fluid (Pa·s)

u : velocity vector (m/s)

ρ : fluid density (kg/m^3)

p : pressure (Pa)

ε_p : porosity

k : permeability of porous medium (m^2)

Q_{br} : mass source or mass sink (m^3/s) [mass creation or deposit in porous domains, assumed to occur at zero velocity]

F : volume forces vector (kg/m^{2}s^2)

In the case of incompressible fluid flow, the density is constant and the condition becomes:

$$\frac{\partial}{\partial t}(\varepsilon_p \rho) + u \cdot \nabla \rho = 0$$

Combining this with the Brinkman continuity equation results in,

$$\rho \nabla \cdot \mathrm{u} = \mathrm{Q}_{\mathrm{br}}$$

The boundary conditions for Laminar fluid flow is specified at the inlet, outlet and at the walls. Wall boundary could be modeled as 'slip' or 'sliding wall' conditions. The 'Slip' condition is used for the boundary condition at the wall. The Slip condition assumes that there are no viscous stresses at the wall and therefore no development of boundary layers. This is a very reasonable assumption for the wall conditions, since from a modeling stand point the purpose of the wall is to avoid fluid flow through it. This condition can be mathematically computed using,

$$u \cdot n = 0 \qquad [-pI + \mu(\nabla u + (\nabla u)^T)]n = 0$$

n: normal vector

For the inlet conditions in single-phase flow, the 'pressure, no viscous stress' condition or the 'normal stress' condition can be chosen. The 'pressure, no viscous stress' condition is chosen. This condition assumes that the viscous stress is vanishing along with a Dirichlet condition for pressure, mathematically written as:

$$\left[\mu(\nabla u + (\nabla u)^T) - \frac{2}{3}\mu(\nabla \cdot u)I\right]n = 0, \qquad p = p_0$$

for compressible fluid flow. Physically, this boundary condition is equivalent to a boundary that is adjacent to a large domain (for inlet) or exiting into a large domain (for outlet). Hence,

pressure is assumed to be constant along the entire boundary and the condition is considered numerically stable.

CHAPTER 4: RESULTS AND DISCUSSION

The modeling and simulation of the electrolyte-supported button type Solid Oxide Fuel Cell was carried out using the Batteries and Fuel Cells module of COMSOL Multiphysics® version 4.2a. The geometry modeling, meshing, solution process and post-processing were all carried out in COMSOL. This section will include the SOFC geometry design, the results from the simulations of the YSZ and SCSZ layered electrolyte SOFC and some analysis of these results. In addition, a study to understand the most significant parameters that affect SOFC performance was conducted, which will be covered under the section titled parametric study.

4.1 SOFC Geometry and material properties

The SOFC button cell was modeled to represent the cell that is developed in the lab, and hence the dimensions used of the cell were just as the SOFC produced in the lab. The dimensions of the cell have been summarized in the Table 4 below.

Table 4. Dimensions of the button SOFC to be produced in the lab.

SOFC Dimensions	
Anode & Cathode thickness	50 µm
Electrolyte layer thickness	30 µm
Anode & Cathode diameter	10 mm
Electrolyte diameter	20 mm
Gas flow channel height (Anode & Cathode)	1 mm
Gas flow channel diameter (Anode & Cathode)	10 mm

The figure 11 and figure 12 show the modeled geometry of the SOFC in COMSOL. Figure # shows the parts of the SOFC labeled. As can be seen the SOFC has a disk-like structure with the electrolyte having the largest diameter. The thickness of the electrodes is small compared to

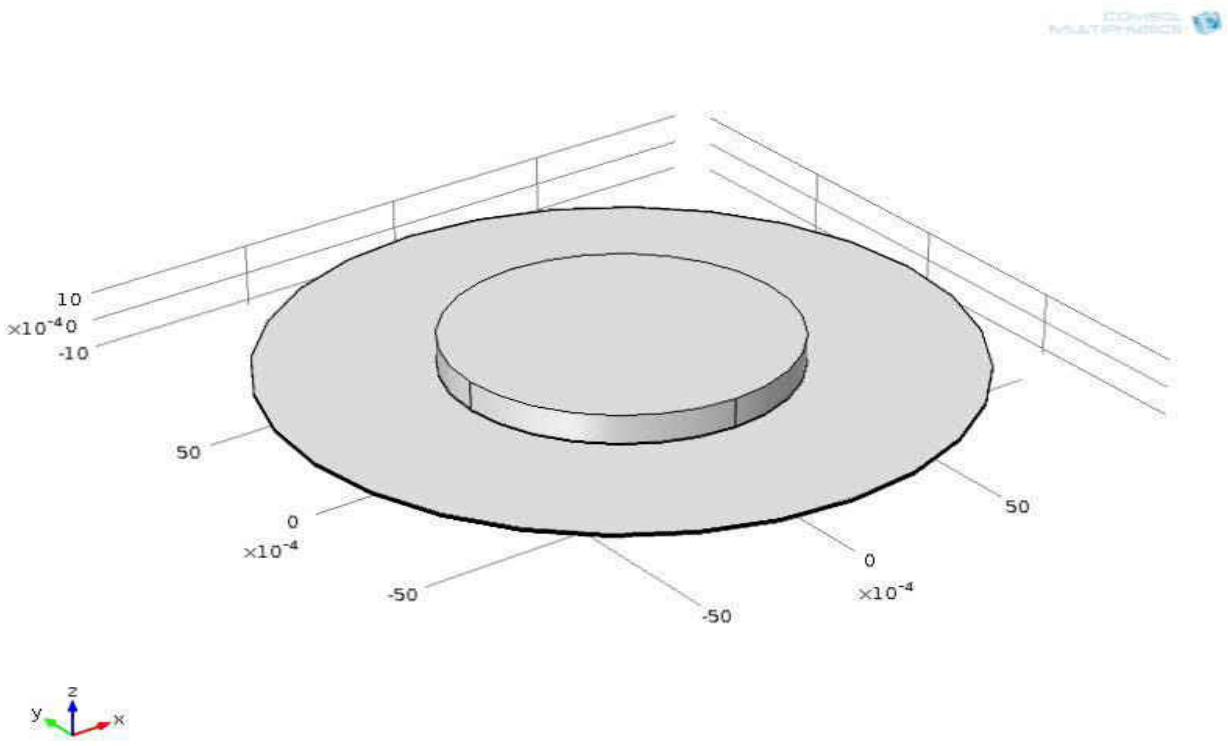

Figure 11. SOFC geometry.

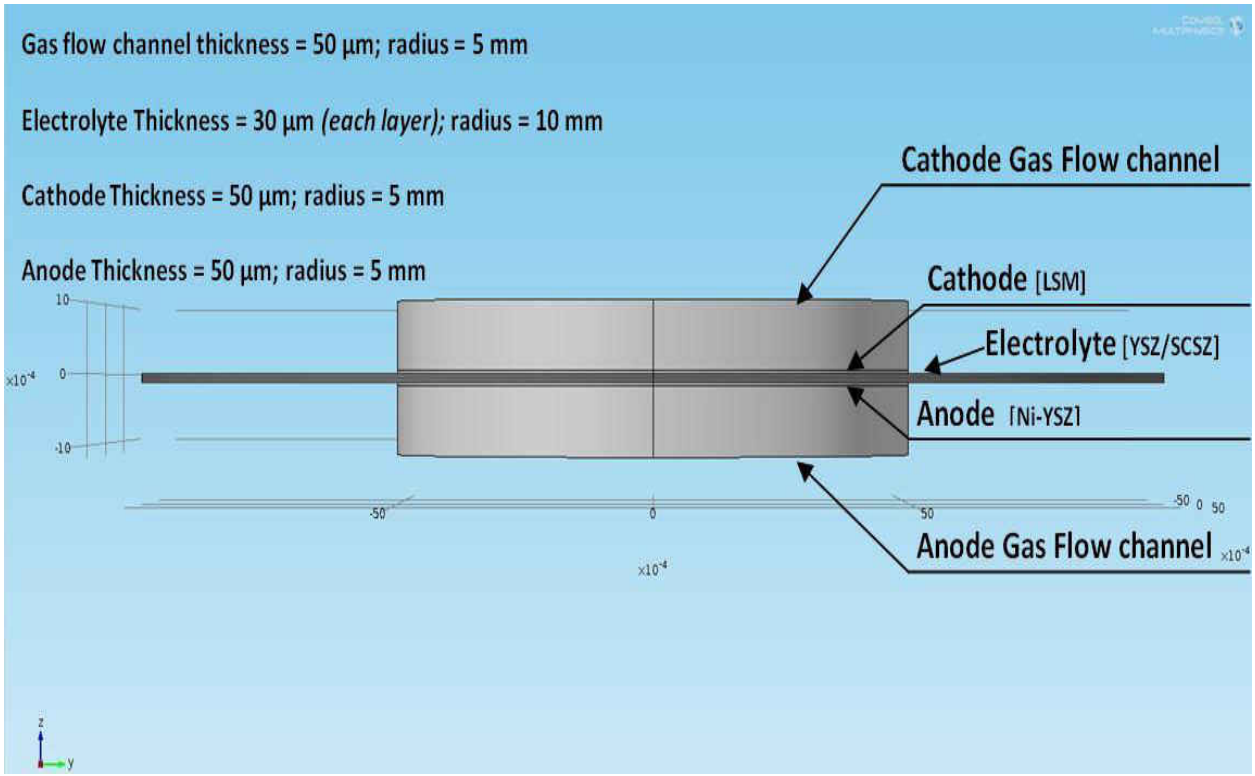

Figure 12. SOFC geometry – side view, labeled.

the thickness of the gas flow channels and hence it could be hard to see in figure 12. The electrolyte is non-porous modeled to allow the transfer of ions only. The electrodes, on the other hand, are porous and allow the flow of gases, ions and electrons. The interface of the electrodes and electrolyte is the location of Triple Phase Boundaries (TPBs) where the major chemical reactions of the fuel cell occur. The gas flow channels are the domains through which gases flow. Air (oxidant) flows into the fuel cell through the cathode gas flow channel and Hydrogen (fuel) flows into the cell through the anode gas flow channel. The flow is designed such that the outlet of gases is through the peripheral walls of the electrodes. This flow design was chosen to maximize the flow through the electrodes and a detailed study of this was carried out through simulations. The results of these simulations are shown below in figure 13 and figure 14. A

straight channel has been used here for demonstration. By comparing the results it is clearly understood why this particular flow design was chosen. The mass fraction of oxygen is almost evenly distributed throughout the electrode as seen in figure 13, but the mass flow distribution is not even in the cross-flow condition as seen in figure 14. This effect although may look insignificant, in a fuel cell system which may contain hundreds of single cells, these effects could become very significant.

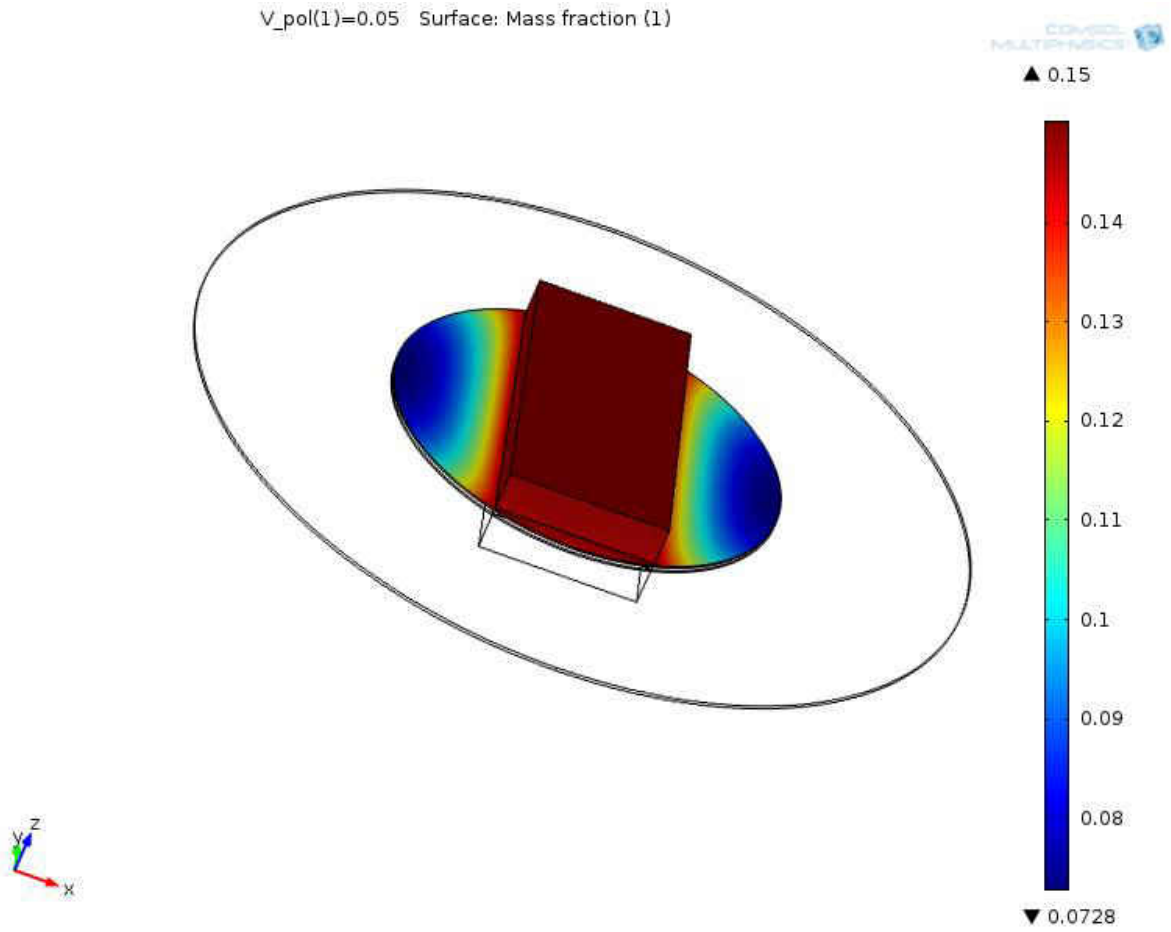

Figure 13. Custom-flow: Oxygen mass fraction distribution in SOFC cathode and cathode flow channel.

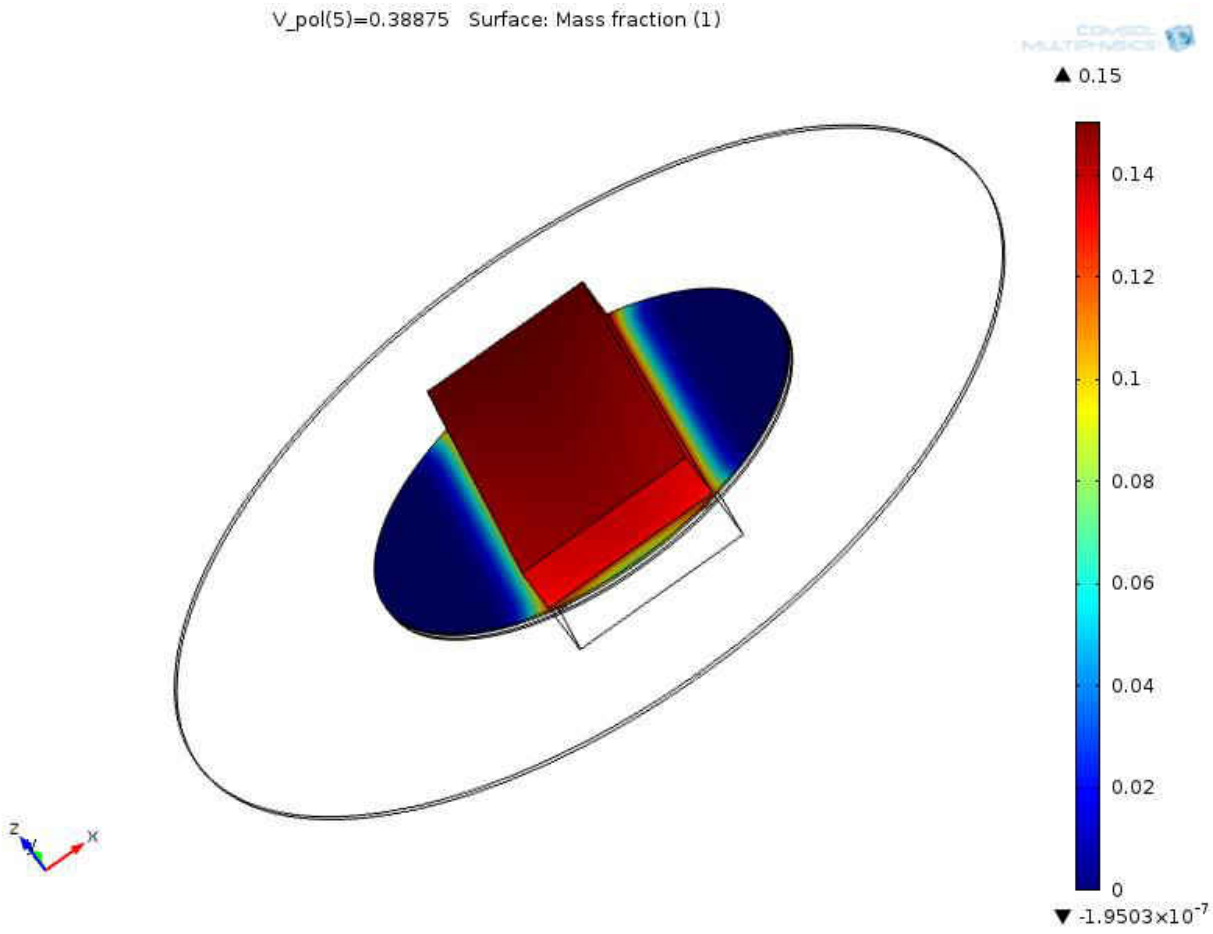

Figure 14. Cross-flow: Oxygen mass fraction distribution in SOFC cathode and cathode flow channel

The properties of the anode and cathode were chosen from referring to the published data. The anode properties were chosen from references [44-47] and cathode properties were chosen from references [48-52]. The electrolyte properties will be discussed in section 4.3. The following Table 6 summarizes the material properties of the electrodes and electrolyte.

Table 5. Material properties of the electrodes and electrolyte

Material property	Anode – Ni-YSZ	Cathode - LSCF	Electrolyte – YSZ	Electrolyte - SCSZ
Ionic Conductivity [S/m]	1	5.15	4.24 – 4.62	10.58 – 11.93
Electronic Conductivity [S/m]	650000	2300	negligible	negligible
Porosity	40 %	40 %	0	0

4.2 Meshing

Meshing is a very important aspect of multiphysics modeling. Meshing is essentially breaking down the model domains into small discrete elements and the physical equations (partial differential equations) associated with the problem are solved within each of these elements. For this reason, it is important to make the elements small enough to capture all the necessary reactions or phenomena associated with the problem to get the most accurate results. The process of meshing a geometry is a balance between reducing the element size and the computational cost of doing so. The smaller the elements are, the higher the number of elements in the model and therefore the computation will take longer time, demand higher computational capabilities and larger memory space. Meshing is an aspect in which experience matters a lot. A good modeler will be able to intuitively judge the apt technique and extent to which the model needs to be meshed. There are two types of meshing – Structured, Unstructured and Hybrid. Structured meshing involves fixing the element shape and using the same element to fill the entire domain. Unstructured meshing is one in which the user has more control of the meshing process and the

element shape and size can vary to a large extent. Unstructured meshing can be interpreted as 'custom meshing', customized depending on the problem and each domain or part of the domain. Hybrid meshing combines aspects of both structured and unstructured meshing. The type of meshing to be used really depends on the problem at hand. In the recent past certain modelers have come up with meshless designs, but that is out of the scope of this thesis.

Apart from the meshing technique, meshing can also be classified based on the shape of the mesh element. Some of the commonly used element shapes are triangles and quadrilaterals for 2D modeling, while 3D modeling may have pyramids, prisms, tetrahedron and hexahedron. It is important to arrive at the most optimum mesh for any model. This can be accomplished a few ways. One of the ways is the keep increasing the number of elements in the model, as the number of elements is increased the accuracy of the results will improve. At some point, the variation in the accuracy of the results will start reducing. The number of elements to be chosen will then be based on a particular range of accuracy of the results desired. This method was inculcated in this particular model. Unstructured meshing was used and the approximate number of mesh elements chosen was between 116,000 and 1,035,000. The table 5 below gives a summary of the meshing specifications.

Table 6. Summary of meshing specifications.

Meshing technique	Unstructured
Mesh element type	Tetrahedral, Triangular, Edge, Vertex
Number of elements	116,000 to 1,035,000
Smallest element size	1.32×10^{-4} m
Largest element size	0.002 m

4.3 Modeling approach

One of the challenges involved in modeling is assessing the best way to model a particular system. Often times the modeling process may include omission of certain aspects of the real system, or inclusion of a certain aspect that is not part of the real system, or even modifying the system on the computer to make the model computationally more accurate, efficient or economical. An example is that the electrodes and electrolyte are assumed to have uniform properties throughout, but in reality this is not the case. The microstructure and properties of the electrodes and electrolyte is not uniform and the properties may vary throughout. But, the uniform properties assumption may be made if such an assumption will not affect the results to a large extent. The reason behind making such assumptions is either to save computational time and resources or because of lack of data available.

The significant assumptions made in this model are:

- Steady state condition
- Material properties is considered to be constant
- Focus is on the cell-level modeling only, without considering interconnect, pore-formers and other aspects of the fuel cell system.
- All fluids (H_2, O_2, H_2O, N_2) are considered to follow ideal gas law and treated as incompressible
- Heat transfer effects are not considered

The algorithm used in this modeling is given in the Figure 13 below:

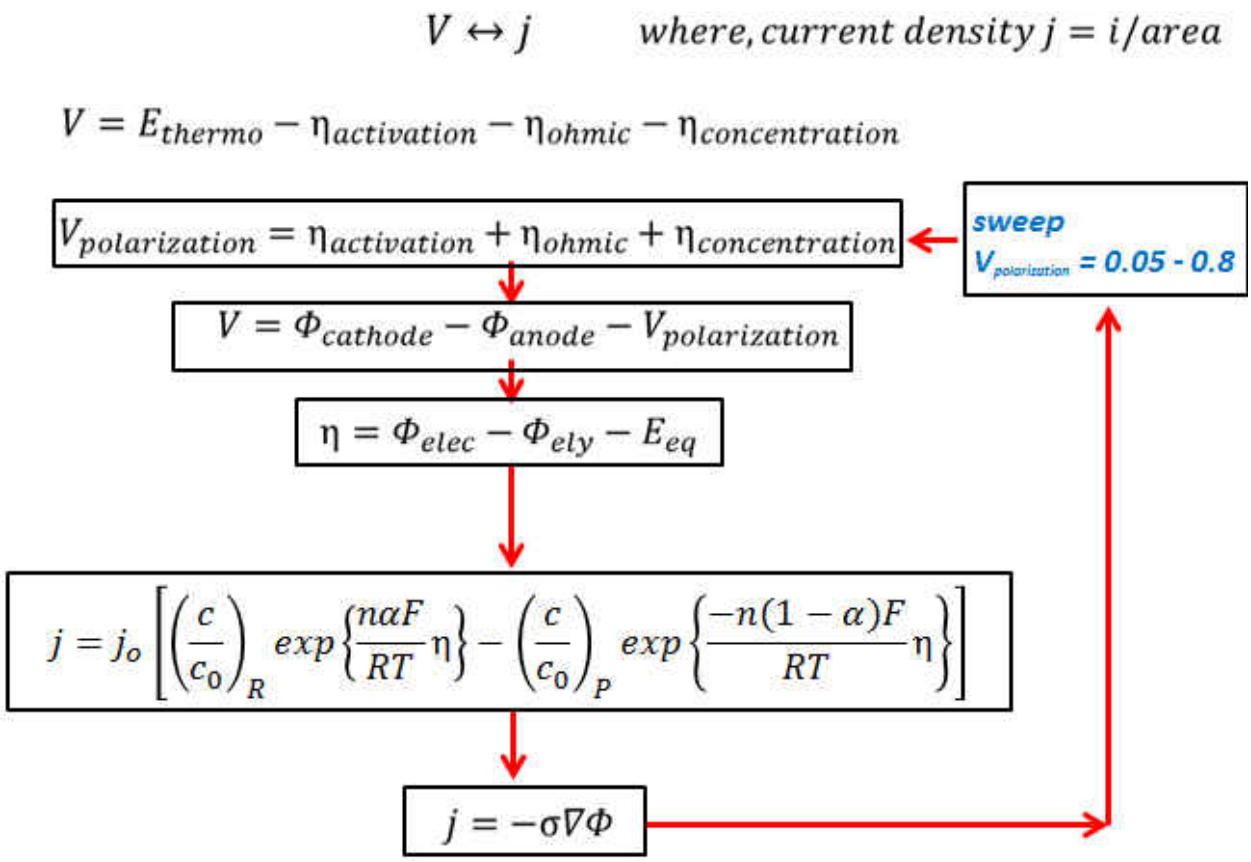

Figure 15. Algorithm of the modeling process

In the modeling of this particular electrolyte-supported cell, one of the questions encountered was as to how a layered electrolyte should be modeled in the computer. Consider the 3-layered electrolyte. The electrolyte can be modeled as three different domains of 30µm thickness each stacked one on top of the other or as one big block of 90µm thickness. The electrolyte conductivity data is only available for whole 3 - layered electrolyte and not for each individual layer. Also, since the uniform properties assumption was made then does it really matter if the electrolyte is modeled as one domain or three layered domains? The best way to answer this question is to try out two different approaches. As can be seen in table 6, the measured

electrolyte conductivity data is only available for pure and composite 3, 4 and 6 - layered electrolytes, but not for a single layer. The graph 3 shows that the conductivity of YSZ and SCSZ does not vary significantly. Therefore, it seems safe to assume that the electrolyte conductivity of a single layer is an average of the conductivities of 3, 4 and 6 – layered electrolytes of the same material.

Table 7. Measured electrolyte conductivities and average of YSZ & SCSZ conductivities.

SOFC Electrolyte Conductivities [S/m]			
	YSZ	**SCSZ**	**YSZ-SCSZ-YSZ**
3-layered (Block)	4.53	10.58	6.01
4-layered (Block)	4.62	11.93	6.89
6-layered (Block)	4.24	11.62	8.86
Single layer - average of 3, 4, 6-layered	4.47	11.38	-

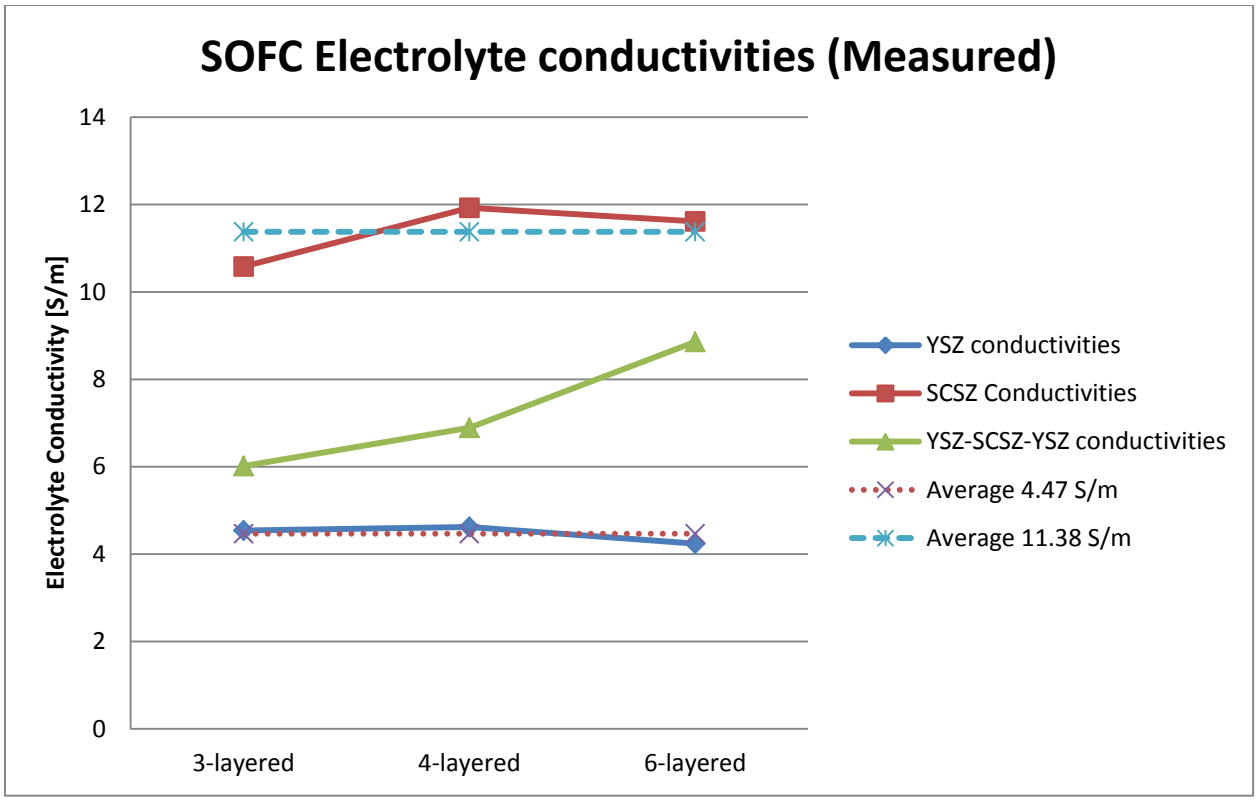

Figure 16. Measured SOFC electrolyte conductivities.

Therefore, two different approaches are suggested. The first approach is called ‘block’, where the electrolyte is model as one whole domain with the complete thickness (instead of layers) and the measured electrolyte values are used. The other approach called ‘layered’, models the electrolyte as separate layers stacked one on top of the other and the average or single layer conductivity value is used. These two approaches are demonstrated in the figure 13 below. These two modeling approaches will be adopted.

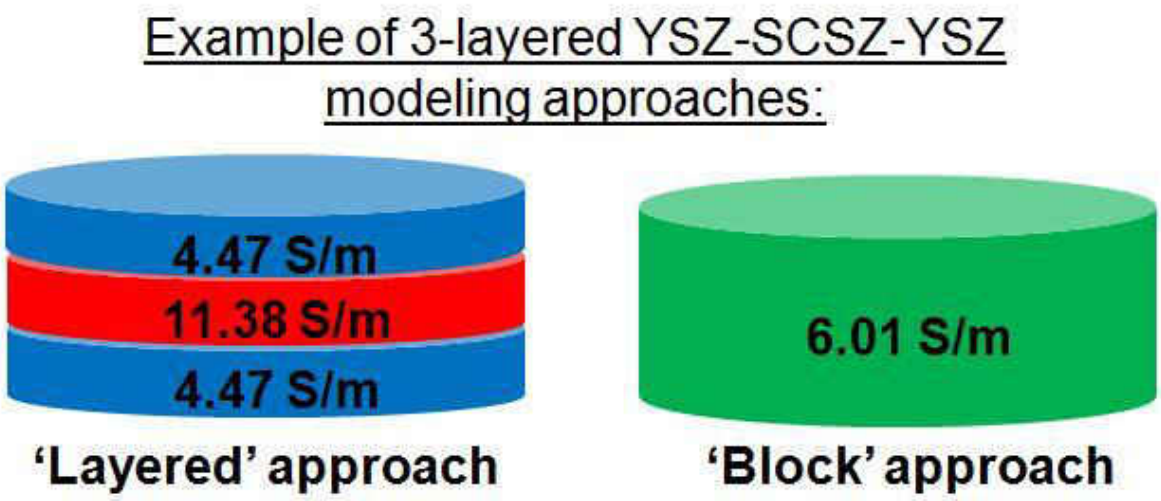

Figure 17. Comparison of the 'Layered' and 'Block' approach used to model the SOFC button cell.

4.4 Simulation Results

The results from the simulations of the 3, 4 and 6 layered electrolyte SOFC is presented in this section. A summary of the results can be seen in table 7. It can be clearly seen that the best performance is displayed by 3-layered SCSZ electrolyte modeled using the 'block' approach. The rest of the results will comprise of the current-voltage (or i-V) plots, power density curves and some pressure and velocity plots. First, we will look at the results for pure YSZ and SCSZ electrolyte SOFC and then we will look at the results from layered YSZ-SCSZ electrolyte cells.

Table 8. Summary of results – Power density.

Max Power Density [W/m^2]						
	Layered approach			Block approach		
	YSZ	SCSZ	YSZ-SCSZ-YSZ	SCSZ	YSZ	YSZ-SCSZ-YSZ
3-layered	1230.38	*1418.27*	1288.60	1403.07	1222.24	1292.60
4-layered	1128.39	1355.68	1231.07	1378.76	1150.14	1260.67
6-layered	997.91	1270.77	1163.75	1273.77	*980.96*	1206.36

Table 9. Summary of results – Current density.

Max Current Density [A/m^2]						
	Layered approach			Block approach		
	YSZ	SCSZ	YSZ-SCSZ-YSZ	SCSZ	YSZ	YSZ-SCSZ-YSZ
3-layered	4811.08	*5711.59*	5080.99	5642.40	4785.57	5112.91
4-layered	4363.71	5421.11	4831.36	5520.44	4454.40	4960.35
6-layered	3788.04	5018.85	4523.73	5035.89	*3716.11*	4722.63

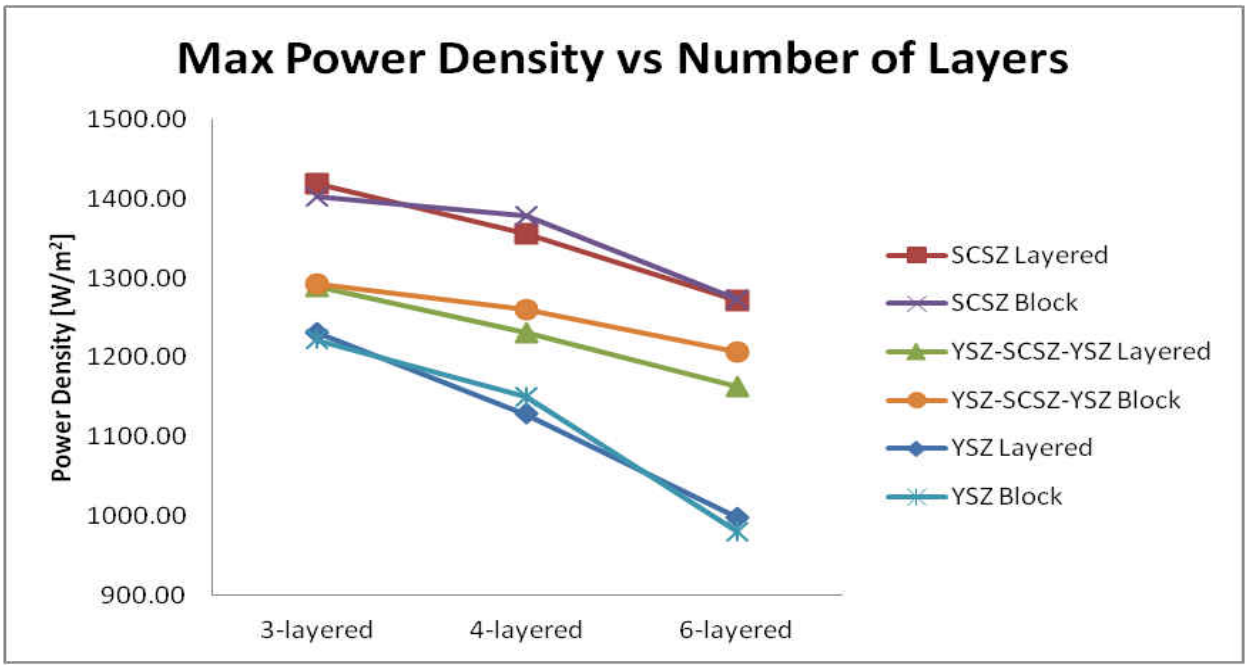

Figure 18 Maximum power density versus number of electrolyte layers.

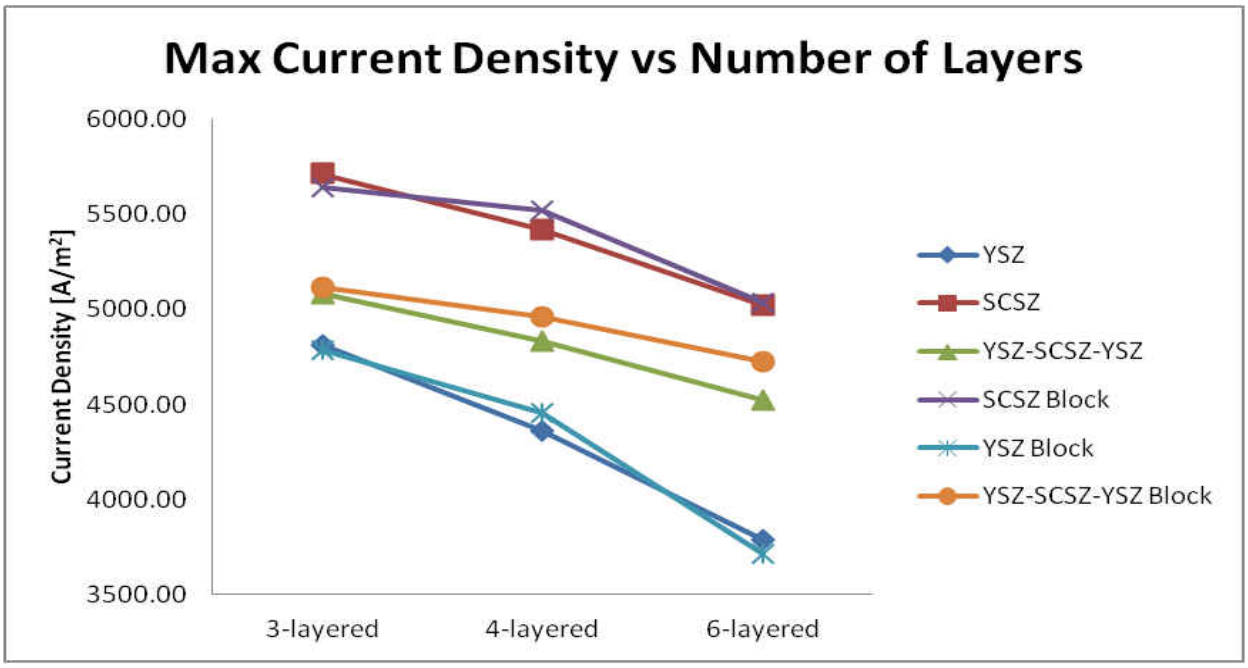

Figure 19 Maximum current density versus number of electrolyte layers.

The rest of the results will comprise of the current-voltage (or i-V) plots, power density curves and some pressure and velocity plots. First, we will look at the results for pure YSZ and SCSZ electrolyte SOFC and then we will look at the results from layered YSZ-SCSZ electrolyte cells.

4.4.1 Results of 3-, 4-, 6-layered electrolyte SOFC

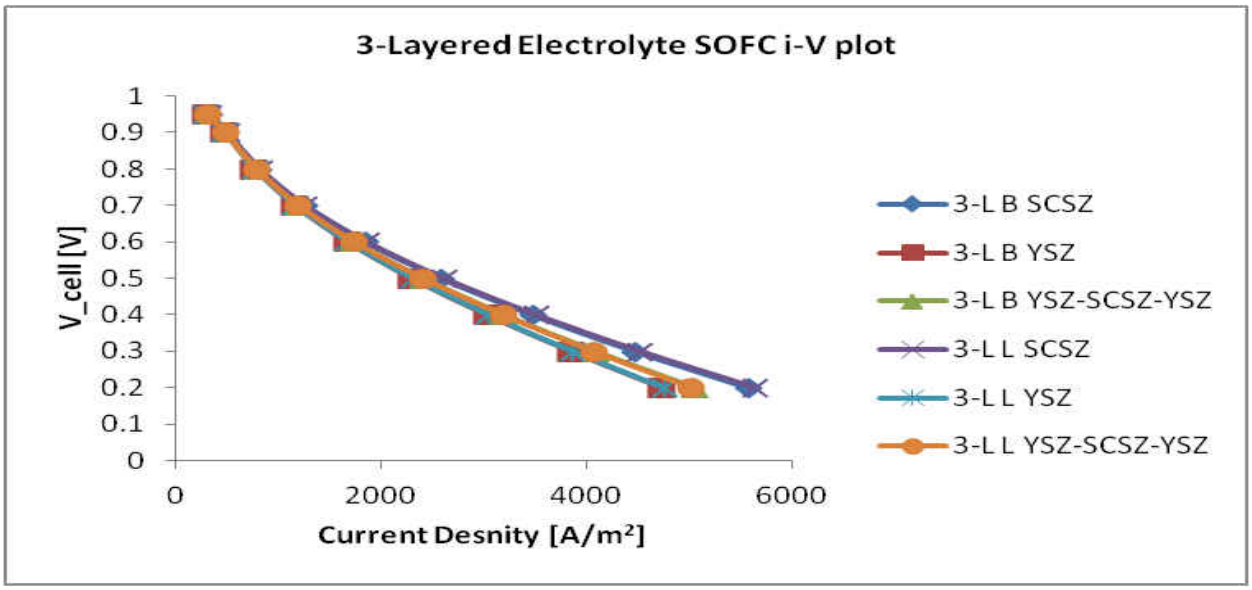

Figure 20 Current-voltage plots of 3-Layered Electrolyte SOFC. Format: 3-Layered Block/Layered Electrolyte Material

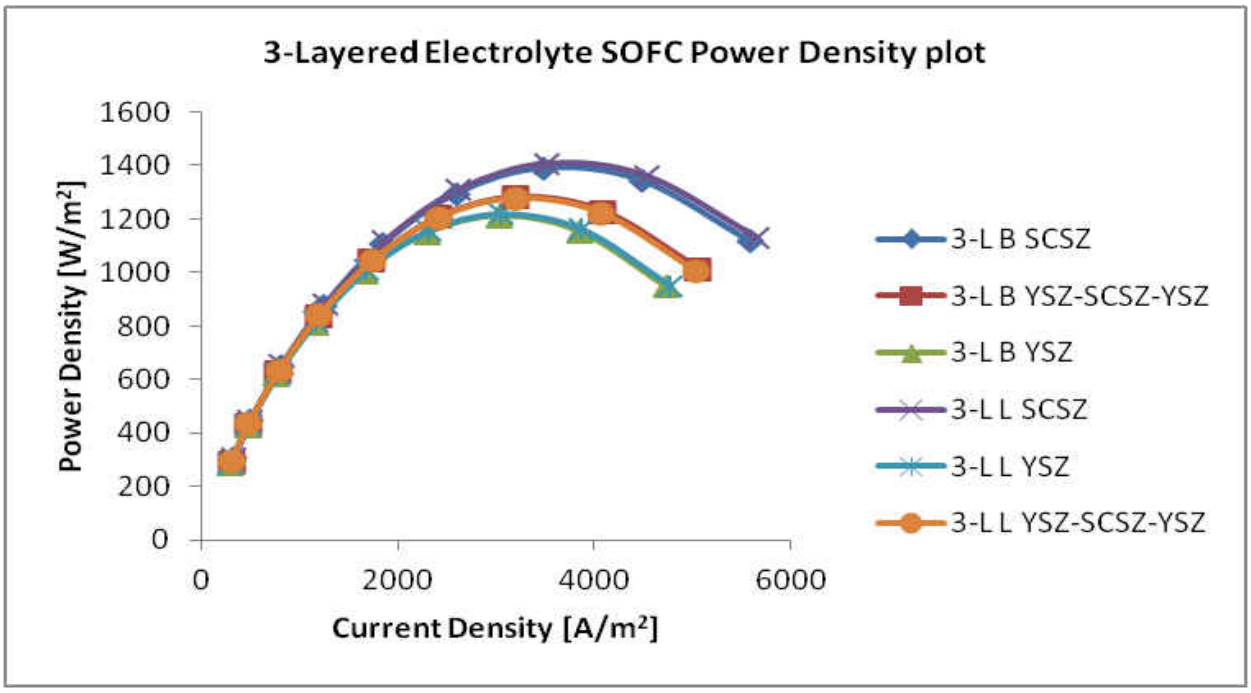

Figure 21 Power-voltage plots of 3-Layered Electrolyte SOFC. Format: 3-Layered Block/Layered Electrolyte Material

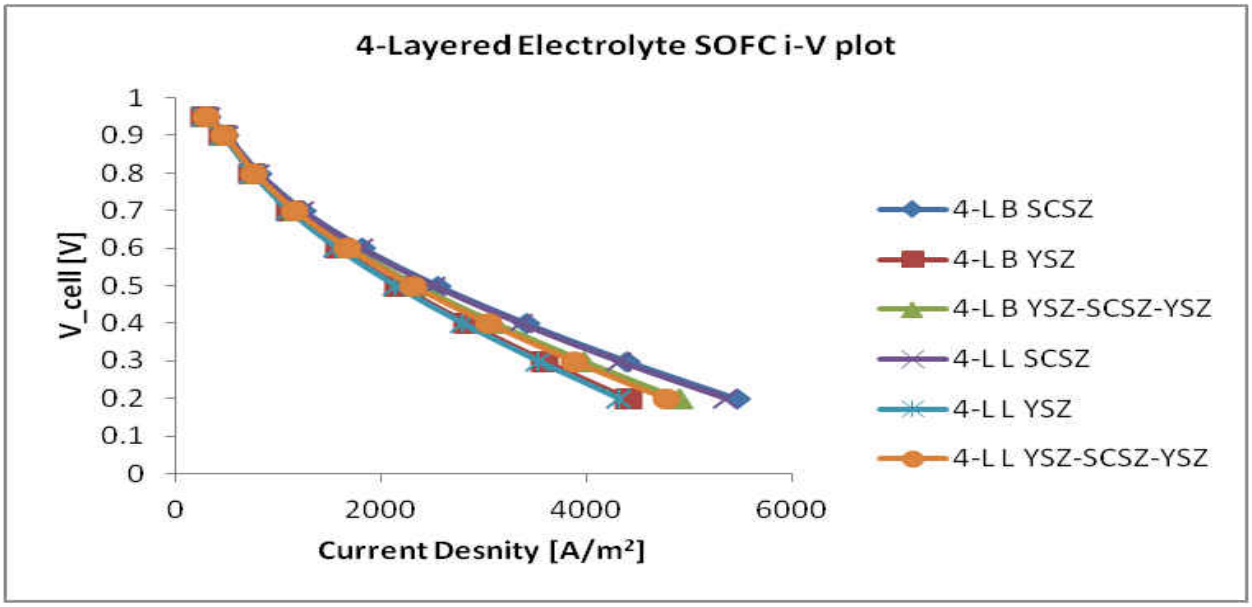

Figure 22 Current-voltage plots of 4-Layered Electrolyte SOFC. Format: 4-Layered Block/Layered Electrolyte Material

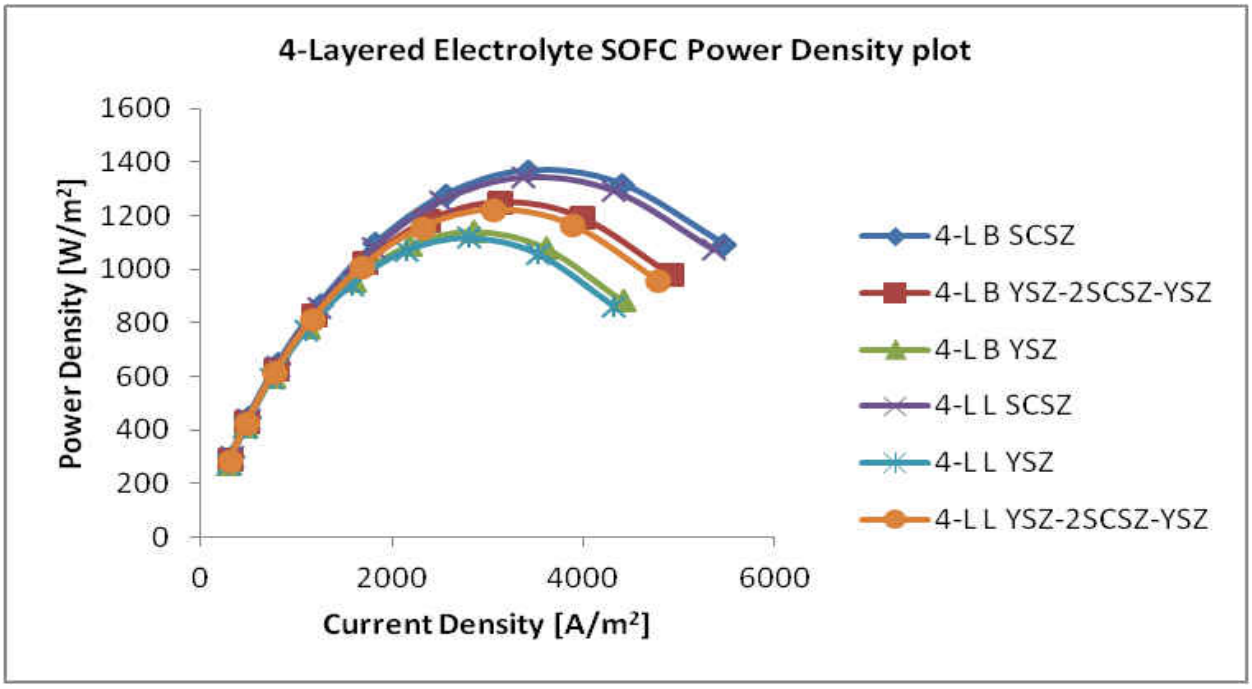

Figure 23 Power density plots of 4-Layered Electrolyte SOFC. Format: 4-Layered Block/Layered Electrolyte Material

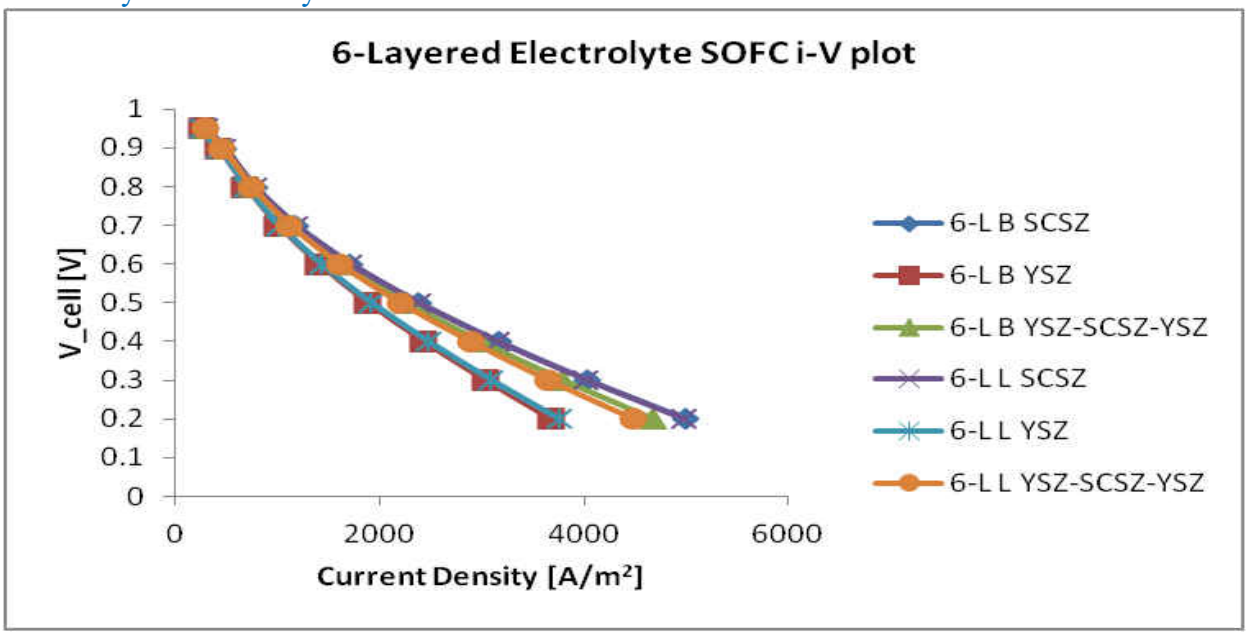

Figure 24 Current-voltage plots of 6-Layered Electrolyte SOFC. Format: 6-Layered Block/Layered Electrolyte Material

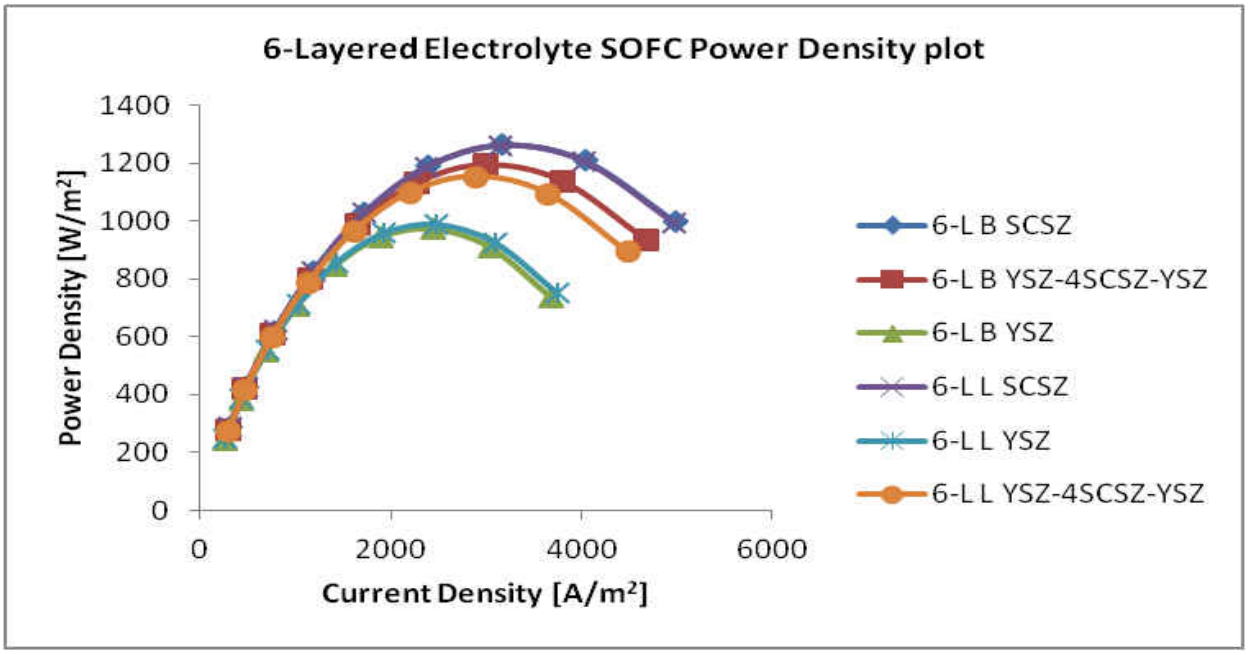

Figure 25 Power-current density plots of 6-Layered Electrolyte SOFC. Format: 6-Layered Block/Layered Electrolyte Material

4.5. Model Validation

Validation of any numerical model is critical to consider the model accurate and reliable. In general researchers validate numerical models or methodology against experimental data. Simulation of SOFC especially, involves a large number of equations and parameters. The final result produced depends on the modeling methodology, algorithm, governing equations, volume & boundary conditions, properties of materials, discretization scheme and post-processing of the data. Once the results from the model matches that of experiments, then the model can be declared as validated. A validated model can be used for optimization of the system, parametric studies and in some cases to validate experimental results. The validation of the model developed in this research was validated by the work of Sembler et al. [15]. Three papers were considered initially to be used for validation – Virkar et al [23], Akhtar et al. [16] and Sembler et al [15]. Of

the three papers, Virkar et al. was missing information about a lot of parameters and material properties. The SOFC modeled in Akhtar et al. was very different from the SOFC being modeled in this research, and therefore was not chosen. Sembler et al. provided a lot of required parameters needed. The paper by Sembler at al. is actually a numerical simulation study and it was validated against the experimental results of anode-supported SOFC produced by Joongmyeon Bae et al. [43]. The paper by Joongmyeon Bae et al. showed i-V plots for temperatures of 650 ^{0}C and 750 ^{0}C. The paper by Sembler et al, however, had i-V plots for 650 ^{0}C, 750 ^{0}C and 850 ^{0}C. For this reason the paper by Sembler et al. was chosen.

In the process of validating the model, a lot of important discoveries were made regarding the SOFC modeling methodology. There are some key parameters that cannot be measured by experimental techniques. These parameters are charge transfer coefficient (α) at anode and cathode; and exchange current density at anode and cathode ($j^0{}_o$); appearing in the Butler-Volmer equation.

$$j = j^0{}_0\left[\frac{c_R^*}{c_R^{0*}}\exp\left\{\frac{n\alpha F}{RT}\eta\right\} - \frac{c_P^*}{c_P^{0*}}\exp\left\{\frac{-n(1-\alpha)F}{RT}\eta\right\}\right]$$

It was learned by contacting authors of papers published in SOFC modeling, that these values can be assumed so as to fit the experimental results. The charge transfer coefficient is assumed by most researchers to be equal to be 0.5, and this value makes sense because 0.5 means the forward reaction rate is equal to the backward reaction rate. Therefore, the value of α was assumed to be 0.5. Now the exchange current density at anode and cathode were varied so as to fit the experimental data, by keeping all other conditions and parameters constant. This process

was followed for 1123 K, 1023 K and 923 K. As can be seen in figure #, the simulations results match the results from the paper. This proves the validity of the modeling methodology used and now the model can be declared validated.

Now that the model is validated, the next step would be do a parametric study of the SOFC to determine the significant parameters that affect the efficiency and power output of the cell which will be discussed in the next section.

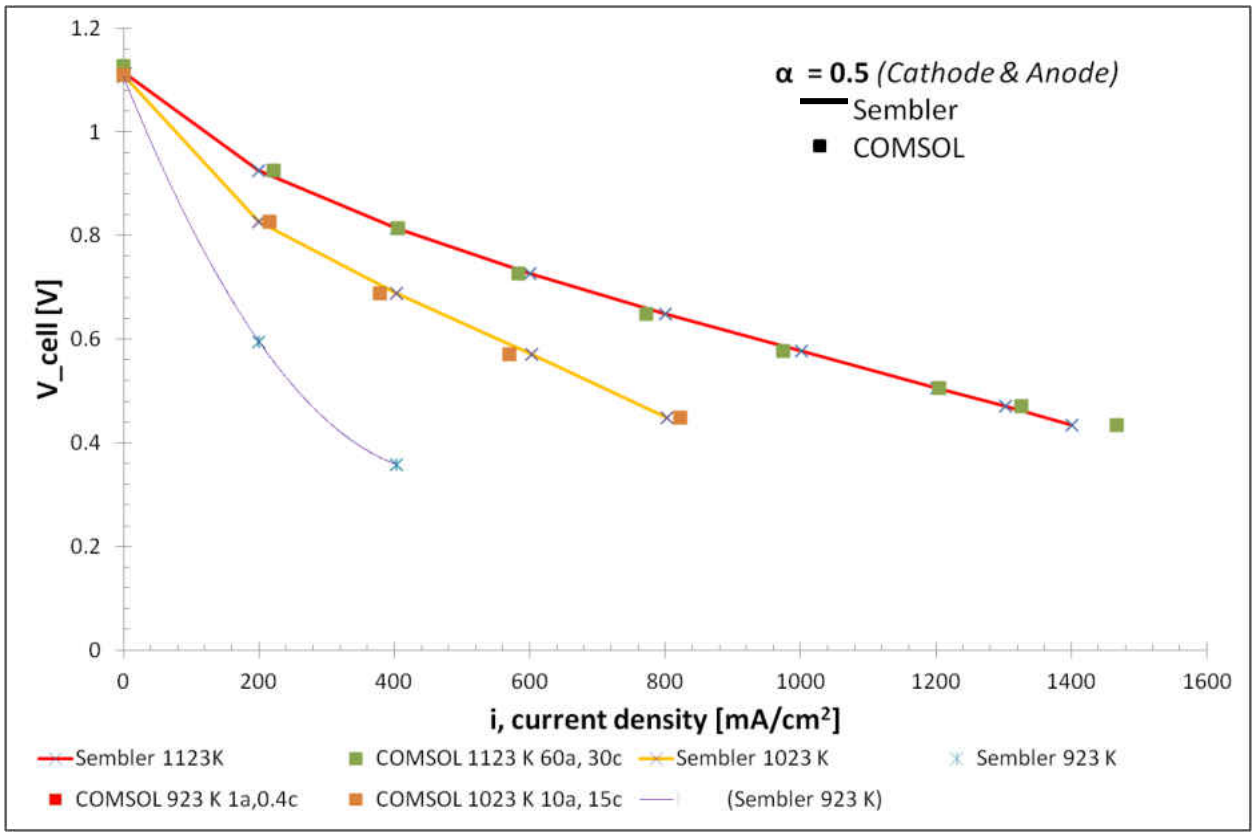

Figure 26. Model validation – the simulation results are plotted against results from Sembler et al. [15] at 1123 K, 1023 K and 923 K.

4.6. Parametric Study

As it can be observed, SOFC modeling involves a large number of parameters that affect the cell performance. These parameters affect different aspects of the cell's performance and hence it is important to study them individually. By this process, the parameters can be narrowed down to a few that have a significant impact and influence on the cell's behavior. The Table 9 below summarizes the effects of different parameters on the maximum current and power density of the cell. Following the table are different plots of these parameters affecting the performance shown individually.

Table 10 Summary of the parametric study on a SOFC

Summary of the parametric study on SOFC					
#	**Parameter**	**Range**	**Max % variation in Power density**	**Max % variation in Current density**	**Notes**
1	Overall Pressure	1 - 100 atm	0	0	
2	Anode Pressure	0.1 - 100 Pa	0	0	
3	Cathode Pressure	0.1 - 100 Pa	0	0	
4	Temperature	0 - 10000 ^{o}C	201.60%	201.60%	Effect on material properties not included
5	Viscosity - Anode	$1x10^{-6}$ - 1 Pa.s	< 1%	< 1%	No solution at 10+ Pa*s, affects flow slightly but not performance
6	Viscosity - Cathode	$3x10^{-7}$- 10 Pa.s	4.83%	4.83%	
7	Exchange current – Anode	0.01 - 100 A/m^2	-42.80%	-42.80%	
8	Exchange current - Cathode	0.001 - 0.1 A/m^2	253.60%	253.60%	
9	Specific Surface Area - Anode	$1x10^{6}$- $1x10^{12}$ m^{-1}	-98.90%	-98.90%	
10	Specific Surface Area - Cathode	$1x10^{6}$ – $1x10^{12}$ m^{-1}	327.22%	327.22%	
11	Permeability - Anode	$1x10^{-13}$ - 1 m^2	0	0	
12	Permeability - Cathode	$1x10^{-13}$ - 1 m^2	0	0	
13	Open Boundary Condition	Yes/no	0	0	Flow properties changed but not current
14	Electrolyte Conductivity	1 - 15 S/m	-63.35%	-63.35%	

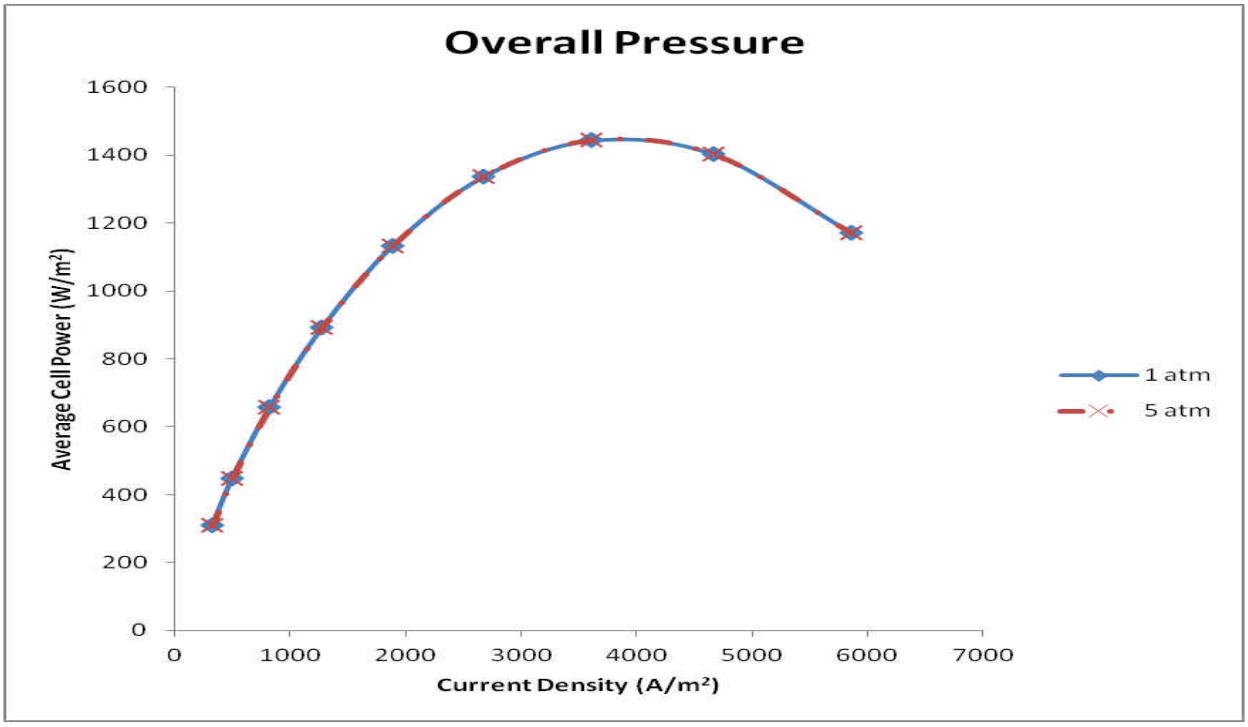

Figure 27 Effect of anode partial pressure on current and power density.

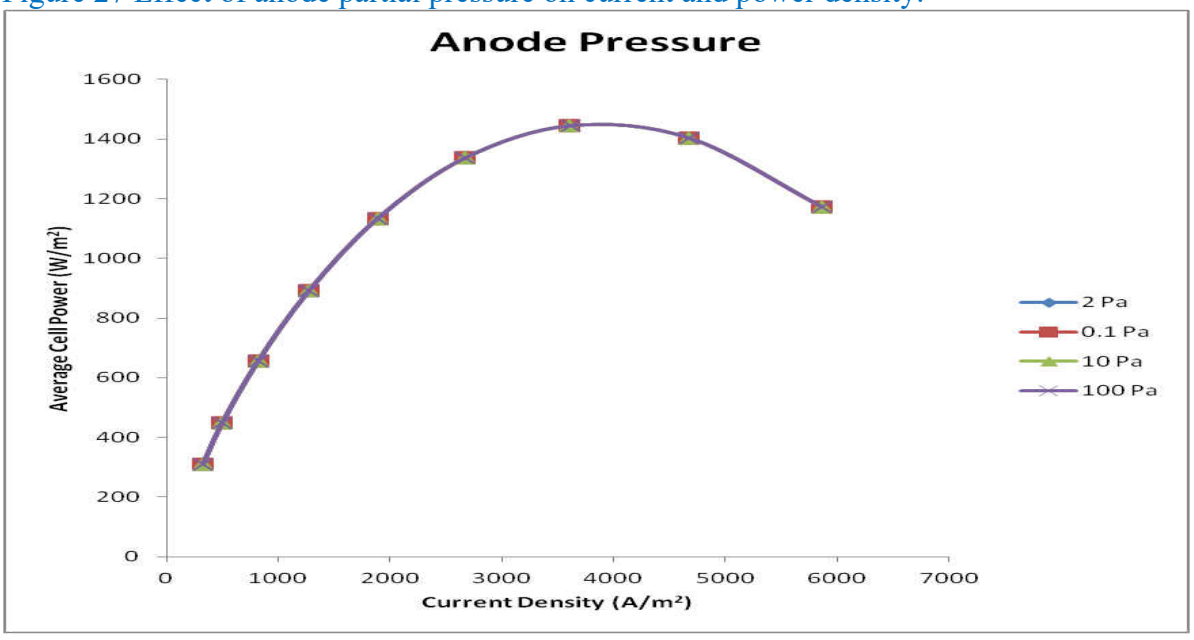

Figure 28 Effect of anode partial pressure on current and power density.

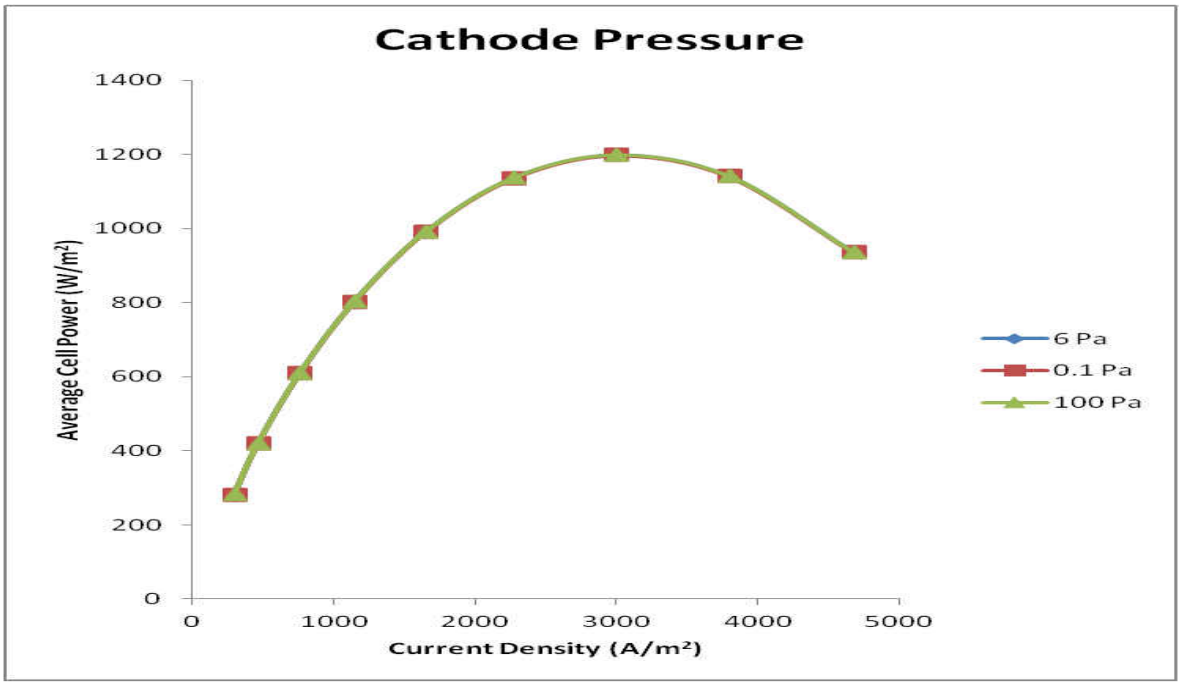

Figure 29 Effect of cathode partial pressure on current and power density.

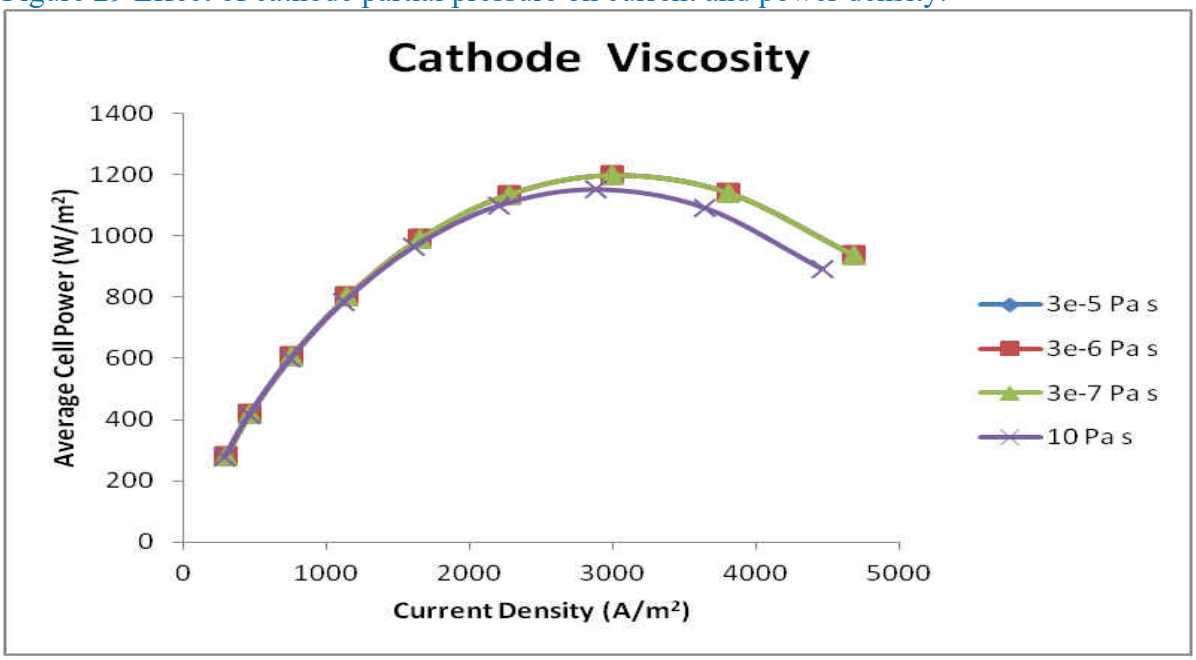

Figure 30 Effect of viscosity of gases at the cathode on current and power density.

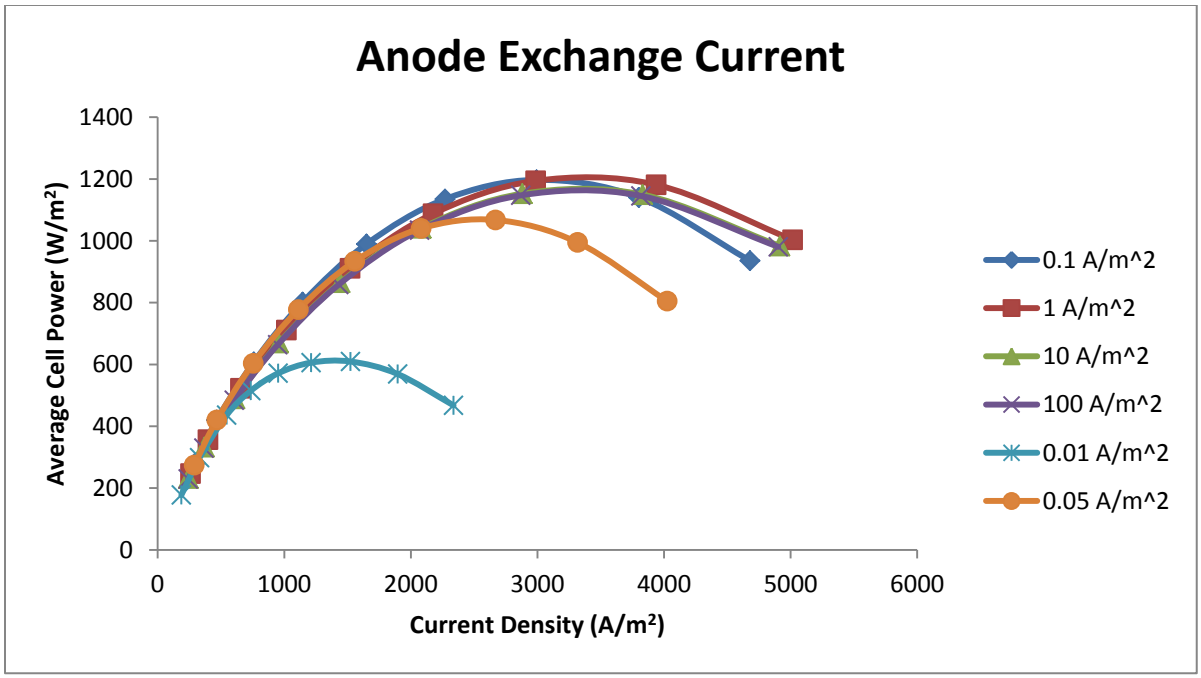

Figure 31 Effect of anode exchange current density on current and power density.

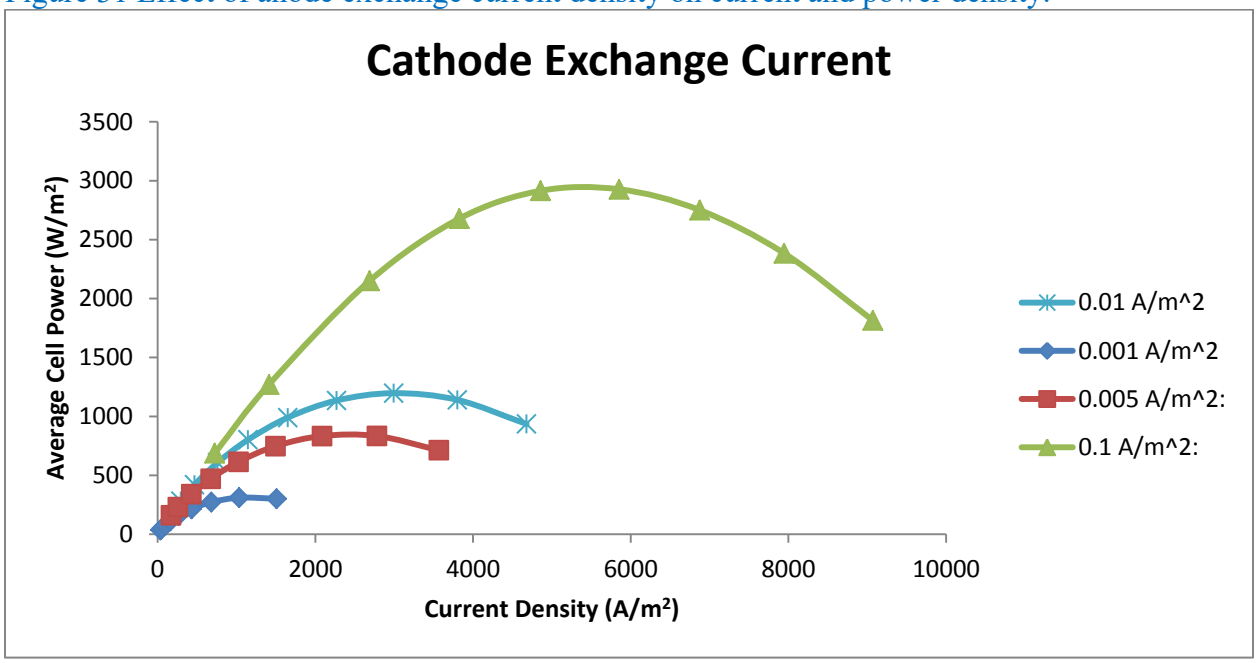

Figure 32 Effect of cathode exchange current density on current and power density.

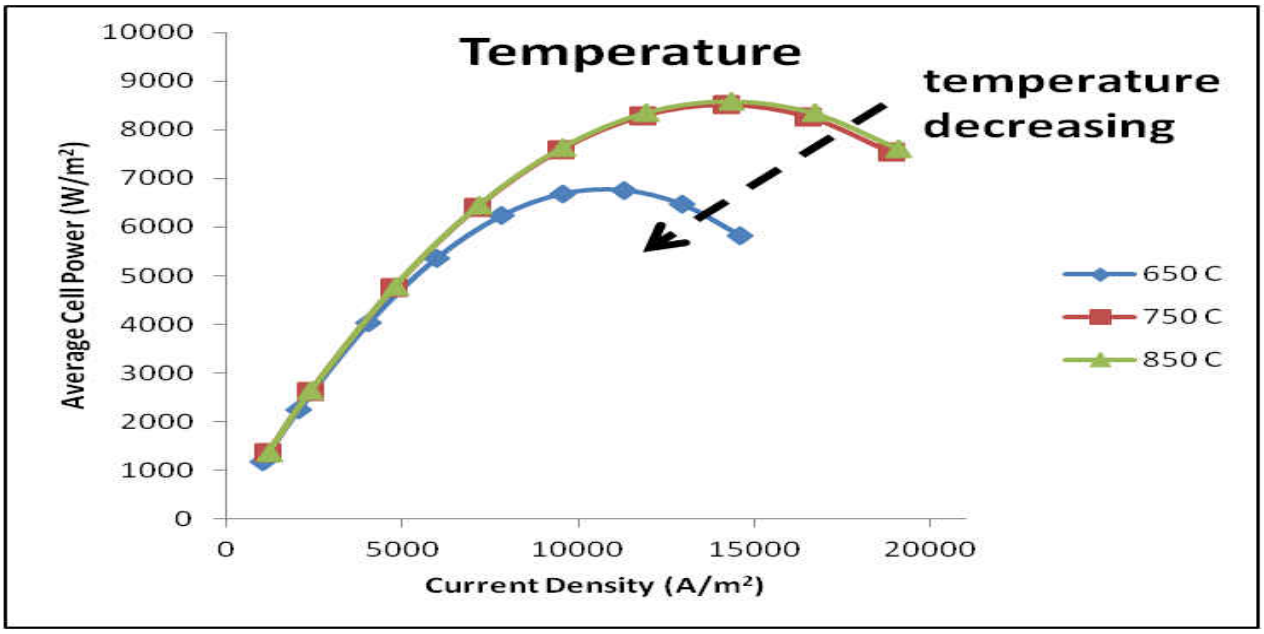

Figure 33 Effect of temperature on current and power density.

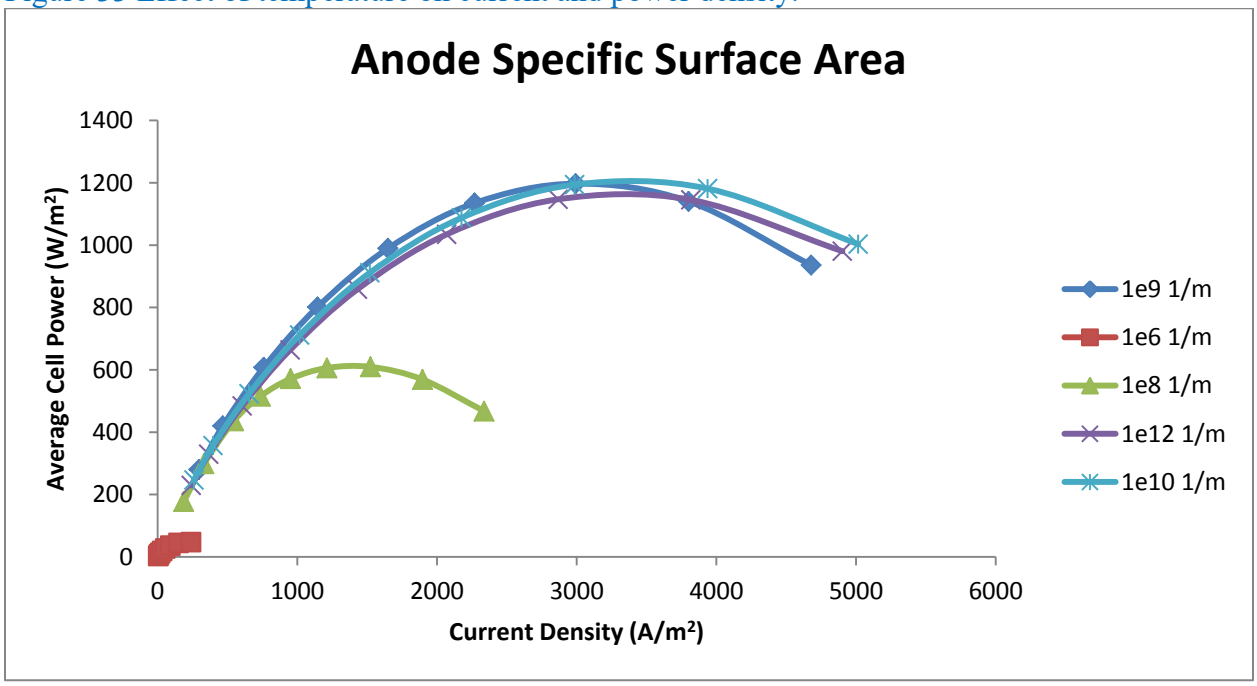

Figure 34 Effect of anode specific surface area on current and power density

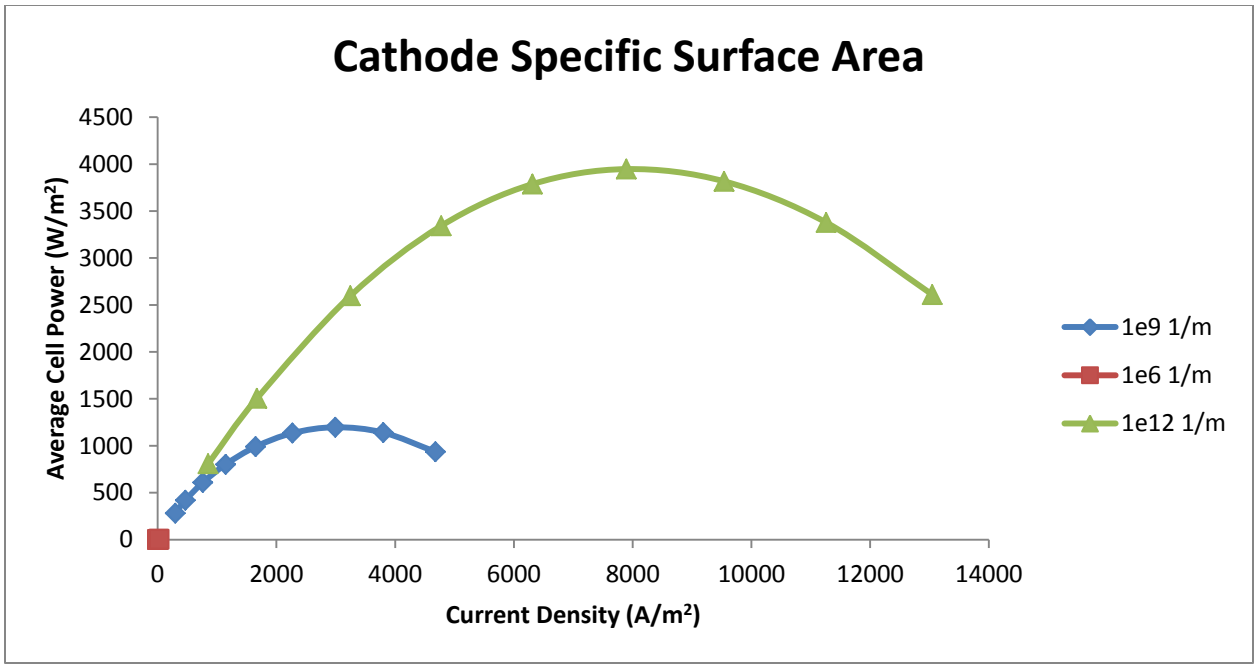

Figure 35 Effect of cathode specific surface area on current and power density

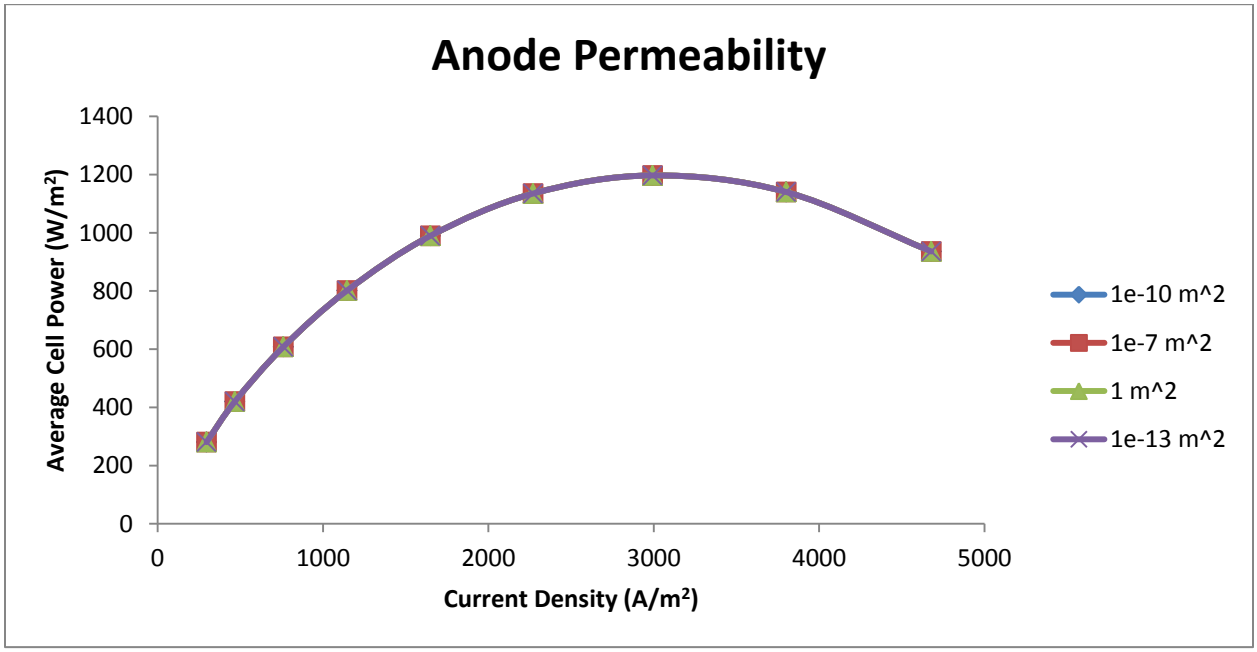

Figure 36 Effect of permeability of anode electrode on current and power density

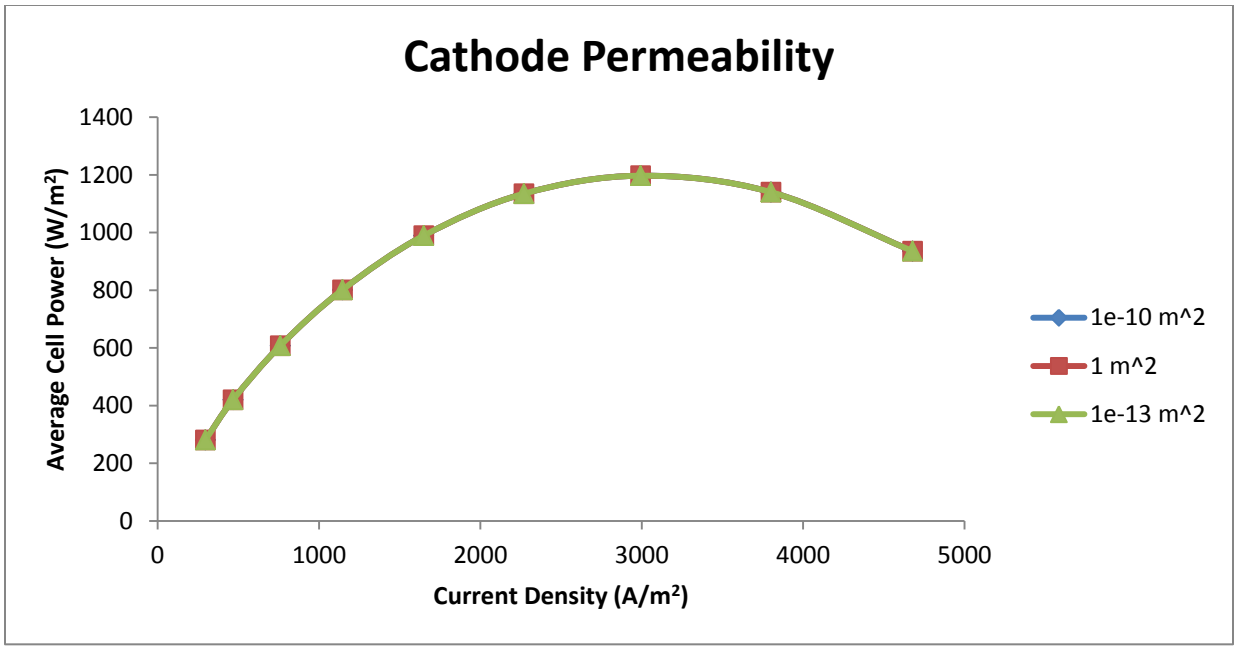

Figure 37 Effect of permeability of cathode electrode on current and power density

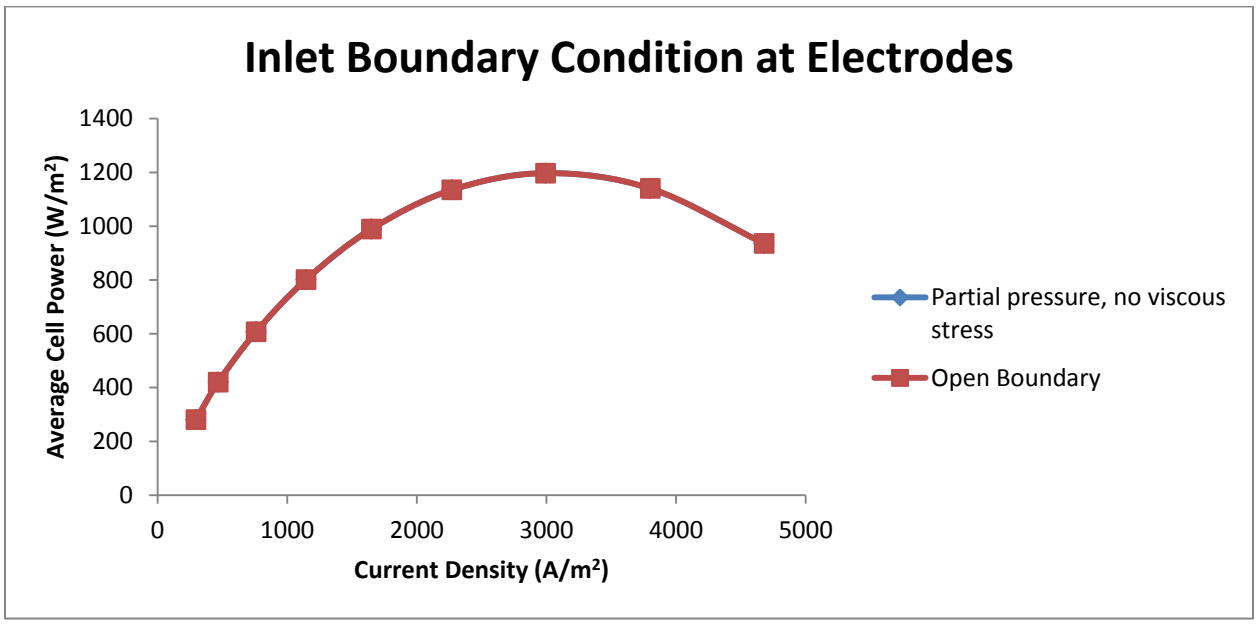

Figure 38 Effect of inlet boundary conditions of gases at electrodes, on current and power density.

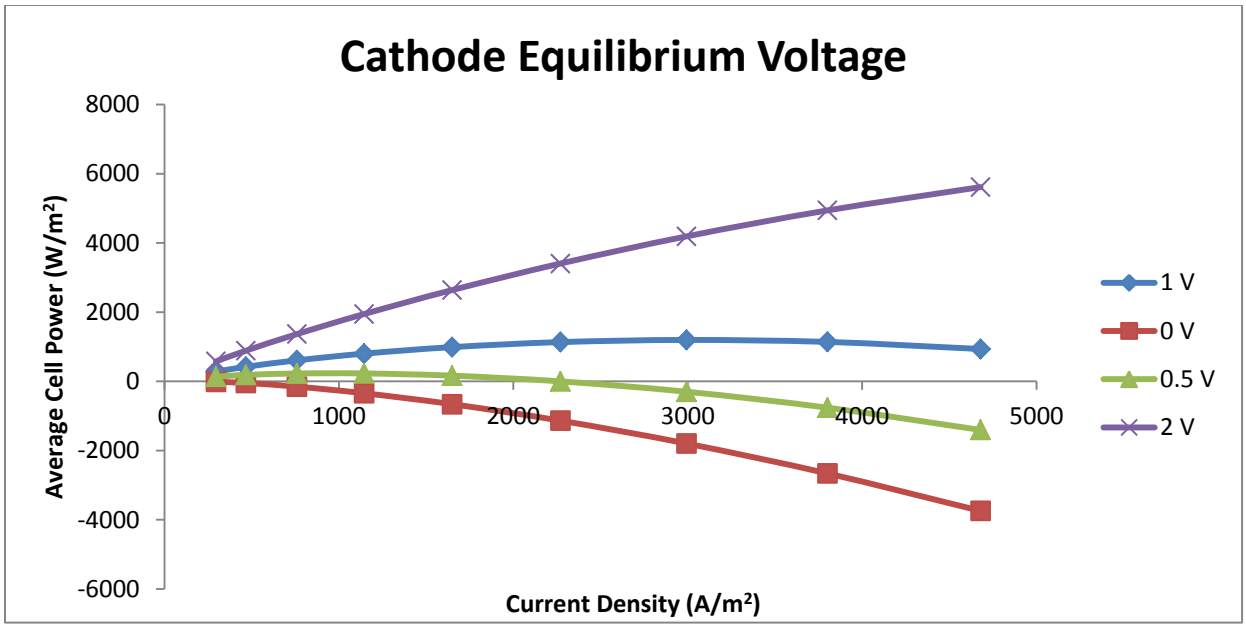

Figure 39 Effect of equilibrium voltage at cathode on current and power density.

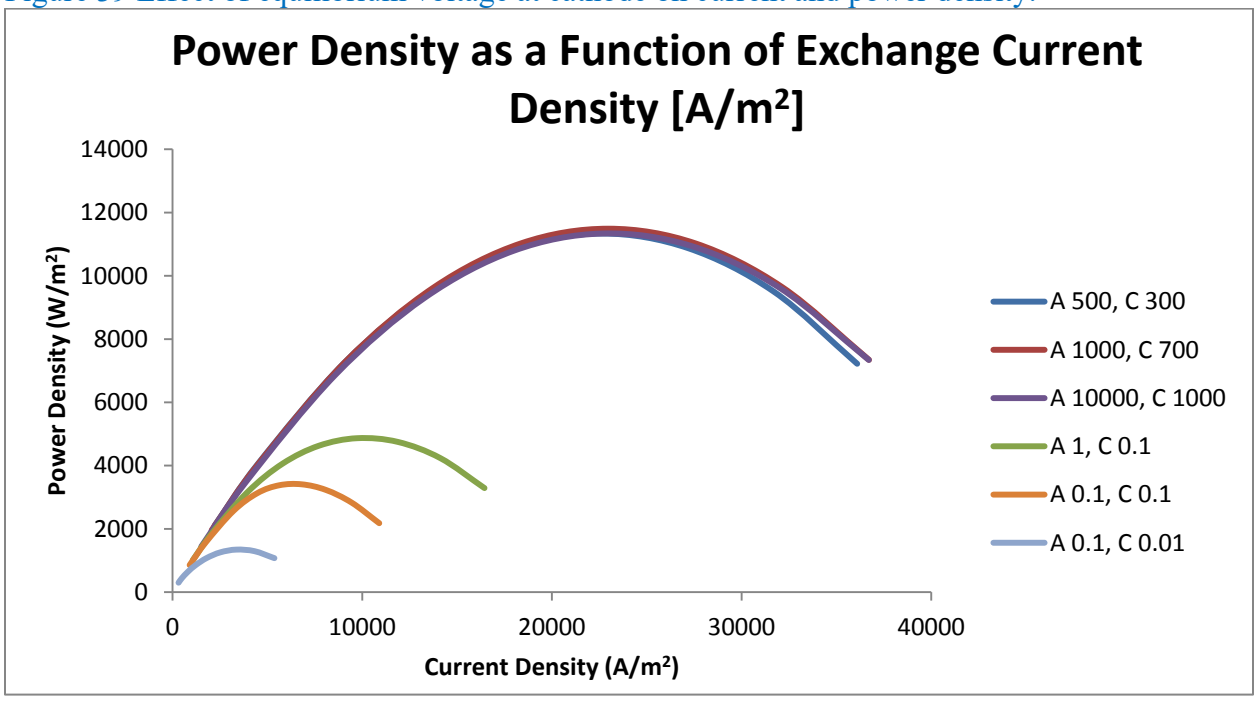

Figure 40 Current and power density of SOFC at various values of anode (A) & cathode (C) exchange current density.

As it can be observed in the graphs above, there are few parameters that have a significant impact on the cell performance. The most significant parameters include temperature, anode exchange current, cathode exchange current, anode specific surface area, cathode specific surface area, equilibrium voltage at cathode, electrolyte conductivity, anode charge transfer coefficient and cathode charge transfer coefficient. On comparing the results with the parametric study done by Akhtar et al. in their paper [35], it can be seen that the results are in agreement although the type of SOFC is different. Pressure and permeability seem to not be significant factors that affect cell performance. On the other hand, cathode exchange current density has a very high impact on the cell performance. Also, the anode exchange current density seems have an effect on performance to a certain limited extent. The conclusion that increasing operating temperature increases cell performance can also be seen in the paper by Arpornwichanop et al. [17]. Using the results above, researchers can focus their attention on the optimizing the parameters that do affect cell performance. This is the advantage of modeling a fuel cell; it supports and forwards the commitment of building high performance fuel cells.

CHAPTER 5: CONCLUSION

The purpose of this thesis was to model a solid oxide fuel cell and use the model to analyze Solid Oxide Fuel Cells (SOFC) with different electrolyte materials and configurations. A working model successfully developed. The SOFC model was built as per specifications of the SOFC that is intended to be developed in the lab. The model was then validated against experimental data of a different SOFC. The purpose of using a layered electrolyte design was to harness the superior ionic conductivity of SCSZ; and the superior mechanical and chemical stability of YSZ. The conductivity tests show that the layered electrolytes using SCSZ and YSZ have proven to have conductivity values better than YSZ, and lower than SCSZ. The results from the modeling seem coherent with the conductivity tests; such that the performance of SOFC with the YSZ-xSCSZ-YSZ layered electrolytes are better than those SOFC using pure YSZ but lower than those SOFC using SCSZ as their electrolyte material. Also, it was seen that as thickness of the electrolyte increased the performance went down. This result is obviously due to the fact that the increase in electrolyte thickness will result in higher Ohmic resistance. The choice of the number of electrolyte layers will then be a balance between the mechanical strength and the ionic conductivity required for the particular application. Other factors involved in the choice could include the fuel cell system design and the density of cells required (number of single cells in a system of given size).

A parametric study of the SOFC was also carried out to identify the significant parameters that affect cell performance. It is to be noted that the exchange current density at anode and cathode electrodes is a critical factor and can be estimated by curve fitting the modeling data against experimental data. The key parameters that seem to significantly affect cell performance include

exchange current density at both electrodes, the specific area of electrodes especially the cathode and the ionic conductivity of the electrolyte.

Future work will include the incorporating heat transfer physics in the model. This will help understand the temperature distribution within the cell, the results thermal stresses and their effect on other aspects of the cell. Once the cells are actually developed and tested in the laboratory the model can be further improved and will aid in better design of the cells being produced. Also, an important future study will be Finite Element Modeling (FEM) of the mechanical strength testing of the electrolytes. The focus will be on the biaxial flexural strength. This will help understand the relationship between the load applied, fracture strength and deflection of the electrolyte. Combining the FEM model results of the electrolytes and the SOFC model discussed in this thesis will provide the opportunity to choose the optimum number of layers of electrolyte, mechanical strength versus the power density of the cell.

APPENDIX: COPYRIGHT PERMISSION LETTER

JOHN WILEY AND SONS LICENSE

TERMS AND CONDITIONS

Jul 12, 2012

This is a License Agreement between Amjad Aman ("You") and John Wiley and Sons ("John Wiley and Sons") provided by Copyright Clearance Center ("CCC"). The license consists of your order details, the terms and conditions provided by John Wiley and Sons, and the payment terms and conditions.

All payments must be made in full to CCC. For payment instructions, please see information listed at the bottom of this form.

License Number

2860900699692

License date

Mar 02, 2012

Licensed content publisher

John Wiley and Sons

Licensed content publication

Wiley Books

Licensed content title

Fuel Cell Fundamentals, 2nd Edition

Licensed content author

Ryan O'Hayre, Suk-Won Cha, Whitney Colella, Fritz B. Prinz

Licensed content date

Jan 1, 2009

Type of use

Dissertation/Thesis

Requestor type

University/Academic

Format

Print and electronic

Portion

Figure/table

Number of figures/tables

3

Number of extracts

Original Wiley figure/table number(s)

From first edition of the book: Fig 1.9, 1.10 From second edition: Fig 2.9

Will you be translating?

No

Order reference number

Total

0.00 USD

Terms and Conditions

TERMS AND CONDITIONS

This copyrighted material is owned by or exclusively licensed to John Wiley & Sons, Inc. or one of its group companies (each a "Wiley Company") or a society for whom a Wiley Company has exclusive publishing rights in relation to a particular journal (collectively WILEY"). By clicking "accept" in connection with completing this licensing transaction, you agree that the following terms and conditions apply to this transaction (along with the billing and payment terms and conditions established by the Copyright Clearance Center Inc., ("CCC's Billing and Payment

terms and conditions"), at the time that you opened your Rightslink account (these are available at any time at http://myaccount.copyright.com)

Terms and Conditions

1. The materials you have requested permission to reproduce (the "Materials") are protected by copyright.

2. You are hereby granted a personal, non-exclusive, non-sublicensable, non-transferable, worldwide, limited license to reproduce the Materials for the purpose specified in the licensing process. This license is for a one-time use only with a maximum distribution equal to the number that you identified in the licensing process. Any form of republication granted by this licence must be completed within two years of the date of the grant of this licence (although copies prepared before may be distributed thereafter). The Materials shall not be used in any other manner or for any other purpose. Permission is granted subject to an appropriate acknowledgement given to the author, title of the material/book/journal and the publisher. You shall also duplicate the copyright notice that appears in the Wiley publication in your use of the Material. Permission is also granted on the understanding that nowhere in the text is a previously published source acknowledged for all or part of this Material. Any third party material is expressly excluded from this permission.

3. With respect to the Materials, all rights are reserved. Except as expressly granted by the terms of the license, no part of the Materials may be copied, modified, adapted (except for minor reformatting required by the new Publication), translated, reproduced, transferred or distributed, in any form or by any means, and no derivative works may be made based on the Materials without the prior permission of the respective copyright owner. You may not alter, remove or suppress in any manner any copyright, trademark or other notices displayed by the Materials. You may not license, rent, sell, loan, lease, pledge, offer as security, transfer or assign the Materials, or any of the rights granted to you hereunder to any other person.

4. The Materials and all of the intellectual property rights therein shall at all times remain the exclusive property of John Wiley & Sons Inc or one of its related companies (WILEY) or their respective licensors, and your interest therein is only that of having possession of and the right to reproduce the Materials pursuant to Section 2 herein during the continuance of this Agreement. You agree that you own no right, title or interest in or to the Materials or any of the intellectual property rights therein. You shall have no rights hereunder other than the license as provided for above in Section 2. No right, license or interest to any trademark, trade name, service mark or other branding ("Marks") of WILEY or its licensors is granted hereunder, and you agree that you shall not assert any such right, license or interest with respect thereto.

5. NEITHER WILEY NOR ITS LICENSORS MAKES ANY WARRANTY OR REPRESENTATION OF ANY KIND TO YOU OR ANY THIRD PARTY, EXPRESS, IMPLIED OR STATUTORY, WITH RESPECT TO THE MATERIALS OR THE ACCURACY

OF ANY INFORMATION CONTAINED IN THE MATERIALS, INCLUDING, WITHOUT LIMITATION, ANY IMPLIED WARRANTY OF MERCHANTABILITY, ACCURACY, SATISFACTORY QUALITY, FITNESS FOR A PARTICULAR PURPOSE, USABILITY, INTEGRATION OR NON-INFRINGEMENT AND ALL SUCH WARRANTIES ARE HEREBY EXCLUDED BY WILEY AND ITS LICENSORS AND WAIVED BY YOU.

6. WILEY shall have the right to terminate this Agreement immediately upon breach of this Agreement by you.

7. You shall indemnify, defend and hold harmless WILEY, its Licensors and their respective directors, officers, agents and employees, from and against any actual or threatened claims, demands, causes of action or proceedings arising from any breach of this Agreement by you.

8. IN NO EVENT SHALL WILEY OR ITS LICENSORS BE LIABLE TO YOU OR ANY OTHER PARTY OR ANY OTHER PERSON OR ENTITY FOR ANY SPECIAL, CONSEQUENTIAL, INCIDENTAL, INDIRECT, EXEMPLARY OR PUNITIVE DAMAGES, HOWEVER CAUSED, ARISING OUT OF OR IN CONNECTION WITH THE DOWNLOADING, PROVISIONING, VIEWING OR USE OF THE MATERIALS REGARDLESS OF THE FORM OF ACTION, WHETHER FOR BREACH OF CONTRACT, BREACH OF WARRANTY, TORT, NEGLIGENCE, INFRINGEMENT OR OTHERWISE (INCLUDING, WITHOUT LIMITATION, DAMAGES BASED ON LOSS OF PROFITS,

DATA, FILES, USE, BUSINESS OPPORTUNITY OR CLAIMS OF THIRD PARTIES), AND WHETHER OR NOT THE PARTY HAS BEEN ADVISED OF THE POSSIBILITY OF SUCH DAMAGES. THIS LIMITATION SHALL APPLY NOTWITHSTANDING ANY FAILURE OF ESSENTIAL PURPOSE OF ANY LIMITED REMEDY PROVIDED HEREIN.

9. Should any provision of this Agreement be held by a court of competent jurisdiction to be illegal, invalid, or unenforceable, that provision shall be deemed amended to achieve as nearly as possible the same economic effect as the original provision, and the legality, validity and enforceability of the remaining provisions of this Agreement shall not be affected or impaired thereby.

10. The failure of either party to enforce any term or condition of this Agreement shall not constitute a waiver of either party's right to enforce each and every term and condition of this Agreement. No breach under this agreement shall be deemed waived or excused by either party unless such waiver or consent is in writing signed by the party granting such waiver or consent. The waiver by or consent of a party to a breach of any provision of this Agreement shall not operate or be construed as a waiver of or consent to any other or subsequent breach by such other party.

11. This Agreement may not be assigned (including by operation of law or otherwise) by you without WILEY's prior written consent.

12. Any fee required for this permission shall be non-refundable after thirty (30) days from receipt.

13. These terms and conditions together with CCC's Billing and Payment terms and conditions (which are incorporated herein) form the entire agreement between you and WILEY concerning this licensing transaction and (in the absence of fraud) supersedes all prior agreements and representations of the parties, oral or written. This Agreement may not be amended except in writing signed by both parties. This Agreement shall be binding upon and inure to the benefit of the parties' successors, legal representatives, and authorized assigns.

14. In the event of any conflict between your obligations established by these terms and conditions and those established by CCC's Billing and Payment terms and conditions, these terms and conditions shall prevail.

15. WILEY expressly reserves all rights not specifically granted in the combination of (i) the license details provided by you and accepted in the course of this licensing transaction, (ii) these terms and conditions and (iii) CCC's Billing and Payment terms and conditions.

16. This Agreement will be void if the Type of Use, Format, Circulation, or Requestor Type was misrepresented during the licensing process.

17. This Agreement shall be governed by and construed in accordance with the laws of the State of New York, USA, without regards to such state's conflict of law rules. Any legal action, suit or proceeding arising out of or relating to these Terms and Conditions or the breach thereof shall be instituted in a court of competent jurisdiction in New York County in the State of New York in the United States of America and each party hereby consents and submits to the personal jurisdiction of such court, waives any objection to venue in such court and consents to service of process by registered or certified mail, return receipt requested, at the last known address of such party.

Wiley Open Access Terms and Conditions

All research articles published in Wiley Open Access journals are fully open access: immediately freely available to read, download and share. Articles are published under the terms of the Creative Commons Attribution Non Commercial License. which permits use, distribution and reproduction in any medium, provided the original work is properly cited and is not used for commercial purposes. The license is subject to the Wiley Open Access terms and conditions:
Wiley Open Access articles are protected by copyright and are posted to repositories and websites in accordance with the terms of the Creative Commons Attribution Non Commercial License. At the time of deposit, Wiley Open Access articles include all changes made during peer review, copyediting, and publishing. Repositories and websites that host the article are responsible for incorporating any publisher-supplied amendments or retractions issued subsequently.

Use by commercial "for-profit" organizations

Use of Wiley Open Access articles for commercial, promotional, or marketing purposes requires further explicit permission from Wiley and will be subject to a fee. Commercial purposes include:

Copying or downloading of articles, or linking to such articles for further redistribution, sale or licensing;

Copying, downloading or posting by a site or service that incorporates advertising with such content;

The inclusion or incorporation of article content in other works or services (other than normal quotations with an appropriate citation) that is then available for sale or licensing, for a fee (for example, a compilation produced for marketing purposes, inclusion in a sales pack)

Use of article content (other than normal quotations with appropriate citation) by for-profit organisations for promotional purposes

Linking to article content in e-mails redistributed for promotional, marketing or educational purposes;

Use for the purposes of monetary reward by means of sale, resale, licence, loan, transfer or other form of commercial exploitation such as marketing products

Print reprints of Wiley Open Access articles can be purchased from: corporatesales@wiley.com

Other Terms and Conditions:

BY CLICKING ON THE "I AGREE..." BOX, YOU ACKNOWLEDGE THAT YOU HAVE READ AND FULLY UNDERSTAND EACH OF THE SECTIONS OF AND PROVISIONS SET FORTH IN THIS AGREEMENT AND THAT YOU ARE IN AGREEMENT WITH AND ARE WILLING TO ACCEPT ALL OF YOUR OBLIGATIONS AS SET FORTH IN THIS AGREEMENT.

v1.7

If you would like to pay for this license now, please remit this license along with your payment made payable to "COPYRIGHT CLEARANCE CENTER" otherwise you will be invoiced within 48 hours of the license date. Payment should be in the form of a check or money order referencing your account number and this invoice number RLNK500731390.

Once you receive your invoice for this order, you may pay your invoice by credit card. Please follow instructions provided at that time.

Make Payment To:

Copyright Clearance Center

Dept 001

P.O. Box 843006

Boston, MA 02284-3006

LIST OF REFERENCES

[1] Ryan O'Hayre, Suk-Won Cha, Whitney Colella, and Fritz B. Prinz, *Fuel Cell Fundamentals*, Wiley; 2nd edition, 2009.

[2] Subhash C Singhal and Kevin Kendall, *High-temperature Solid Oxide Fuel Cells: Fundamentals, Design and Applications*, Elsevier Science; 1st edition, 2003.

[3] Kevin Huang and John B. Goodenough, Solid oxide fuel cell technology: Principles, performance and operations, CRC Press; 1st edition, 2009.

[4] E. Bauer and H. Preis, 'Über Brennstoff-Ketten mit Festleitern', *Z. Elektrochem.*, 1937 **43** 727-732.

[5] B. A. Haberman and A. J. Marquis, A Numerical Investigation Into the Interaction Between Current Flow and Fuel Consumption in a Segmented-in-Series Tubular SOFC, *Journal of Fuel Cell Science and Technology,* August 2009, Vol. 6 / 031002-1.

[6] Yutong Qi, Biao Huang and Jingli Luo, Nonlinear State Space Modeling and Simulation of A SOFC Fuel Cell, *Proceedings of the 2006 American Control Conference Minneapolis*, Minnesota, USA, June 14-16, 2006.

[7] Mark C. Williams, Joseph P. Strakey and Wayne A. Surdoval, U.S. Department of Energy's Solid Oxide Fuel Cells: Technical Advances, *Int. J. Appl. Ceram. Technol.,* 2 [4] 295–300 (2005).

[8] Wolfgang Winkler and Hagen Lorenz, Design studies of mobile applications with SOFC–heat engine modules, Journal of Power Sources 106 (2002) 338–343.

[9] http://www.bloomenergy.com/

[10] www.comsol.com

[11] COMSOL® Multiphysics® 4.2 Help – Documentation.

[12] Raphaèle Herbin, Jean Michel Fiard, James R. Ferguson, Three-Dimensional Numerical Simulation of the Temperature, Potentail and Concentration Distributions of a Unit Cell for Various Geometries of SOFCs, *First European Solid Oxide Fule Cell Forum; proceedings;* 3-7 October 1994, Lucerne/ Switzerland. Pages: 317 – 326.

[13] Henning Severson, Mohsen Assadi, Modeling of Overpotentials in an Anode-Supported Planar SOFC Using a Detailed Simulation Model, *Journal of Fuel Cell Science and Technology*, October 2011, Vol. 8.

[14] Thinh X. Ho, Pawel Kosinski, Alex C. Hoffmann, Arild Vik, Numerical analysis of a planar anode-supported SOFC with composite electrodes, *International Journal of Hydrogen Energy*, 34 (2009) 3488-3499.

[15] William J. Sembler, Sunil Kumar, Optimization of a Single-Cell Solid-Oxide Fuel Cell Using Computational Fluid Dynamics, *Journal of Fuel Cell Science and Technology*, April 2011, Vol. 8.

[16] Naveed Akhtar, Stephen P. Decent, Daniel Loghin, Kevin Kendall, Modeling of Co-planar Type Single-Chamber Solid Oxide Fuel Cells, *Journal of Fuel Cell Science and Technology*, April 2011, Vol. 8 / 041014.

[17] Yaneeporn Patcharavorachot, Amornchai Arpornwichanop, Anon Chuachuensuk, Electrochemical study of a planar solid oxide fuel cell: Role of support structures, *Journal of Power Sources*, 177 (2008) 254-261.

[18] N. Autissier, D. Larrain, J. Van herle, D. Favrat, CFD simulation tool for solid oxide fuel cells, *Journal of Power Sources*, 131 (2004) 313-319.

[19] Chiara Ciano, A Model for Tubular Solid Oxide Fuel Cells, *Excerpt from the Proceedings of the COMSOL Users Conference*, 2006, Milano.

[20] Daan Cui, Mojie Cheng, Numerical Analysis of Thermal and Electrochemical Phenomena for Anode Supported Micrtotubular SOFC, *Americal Institute of Chemical Engineers Journal*, May 2009, Vol. 55, No. 3.

[21] Mustafa Fazil Serincan, Ugur Pasaogullari, Nigel M. Sammes, Effects of operating conditions on the performance of a micro-tubular solid oxide fuel cell (SOFC), *Journal of Power Sources*, 192 (2009) 414-422.

[22] Joonguen Park, Joongmyeon Bae, Jae-Yuk Kim, A numerical study on anode thickness and channel diameter of anode-supported flat-tube solid oxide fuel cells, *Journal of Renewable Energy*, 42 920120 180-185.

[23] Feng Zhao, Anil V. Virkar, Dependence of polarization in anode-supported solid oxide fuel cells on various cell parameters, *Journal of Power Sources*, 141 (2005) 75-95.

[24] M. M. Hussain, X. Li, I. Dincer, A general electrolyte-electrode-assembly model for the performance characteristics of planar anode-supported solid oxide fuel cells, *Journal of Power Sources*, 189 (2009) 916-928.

[25] V. A. C. Haanappel, N. Jordan, A. Mai, J. Mertens, J. M. Serra, F. Tietz, S. Uhlenbruck, I. C. Vinke, M. J. Smith, L. G. J. de Haart, Advances in Research, Development, and Testing of Single Cells at Forschungszentrum Jülich, *Journal of Fuel Cell Science and Technology*, May 2009, Vol. 6 / 021302.

[26] Ugur Pasaogullari, Chao-Yang Wang, Computational Fluid Dynamics Modeling of Solid Oxide Fuel Cells, Electrochemical Engine Center, and Department of Mechanical and Nuclear Engineering, The Pennsylvania State University, USA.

[27] Marco A. Buccheri, Anand Singh, Josephine M. Hill, Anode- versus electrolyte-ssupported Ni-YSZ/YSZ/Pt SOFCs: Effect of cell design on OCV, performance and carbon formation for the direct utilization of dry methane, *Journal of Power Sources*, 196 (2011) 968-976.

[28] Junxiang Shi, Xingjian Xue, Bifuntionally Graded Electrode Supported SOFC Modeling and Computational Thermal Fluid Analysis for Experimental Design, *Journal of Fuel Cell Science and Technology*, February 2011, Vol. 8 / 011005.

[29] R. b. Bird, W. E. Stewart, E. N. Lightfoot, *Transport Phenomena*, 2nd edition, John Wiley & Sons, 2005.

[30] R. J. Kee, M. E. Coltrin, P. Glarborg, *Chemically Reacting Flow*, Jon Wiley & Sons, 2003.

[31] M. L. Bars, M. G. Worster, Interfacial Conditions Between a Pure Fluid and a Porous Medium: Implications for Binary Alloy Solidification, *Journal of Fluid mechanics*, vol. 550, pp. 149-173, 2006.

[32] G. K. Batchelor, *An Introduction To Fluid Dynamics*, Cambridge University Press, 1967.

[33] R. L. Panton, *Incompressible Flow*, 2nd edition, John Wiley & Sons, 1996.

[34] D. Nield, A. Bejan, *Convection in Porous Media*, 3rd edition, Springer, 2006.

[35] Naveed Akhtar, Stephen P. Decent, Kevin Kendall, A parametric analysis of a micro-tubular, single-chamber solid oxide fuel cell, *International Journal of Hydrogen Energy*, 36 (2011) 765-772.

[36] Penyarat Chinda, Somchai Chanchaona, Pascal Brault, Wishsanuruk, A Planar Anode-Supported Solid Oxide Fuel Cell Model with Internal Reforming of Natural Gas, *European Physical Journal Applied Physics*, 54 (2011) 23405 (15 pages).

[37] Laurencin, J., Simulation Results and Experimental Validation of SOFC Operation under Hydrogen, *Solid Oxide Fuel Cells IX; Proceedings of the International Symposium*, 2005, pages 806-813.

[38] Tae Seok lee, J. N. Chung, Yen-Cho Chen, Design and optimization of a combined fuel reforming and solid oxide fuel cell system with anode off-gas recycling, *Energy Conversion and Management*, 52 (2011) 3214-3226.

[39] Hocine. Mahcene, Hocine Ben Maussa, Hamza. Bouguettaia, Djamel. Bechki, Mostefa Zeroual, Computational modeling of the transport and electrochemical phenomena in solid oxide fuel cells, *Energy Procedia*, 6 (2011) 65-74.

[40] Kyung Joong Yoon, Srikanth Gopalan, Uday B. Pal, Effect of Anode Active Layer on Performance of Single-Step Cofired Solid Oxide Fuel Cells, *Journal of The Electrochemical Society*, 155 (6) B610-B617 (2008).

[41] Kenjo, T., Exchange current densities of Pt/YSZ oxygen electrodes as a function of yttria content in YSZ electrolyte, *Proceedings of the Fifth International Syposium of Solid Oxide Fuel Cell*, 1997, pages 431-40.

[42] Yixin Lu, Laura Schaefer, Peiwen Li, Numerical study of a flat-tube high power density solid oxide fuel cell Part I. Heat/mass transfer and fluid flow, *Journal of Power Sources*, 140 (2005) 331-339.

[43] Joongmyeon Bae, Singkwang Lim, Hyunjin Jee, Jung Hyun Kim, Young-Sung Yoo, Taehee Lee, Small stack performance of intermediate temperature-operating solid oxide fuel cells using stainless steel interconnects and anode-supported single cell, *Journal of Power Sources*, 172 (2007) 100-107.

[44] D. W. Dees, T. D. Claar, T. E. Easier, D. C. Fee, and F. C. Vlrazek, Conductivity of Porous Ni/ZrO2-Y203 Cermets, *J. Electrochem. Soc.: Electrochemical Science And Technology*, September 1987.

[45] D. Simwonis, F. Tietz, D. Stöver, Nickel coarsening in annealed Ni/8YSZ anode substrates for solid oxide fuel cells, *Solid State Ionics*, 132 (2000) 241–251.

[46] Ying Li, Yusheng Xie, Jianghong Gong, Yunfa Chen, Zhongtai Zhang, Preparation of Ni/YSZ materials for SOFC anodes by buffer-solution method, *Materials Science and Engineering B*, 86 (2001) 119–122.

[47] Swadesh K Pratihar, A. Dassharma and H.S. Maiti, Processing Microstructure Property Correlation of Porous Ni-YSZ Cermets Anode for SOFC Application, *Published in Materials Research Bulletin, 2005, Department of Ceramic Engineering, National Institute of Technology, Rourkela, India.*

[48] Atsushi Mineshige, Junko Izutsu, Maiko Nakamura, Kengo Nigaki, Jiro Abe, Masafumi Kobune, Satoshi Fujii, Tetsuo Yazawa, Introduction of A-site deficiency into

$La_{0.6}Sr_{0.4}Co_{0.2}Fe_{0.8}O_{3-\delta}$ and its effect on structure and conductivity, *Solid State Ionics*, 176 (2005) 1145– 1149.

[49] Shaorong Wanga, Masatoshi Katsukib, Masayuki Dokiyab, Takuya Hashimotoa, High temperature properties of $La_{0.6}Sr_{0.4}Co_{0.8}Fe_{0.2}O_{3-\delta}$ phase structure and electrical conductivity, *Solid State Ionics*, 159 (2003) 71– 78.

[50] Baoan Fan, Jiabao Yan, Xiaochao Yan, The ionic conductivity, thermal expansion behavior, and chemical compatibility of $La_{0.54}Sr_{0.44}Co_{0.2}Fe_{0.8}O_{3-\delta}$ as SOFC cathode material, *Solid State Sciences*, 13 (2011) 1835-1839.

[51] H. Ullmann, N. Trofimenko, F. Tietz, D. Stöver, A. Ahmad-Khanlou, Correlation between thermal expansion and oxide ion transport in mixed conducting perovskite-type oxides for SOFC cathodes, *Solid State Ionics*, 138 (2000) 79–90.

[52] L.-W. Tai, M.M. Nasrallah, H.U. Anderson, D.M. Sparlin, S.R. Sehlin, Structure and electrical properties of $La_{1-x}Sr_xCo_{1-y}Fe_yO_3$. Part 2. The system $La_{1-x}Sr_xCo_{0.2}Fe_{0.8}O_3$, *Solid State Ionics*, 76 (1995) 273-283.